PEOPLE'S DEMOCRATIC REPUBLIC OF ALGERIA

Ministry of Higher Education and Scientific Research

Ecole Nationale Polytechnique

المدرسة الوطنية المتعددة التقنيات
Ecole Nationale Polytechnique

مخبر التحكم في العمليات التصنيعية
Laboratoire de Commande des Processus

Department of Control Engineering

Laboratory of Process Control

Ph.D thesis in Control Engineering

A HYBRID GLOBAL MAXIMUM POWER POINT TRACKER FOR PHOTOVOLTAIC SYSTEMS UNDER COMPLEX PARTIAL SHADING CONDITIONS

Mostefa KERMADI

Presented and sustained on 06 November 2018

Composition of Jury :

President:	Mohamed TADJINE	Pr	Ecole Nationale Polytechnique
Examinators:	Mohand Oulhadj MAHMOUDI	Pr	Ecole Nationale Polytechnique
	Cherif LARBES	Pr	Ecole Nationale Polytechnique
	Khelifa BENMANSOUR	Pr	Ecole supérieure de la défense aérienne du territoire
	Tarek GHENNAM	MCA	Ecole Militaire Polytechnique
Supervisors:	El Madjid BERKOUK	Pr	Ecole Nationale Polytechnique
	Zainal SALAM	Pr	Universiti Teknologi Malaysia

ENP 2018

PEOPLE'S DEMOCRATIC REPUBLIC OF ALGERIA

Ministry of Higher Education and Scientific Research

Ecole Nationale Polytechnique

المدرسة الوطنية المتعددة التقنيات
Ecole Nationale Polytechnique

مخبر التحكم في العمليات التصنيعية
Laboratoire de Commande des Processus

Department of Control Engineering

Laboratory of Process Control

Ph.D thesis in Control Engineering

A HYBRID GLOBAL MAXIMUM POWER POINT TRACKER FOR PHOTOVOLTAIC SYSTEMS UNDER COMPLEX PARTIAL SHADING CONDITIONS

Mostefa KERMADI

Presented and sustained on 06 November 2018

Composition of Jury :

President:	Mohamed TADJINE	Pr	Ecole Nationale Polytechnique
Examinators:	Mohand Oulhadj MAHMOUDI	Pr	Ecole Nationale Polytechnique
	Cherif LARBES	Pr	Ecole Nationale Polytechnique
	Khelifa BENMANSOUR	Pr	Ecole supérieure de la défense aérienne du territoire
	Tarek GHENNAM	MCA	Ecole Militaire Polytechnique
Supervisors:	El Madjid BERKOUK	Pr	Ecole Nationale Polytechnique
	Zainal SALAM	Pr	Universiti Teknologi Malaysia

ENP 2018

REPUBLIQUE ALGERIENNE DEMOCRATIQUE ET POPULAIRE

Ministère de l'Enseignement Supérieur et de la Recherche Scientifique

Ecole Nationale Polytechnique

المدرسة الوطنية المتعددة التقنيات
Ecole Nationale Polytechnique

مخبر التحكم في العمليات التصنيعية
Laboratoire de Commande des Processus

Département d'Automatique

Laboratoire de Commande des Processus

Thèse de Doctorat en Automatique

COMMANDE HYBRIDE DE LA POURSUITE DE LA PUISSANCE MAXIMALE D'UN SYSTEME PHOTOVOLTAIQUE SOUS LES CONDITIONS COMPLEXES D'OMBRAGE PARTIEL

Mostefa KERMADI

Présentée et soutenue en 06 Novembre 2018

Composition du Jury :

Président:	Mohamed TADJINE	Pr	Ecole Nationale Polytechnique
Examinateurs:	Mohand Oulhadj MAHMOUDI	Pr	Ecole Nationale Polytechnique
	Cherif LARBES	Pr	Ecole Nationale Polytechnique
	Khelifa BENMANSOUR	Pr	Ecole Supérieure de la Défense Aérienne du Territoire
	Tarek GHENNAM	MCA	Ecole Militaire Polytechnique
Rapporteurs:	El Madjid BERKOUK	Pr	Ecole Nationale Polytechnique
	Zainal SALAM	Pr	Universiti Teknologi Malaysia

ENP 2018

To my lovely mother and father, *who gave me endless love, trust, constant encouragement over the years, and for their prayers.*

To my spouse, *for being very understanding and supportive in keeping me going, enduring the ups and downs during the completion of this thesis.*

To my family and friends, *for their patience, support, love and prayers.*

This thesis is dedicated to them.

ACKNOWLEDGEMENT

I wish to express my deepest appreciation to all those who helped me, in one way or another, to complete this thesis. First and foremost I thank ALLAH almighty who provided me with strength, direction and showered me with blessings throughout.

My sincerest gratitude to my supervisors **Prof. El Madjid Berkouk** and **Prof. Zainal Salam** for their continuous guidance and support. With their expert guidance and immense knowledge I was able to overcome all the obstacles that I encountered during my journey of PhD. I could not have imagined having a better advisors and mentors who have been more like a fatherly figure to me.

I also wish to sincerely thank the President of jury **Prof. Mohamed Tadjine** and the members of jury: **Prof. Mohand Oulhadj Mahmoudi**, **Prof. Cherif Larbes**, from Ecole Nationale Polytechnique, **Prof. Khelifa Benmansour** from Ecole Supérieure de la Defense Aérienne du Territoire, and **Dr. Tarek Ghennam** from Ecole Militaire Polytechnique for accepting to be members of the reading committee and for their constructive analysis of the present work.

Last but not least, I would like to take this opportunity to express my appreciation and gratitude to Prof. **Djamel Boukhetala**, Deputy Director of the School and Director of the Post-Graduation and Scientific Research, Prof. **Rachid Illoul**, Head of the Department of Control Engineering, Prof. **Boualem Hemici**, Head of the Laboratory of Process Control, and Prof. **Mohamed Seghir Boucherit**, Responsible of the Conversion Energy Systems Control Doctoral School, for their support throughout the preparation of this work.

ملخص

تعتبر تتبع نقطة الإستطاعة القصوى (MPPT) مهمة لا غنى عنها في الأنظمة الكهروضوئية (Photovoltaic systems). حتى الآن، تم اقتراح العديد من تقنيات MPPT باستخدام أساليب مختلفة. في البداية، قمنا بحوصلة أهم التقنيات المقترحة وقدمنا كذلك دراسة مقارنة شاملة لأحدث تقنيات MPPT المعتمدة على الذكاء الإصطناعي. بعد ذلك، اقترحنا نظاما هجينا لتعقب الطاقة القصوى (MPPT) خاصا بالأنظمة الكهروضوئية (PV) تحت ظروف التظليل الجزئي المعقدة. تجمع الخوارزمية المقترحة بين التقنيات التقليدية والخوارزميات المعتمدة على الذكاء الإصطناعي. من خلال القيام بذلك، يتم ضمان تتبع سريع، دقيق وموثوق لنقطة الإستطاعة القصوى (GMPP). يضمن النظام المقترح فحصا كاملا و سريعا لمساحة البحث بحيث يتم ضمان تعقب نقطة الإستطاعة القصوى في وقت قياسي. تمت مقارنة أداء التقنية المقترحة مقابل خوارزميات MPPT ذات قدرة تنافسية عالية مقترحة حديثا. تم أيضا إجراء اختبارات للتحقق من صحة تتبع GMPP تحت ظروف التظليل الجزئي المعقدة باستعمال المحاكاة و التجربة. للتحقق التجريبي، تم استخدام جهاز محاكاة المولد الكهروضوئي موصول بمحول محول عكسي لفرق الجهد. تم تنفيذ الخوارزمية المقترحة باستخدام TMS320F240 DSP المضمن داخل لوحة dSPACE DS1104.

الكلمات المفتاحية: تتبع نقطة الإستطاعة القصوى. الأنظمة الكهروضوئية. التظليل الجزئي.

RESUME

Dans les systèmes photovoltaïques (PV), le suivi de point de puissance maximum (MPPT) est une tâche indispensable. A ce jour, diverses techniques MPPT ont été proposées dans la littérature en utilisant différentes méthodes. Dans ce travail, nous avons résumé d'abord et donne une étude comparative complète des techniques MPPT les plus adoptées. Par la suite, nous avons proposé un algorithme de suivi de puissance maximale (MPPT) hybride pour le système photovoltaïque (PV) dans des conditions d'ombrage partiel complexe. L'algorithme proposé combine des techniques classiques avec un algorithme méta-heuristique, c'est-à-dire l'optimisation de l'essaim de particules (PSO). En ce faisant, un suivi rapide, précis et fiable du point de puissance maximale globale (GMPP) est garanti. L'espace de recherche est entièrement examiné minutieusement de sorte que la convergence vers GMPP est garantie. Les performances de la technique proposée sont évaluées par rapport à des algorithmes MPPT hautement compétitifs. Des tests sont effectués pour vérifier le suivi de l'exactitude du GMPP dans des conditions d'ombrage partiel complexes. Pour la vérification expérimentale, le simulateur de générateur photovoltaïque est utilisé conjointement avec un convertisseur abaisseur-élévateur (Buck-boost). L'algorithme proposé a été implémenté en utilisant le DSP TMS320F240 de la carte dSPACE DS1104.

Mots Clés: Photovoltaïque, Extraction de la puissance maximale, Effet d'ombrage partiel.

ABSTRACT

In Photovoltaic (PV) systems, maximum power point tracking (MPPT) is an indispensable task. To date, various MPPT techniques have been proposed in the literature using different methods. In this work, we performed initially a comprehensive comparative study of the most adopted MPPT techniques. Thereafter, we proposed a hybrid maximum power point tracker (MPPT) for photovoltaic (PV) system under complex partial shading conditions. The proposed algorithm combines conventional techniques with meta-heuristic algorithm i.e., the particle swarm optimization (PSO). By doing so, a fast, accurate and reliable tracking of the global maximum power point (GMPP) is guaranteed. The search space is fully scrutinized such that the convergence to GMPP is guaranteed. The performance of the proposed technique is evaluated against highly competitive MPPT algorithms. Tests are made to verify the correctness tracking of the GMPP under complex partial shading conditions. For experimental verification, hardware based photovoltaic array simulator is used in conjunction with a buck-boost converter. The proposed algorithm was implemented using the TMS320F240 DSP of dSPACE DS1104 board.

Key Words: Maximum power point tracking (MPPT), Photovoltaic (PV), partial shading condition (PSC).

TABLE OF CONTENTS

LIST OF TABLES

TABLE NO **TITLE** **PAGE**

LIST OF FIGURES

FIGURE NO **TITLE** **PAGE**

LIST OF ABBREVIATIONS

GMPP	-	Global Maximum Power Point
PSC	-	Partial shading condition
AI	-	Artificial Intelligence
PID	-	Proportional-Integral-Derivative
FL	-	Fuzzy Logic
ANN	-	Artificial Neural Network
GA	-	Genetic Algorithms
PSO	-	Particle Swarm Optimization
T	-	Cell temperature
G	-	Solar irradiance
I_{PV}	-	PV current
I_{light}	-	Photo-cell current
L_{diode}	-	Direct Diode current
I_{sc}	-	Short-circuit current
I_0	-	Reverse bias saturation current
V_{pv}	-	Voltage across the cell
I_{scref}	-	Short-circuit current in standard temperature conditions
I_{oref}	-	Reverse bias saturation current in standard temperature conditions
T_{ref}	-	Reference temperature
G_{ref}	-	Solar irradiance reference

R_s	-	Series resistance
n	-	Diode ideality factor
V_T	-	Heat Potential
K	-	Boltzmann constant
q	-	The electron charge
μ_{Isc}	-	Short-Circuit Current Temperature Coefficient
E_g	-	Band gap of the semiconductor
N_s	-	Series connected cells number
N_p	-	Parallel connected cells number
$I_{pv}{}^G$	-	Global Current supplied by PV module
$V_{pv}{}^G$	-	Global voltage of PV module
P_{mp}	-	Maximum power available
V_{mp}	-	Operating voltage value at maximum power
V_{oc}	-	The open circuit voltage
I_{sc}	-	Short-circuit current
D	-	Duty cycle
T_d	-	The switching period
i_i	-	Input current of the converter
v_i	-	Input voltage of the converter
i_o	-	Output current of the converter
v_o	-	Output voltage of the converter
S	-	State of the converter switch
R_L	-	Resistive load
L	-	Inductance of the converter
C_1	-	Input capacitor of the converter
C_2	-	Output capacitor of the converter

G_v	-	Voltage conversion ratio
S_1	-	The sliding surface
K	-	Switching gain of the sliding mode controller
v_{iref}	-	Reference voltage
K_p	-	Proportional gain of MPPT controller
K_I	-	Integral gain of MPPT controller
K_D	-	Derivative gain of MPPT controller
μ_i	-	Firing strength
W_h	-	Weight of hidden layer
W_o	-	Weight of output layer
b_h	-	Biases of hidden layer
b_o	-	Biases of output layer
V_{mp}	-	Estimated maximum power voltage
MSE	-	Mean Square Error
$FSTS$	-	Fixed Sampling Time Strategy
$ASTS$	-	Adaptive Sampling Time Strategy
v_i	-	Agent velocity
p_{ibest}	-	Agent's best position
g_{best}	-	Best position attained in the swarm
P_{max}	-	Theoretical maximum power
e_m	-	Tracking error
E_m	-	Average value of the tracking error
V_m	-	Variance of the tracking error
t_{rep}	-	Convergence time towards MPP
η	-	Photovoltaic efficiency (%)
D_{MPP}	-	The optimum duty cycle

D_{ref}	-	Reference duty cycle
ΔP	-	The change in power
ΔV	-	The change in voltage
P_{act}	-	Actual measured power
V_{act}	-	Actual measured voltage
P_{pre}	-	Previous value of power
V_{pre}	-	Previous value of voltage
R_{PV}	-	Equivalent resistance
Φ_D	-	The duty cycle perturbation
Φ_V	-	The voltage perturbation
n_{pts}	-	The number of operating points in the search space
V_{oc_mod}	-	Open circuit voltage of the module
V_{oc_str}	-	Open circuit voltage of the string
V_{GMPP}	-	Voltage of the GMPP
V_{skip}	-	Upper limit of the skipped voltage interval
MHP	-	Middle Higher Peak
SSJ	-	Search-skip-judg
SDP	-	Section Dividing Point

CHAPTER 1

GENERAL INTRODUCTION

1.1 Overview

Electrical energy is the backbone of modern industry and an essential tool for modern life. Because of the growing demand for energy and the stress on conventional energy resources with undesirable impact on environment, the industry has been urged to accelerate the researches on alternative energy resources. Among the available alternative energies, Photovoltaic (PV) energy is one of the most promising renewable energy. PV energy is freely available and environment friendly. PV equipment generates electricity without any gas emissions and its operation is virtually silent. Moreover, it is simple in design and requires little maintenance. Large PV power systems are now widely being installed around the world and the demand of such power is increasing every year.

Algeria has launched an ambitious program to develop renewable energies (photovoltaics (PV), concentrated solar power (CSP) and wind power) to diversify energy sources and engage in sustainable energy use [1]. The Algerian energy strategy is mainly based on solar energy development due to the huge solar potential in the country. PV power should achieve by 2030 more than 37% of national electricity production. In addition, the program aims to export the solar power to Europe through undersea cables. Although large scale PV power systems in general require high initial investment cost, several projects are realized in many regions in Algeria to strengthen the national utility grid.

Notwithstanding the success of the building integrated PV (BIPV) initiatives in various countries, the integration of these systems in Algeria still could not attain the grid-parity, i.e. the point at which the cost of the generated power is less than or equal to the price of purchasing power from the electricity grid. The main obstruction is the high capital investment [2]. However, BIPV is expected to be cost-effective in the near future taking into account the continuous decline of the PV modules price and the continuous depletion of the conventional resources.

Building integrated PV (BIPV) systems can be implemented on unused spaces–such as rooftops of homes, factories and large buildings can be effectively utilized to harvest solar energy. One major problems faces the BIPV is the shadowing that affects the PV systems. It

usually comes from the close proximity of buildings, the nearby trees, soiling of the PV modules etc. which cause energy loss. For instance, 41% of the installed PV systems were affected by shadowing in the German 1000 Roofs Program, which represents a 10% energy loss [3].

The efficiency of the whole PV system depends on three major aspects: the solar cell, power electronics devices and the maximum power point tracking (MPPT) algorithm. At the solar cell level, scientists are still improving the solar cell efficiency continuously. Traditional crystalline silicon solar cells have reached efficiencies between 22% and 26%. The best-reported measurements for 1-sun (non-concentrator) single-junction cells Silicon (Si) crystalline cell is 26.7% [4]. For multi-junction solar cell structure, four-junction wafer-bonded concentrator solar cells efficiency up to 46.1% has been recorded [5]. At the power electronic devices level, a maximum efficiency rating of 98.7 % for photovoltaic inverters has been achieved by the Fraunhofer Institute for Solar Energy Systems ISE in a test prototype using silicon carbide (SiC) transistors [6]. The third major aspect of photovoltaic (PV) system utilization is to enhance its MPPT. Although the popular conventional MPPT methods such as perturb and observe (P&O), incremental conductance (IC) and hill climbing (HC) perform efficiently under uniform irradiance (G), they tend to fail when subjected to partial shading conditions. This is because, when one or more modules in a string are shaded, multiple peaks are generated on the P-V curve. Instead of tracking the global maximum power point (GMPP), the algorithm trapped frequently at a local peak—resulting in a considerable power loss. To overcome this limitation, MPPT based on metaheuristic approach such as particle swarm optimization (PSO) [7], grey wolf optimization (GWO) [8], cuckoo search (CS) [9], flashing fireflies (FF) [10], differential evolution (DE) [11], genetic algorithm (GA), flower pollination algorithm (FPA) [12] and artificial bee colony (ABC) [13] have been proposed in recent literature. These soft computing techniques capitalize on their efficient search and optimization capabilities to locate the GMPP. Despite their advantages—particularly in handling partial shading, they exhibit several drawbacks; the most significant is the sluggishness in the tracking speed due to the random numbers usually used. On the other hand, several conventional MPPT are modified to yield higher performance [14-21]. The ideal scenario is to improve the tracking efficiency, while overcoming the partial shading problem. These objectives can be achieved by incorporating additional intelligence into the MPPT codes.

In the recent literature, a new approach known as the hybrid MPPT is gaining interest [22-28]. It is a combination of the conventional and soft-computing algorithms, with the aim of exploiting the advantages of each type. However, by adopting this approach, it needs to compromise on their weaknesses too. Most of the soft-computing algorithms suffers from the trade-off between the tracking speed and the accuracy of tracking the GMPP (efficiency). The tracking speed can be improved by increasing the step sizes in the iteration. However, this may leads the algorithm to miss certain local maxima points and therefore traps a local maximum power point (LMPP) resulting in drop of the tracking efficiency. On the other hand, reducing the step sizes in addition of using random numbers in the iteration reduces the tracking speed.

Based on these observations, this work proposes a MPPT algorithm which addresses the shortcomings mentioned above. The MPPT has a hybrid structure that combines the modified P&O [29] and PSO. Although the algorithm employs the metaheuristic search (i.e. PSO), the tracking speed is not compromised because it incorporates the SSJ mechanism [15]. The PSO scrutinized the entire search space; thus, the GMPP will not be missed. In addition, unlike the original SSJ, the proposed algorithm does not suffer from slow convergence for GMPP located at the higher end of the P-V curve. This problem is solved by dividing the search region into three parts (lower, middle and upper end); by using three PSO particles, these regions are explored independently. To increase the tracking speed further and to reduce the steady state oscillation, the P&O is made adaptive in nature. As for the practical implementation, only one pair of voltage and current sensors is needed.

1.2 Objective, Scope and Importance of the Research

The objective of this research is to propose, design and implement an effective MPPT algorithm for PV system under complex partial shading condition. The proposed algorithm is based on a hybrid approach that combines the particle swarm optimization (PSO) and an improved perturb and observe (P&O). The scheme incorporates a skipping technique to minimize the region to be searched on the *P-V* curve. In addition, a communication procedure between the particles is inserted so the region that have been previously explored by one particle will not be searched again by another particles. The expected outcome of this work is an efficient MPPT tracking under any complex partial shading condition. This increases the overall efficiency of the BIPV systems frequently subjected to partial shading.

1.3 Organization of the Thesis

The thesis is organized into seven chapters in total. This chapter describes the backgrounds, objectives and scopes of the research. The problem statements are also clearly mentioned and clarified.

Chapter 2 is composed of a review on the recent proposed MPPT methods in the literature. These MPPT methods are subdivided into three categories: 1- MPPT based on improved conventional methods, 2- MPPT based on soft-computing approach and 3- Hybrid MPPT (conventional and soft-computing). The MPPT methods, especially the ones included in the comparative study in this thesis, are extensively described in this chapter.

In Chapter 3, modeling of the different parts constituting the PV system is presented. Then, an adaptive sliding mode control technique for controlling the buck-boost converter used for simulation is proposed. At the end, the experimental set-up where the real tests are carried out is described.

In Chapter 4, the different control structures used for MPPT implementation are analyzed. The analysis study includes the direct control structure based on the duty cycle and the indirect control structure which is based on the voltage. The performance of both control structures is evaluated using simulation and experiment.

Chapter 5 presents a comprehensive comparative study of four Artificial Intelligence (AI)-based MPPT methods namely: Fuzzy Logic (FL), Artificial Neural Networks (ANN), Genetic Algorithms (GA) and Particle Swarm Optimization (PSO). The competing methods are classified according to the tracking performance and the cost of implementation.

In Chapter 6, the improved hybrid PSO MPPT is developed to mitigate the limitations of conventional Soft-computing methods. The working principle of the algorithm, design

structures, flowcharts, software/hardware implementation etc. are described in details. Along with that, the proposed method is tested and compared against recently proposed highly competitive MPPT under several complex shading conditions. The superiority of the proposed method is well highlighted.

Chapter 7 summarizes the research and the contributions are highlighted again. Besides, some probable directions towards the future works are also provided.

CHAPTER 2

LITERATURE REVIEW OF MAXIMUM POWER POINT TRACKING TECHNIQUES

2.1 Introduction

Photovoltaic energy comes from conversion of a part of the solar irradiance into electrical energy. This conversion is based on the photovoltaic effect. This latter is a physical and chemical phenomenon of the creation of voltage and electric current in a material upon exposure to light. PV modules are composed of series and parallel association of many PV cells. The maximum power point of a PV module changes with respect to variation in solar irradiance and temperature levels. Because of the high cost of PV modules and their low efficiency (below 27%), integration of robust MPPT controller is a compulsory task. During uniform solar irradiance (G), *P-V* curve is characterized by a unique MPP. Although the popular conventional MPPT methods such as perturb and observe (P&O), incremental conductance (IC) and hill climbing (HC) perform efficiently under uniform irradiance, they tend to fail when subjected to partial shading condition (PSC). This is because, when one or more modules in a string are shaded, multiple peaks are generated on the P-V curve. Instead of tracking the global maximum power point (GMPP), the algorithm is frequently trapped at a local peak—resulting in a considerable power loss.

This chapter presents a summary and comprehensive literature review of the various MPPT methods dealing with partial shading conditions. Principles of operation of the most prominent MPPT methods proposed in the recent literature are described and their advantages and constraints are highlighted. This would be useful for readers who require a comprehensive background of MPPT methods, as well as keeping up to date with the latest development in this area. The MPPT methods presented in this chapter are divided into three categories:

1- MPPT based on the improved conventional methods.
2- Soft-computing based MPPT methods.
3- MPPT methods based on Hybrid approach, i.e., conventional with soft-computing.

At the end of this chapter, the essential objective of the literature review, i.e., to search for the gap in the existing methods, would be accomplished. This gap shall be the basis for the research that will be carried out in this thesis.

2.2 Group 1: MPPT based on Improved Conventional Methods

Conventional MPPT techniques such as: P&O and IC are simple in implementation and very efficient under uniform insolation. However, they tend to fail in handling partial shading. Recently, conventional methods are modified for the purpose of being able to handle partial shading conditions [14-21]. These objectives can be achieved by incorporating additional intelligence into the MPPT codes. Authors in [17] observed from several shading patterns that the power peaks are displaced from each other by integral multiple of the open circuit voltage of the PV module. By inspiring from this model, Authors in [16] proposed a fast modified IC to cater with partial shading. Another family of MPPT techniques is growing in the recent published literature. In this family, the decreasing *I-V* function is employed to skip scanning certain voltage intervals, resulting significant improvement in the tracking speed [14, 15, 18]. An attempt to review a selection of these methods is made in the present section. Their working principles are described and their advantages and weaknesses are highlighted.

2.2.1 Search-Skip-Judge (SSJ) method

The search-skip-judge (SSJ) improves the convergence of the IC by intelligently skipping the voltage intervals (known as the skipped intervals) which do not contain the GMPP. Since the skipped intervals are avoided, the amount region to be searched is reduced; thus, the tracking speed increases. The SSJ is particularly fast when the GMPP is located at the lower end of the *P-V* curve; however, at the upper end, it is much slower. This is because the search and skip process needs to be repeated for several lower voltage peaks before reaching the GMPP.

To understand the mechanism involved in SSJ, the *P-V* curve shown in Figure 2-1 is considered. The objective of SSJ is to minimize the search region by identifying the sections in which the search can be omitted; hence the name “skipped interval”. First, the nearest LMPP is determined by InCond. Then, the corresponding section dividing point (SDP) is calculated. The SDP is a local minimum point (V_{SDP}, P_{SDP}), located at the right side of the power peak; it is defined as the voltage in the *I-V* curve at which the irradiance (thus the current) steps due to partial shading occurs. For instance, Figure 2.1 shows the *I-V* curve that

composed of four steps due shading pattern of four irradiance levels; the point that divides the step is the SDP. The skipped interval is determined by the following procedure: after initialization, $P(n)$ climbs to the nearest LMPP using the InCond. It records $P_{Pbest}(n)$, $V_{Pbest}(n)$. Then, the operating point is moved forward until tracking the SDP. Note that when the operating voltage V_{PV} is on the right side of V_{SDP}, the string current I_{PV} is always lower than I_{SDP}. Therefore, within the voltage interval [V_{SDP}, V_{skip}], the operating power is always lower than the straight line P_{SDP} drawn in Figure 2-1. Clearly in this condition, P_{Pbest} is guaranteed to be highest within that interval. Hence, since $P_{Pbest}=P_{SDP}|_{\text{at } Vskip}$, the upper bound of the skipped voltage interval V_{skip} can be deduced as

$$V_{skip} = \frac{P_{Pbest}(n)}{I_{SDP}} \tag{2.1}$$

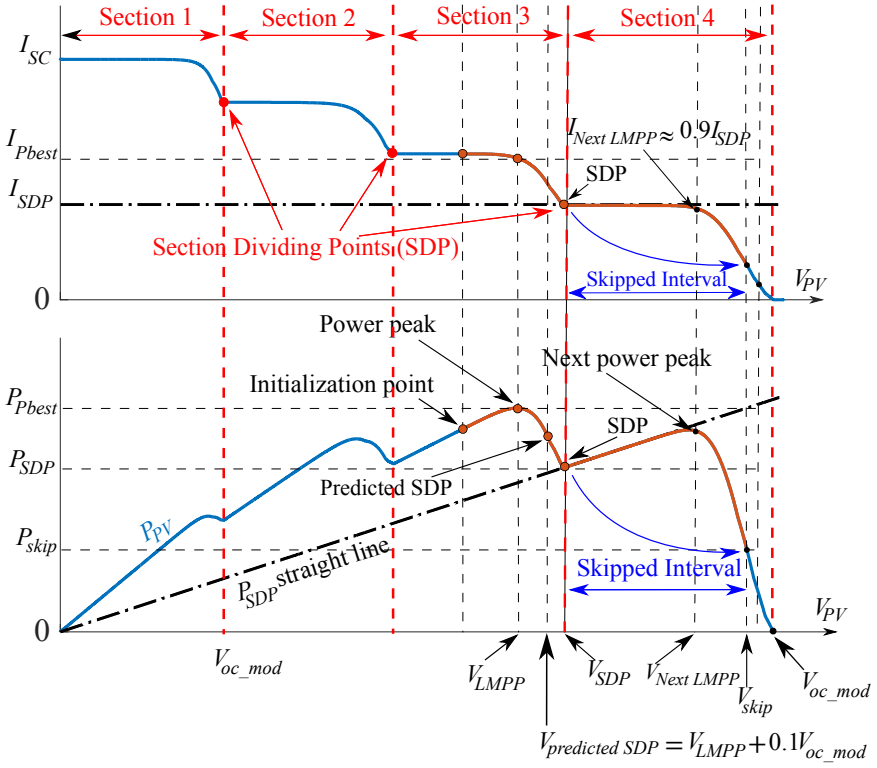

Figure 2-1: Demonstration of skipping voltage interval technique.

Since it is guaranteed that no other peak is higher than P_{Pbest}, the interval [V_{SDP}, V_{skip}] can be exempted from being explored. Thus, the unnecessary scanning is reduced, which leads to a faster convergence.

The SSJ is particularly fast when the GMPP is located at the lower end of the *P-V* curve; however, at the upper end, it is much slower. This is because the search and skip process needs to be repeated for several lower voltage peaks before reaching the GMPP. To explain the issue further, Figure 2-2 is considered. With the SSJ process, the search starts form the lowest local peak and progressively goes towards the GMPP, which is located at the upper end (rightmost peak). In between the search, certain skipped intervals can be made. Obviously, the convergence takes longer time since the GMPP is at the upper end of the *P-V* curve. When the SSJ is initiated from the lower voltage local peak (i.e. the leftmost peak), the incremental conductance (IncCond) is activated until it tracks the first LMPP, i.e. point A. Then, the operating point is moved forward to reach the SDP. After that, the SSJ skips a voltage interval (see Figure 2-2), and a new operating point is judged—thus activating the IncCond again. The same procedure is repeated for points B, C and D—before finally reaching to GMPP. As can be seen, the skipped interval is not very large. Consequently, for *P-V* curve of this nature, a large amount of time is needed to reach the GMPP. However in Figure 2-3, where the GMPP is located in the leftmost side of the *P-V* curve, the SSJ procedure is done only for the region where the GMPP exist. The rest of interval is skipped. Therefore, the tracking time is greatly reduced compared to the *P-V* curve of Figure 2-2.

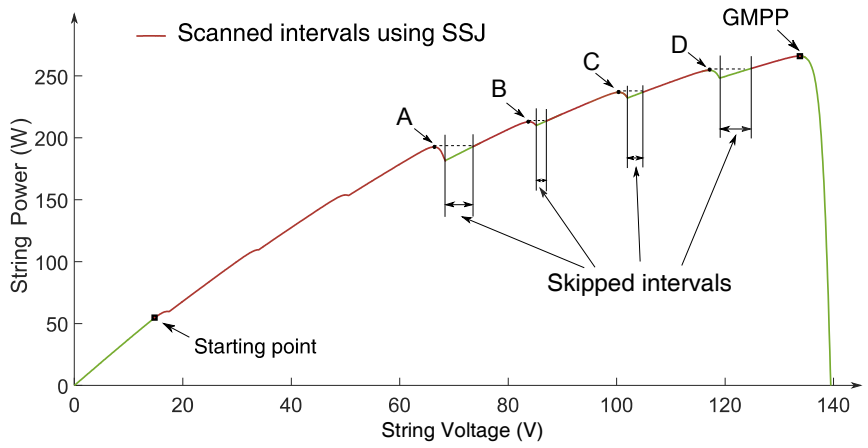

Figure 2-2: Shading pattern where the GMPP is located at the upper end of the *P-V* curve.

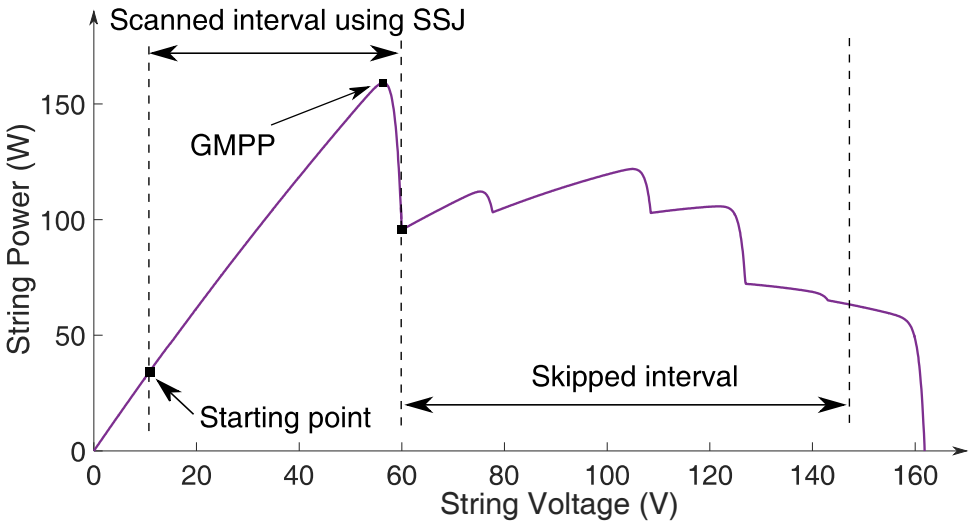

Figure 2-3: Shading pattern where the GMPP is located at the lower end of the P-V curve.

2.2.2 Modified Incremental of Conductance (MIC) method

The modified incremental conductance (MIC) [16] significantly improves the GMPP tracking speed under partial shading. The MIC exhibits very fast convergence to GMPP because it is based on the well-known $0.8\times V_{oc}$ model [17]. The basic MIC operation is illustrated in Figure 2-4. The algorithm considers that the peaks (local and global) are located near the vicinity of multiples of $0.8\times V_{oc\_mod}$, where V_{oc_mod} is the open circuit voltage of the module. The search starts from the lower end (left most) of the *P-V* curve; it stores the first three consecutive peaks—forming the first cluster. The magnitudes of the three peaks are evaluated: if the middle peak is higher than the two accompanying peaks (to its left and right), the GMPP is considered to be found. Consequently, the search is halted. This peak is known as the middle higher peak (MHP). On the other hand, if the middle peak is lower than one of the accompanying peaks, the algorithm assumes that GMPP does not exist within that particular cluster. Then, a successive cluster is formed and this new cluster is scrutinized in the same manner as the previous one. The process continues until the cluster that contains the MHP is found.

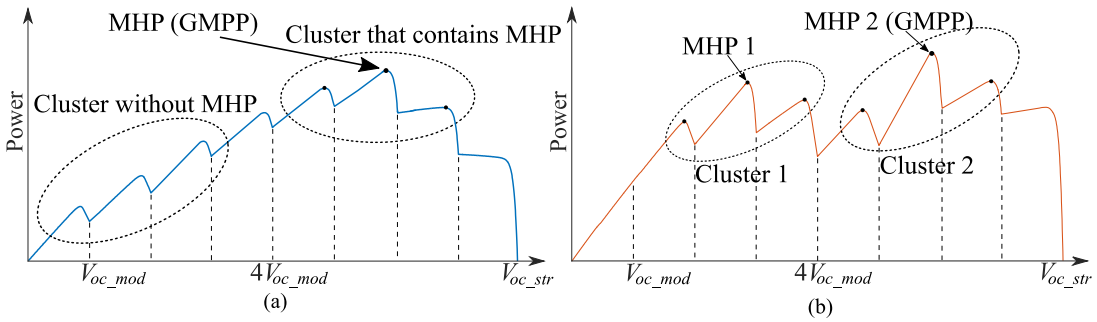

Figure 2-4: (a) *P-V* curve that has only one cluster and unique MHP. (b) With two clusters and two MHP. Note: V_{oc_str} equals $n_{mod} \times V_{oc\_mod}$, where n_{mod} is the number of modules that the string is made of.

One important point to note is that in most PV literature, the MPPT is tested using a simplified multi-peak with unique MHP, similar to the one shown in Figure 2-4(a). Typically, the tracking performance is evaluated GMPP at one particular location on the *P-V* curve. Thus, it is uncertain if the algorithm works equally well when the GMPP is located at the low, medium and high region of the curve. In addition, there are possibilities of complex shading pattern that results in a number of clusters—each with its own MHP, as shown in Figure 2-4(b). This condition imposes a challenging problem, particularly for MIC. In the case where the first cluster has a lower MHP than the second, third and so forth, the MIC will consider the first MHP as the GMPP. In the example shown in Figure 2-4(b), the algorithm found MHP1 in Cluster 1; it decides this point to be the GMPP and thus halts the search process. Obviously, the result is wrong because the true GMPP is located in Cluster 2, i.e. MHP2. This error results in power loss, which is the difference between MHP1 and MHP2.

2.2.3 Voltage Window Search (VWS) method

The Voltage Windows Search (VWS) GMPPT method proposed by [18] is a very efficient tracking method that uses the *I-V* characteristics to skip some unnecessary voltage intervals where the GMPP cannot be found. The main parameters of the VWS algorithm are: the global voltage step (ΔV_{GSTEP}), the voltage window (VW) and the power operating triangle (POT). ΔV_{GSTEP} is the fixed voltage step used to scan the *P-V* curve. Authors in [18] suggested that the optimum value of ΔV_{GSTEP} should be around the voltage difference between two adjacent local power peaks, i.e., within the range $[0.5V_{ocP}, V_{ocP}]$, where V_{ocP} is the open-circuit voltage of single part of a PV module at standard test conditions (STC).

The POT is shown in Figure 2-5. It is the triangle delimited by the x-axis and the straight lines of the open-circuit voltage V_{OC} and short-circuit current I_{SC} at STC.

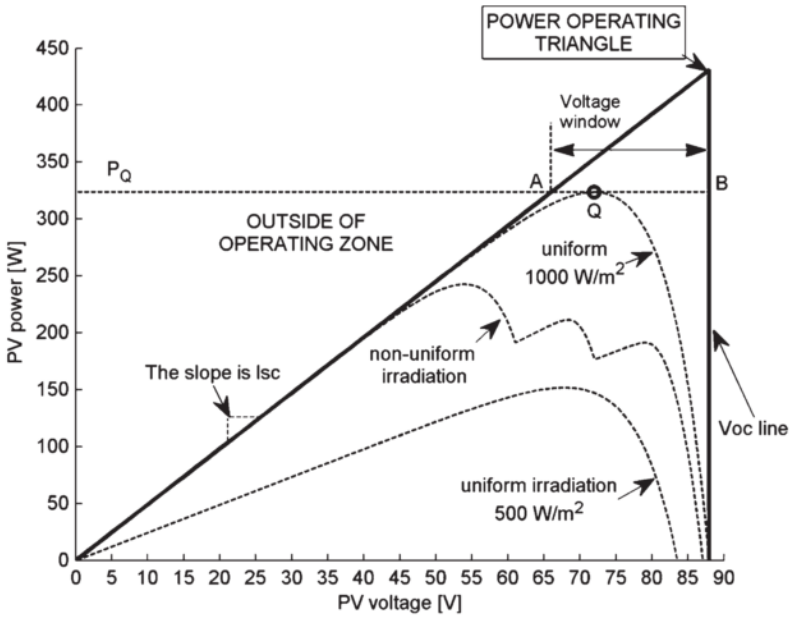

Figure 2-5: Power operating triangle and voltage window illustration [18].

The VW is defined as the voltage range [V_{min}, V_{max}], to be scanned around the GMPP. During the search process, the VW is narrowed from the lower end V_{min}, while the upper end V_{max} is fixed at the maximum possible GMPP voltage. According to a simulation study carried out in [18], the possible GMPP voltage never exceeds $0.887V_{OC}$. Based on this, the upper end of the VW V_{max} was fixed at $0.9V_{OC}$.

Although the VWS technique is very fast, it can fail in tracking the correct GMPP if ΔV_{GSTEP} is not properly chosen. To explain the working principle of the VWS algorithm and to illustrate the failure to track GMPP for certain cases, the shading pattern of Figure 2-6 is considered. It contains two clusters, in which the GMPP exists in the second one. The tracking performance of the VWS is shown in Figure 2-7. As can be seen, the VWS is not able to track the GMPP (73.5V, 126.5W). Instead, it is trapped at the LMPP (34.15V, 119.9W). Its tracking time is very fast (0.13 ms), but that is irrelevant because the algorithm does not converge to GMPP.

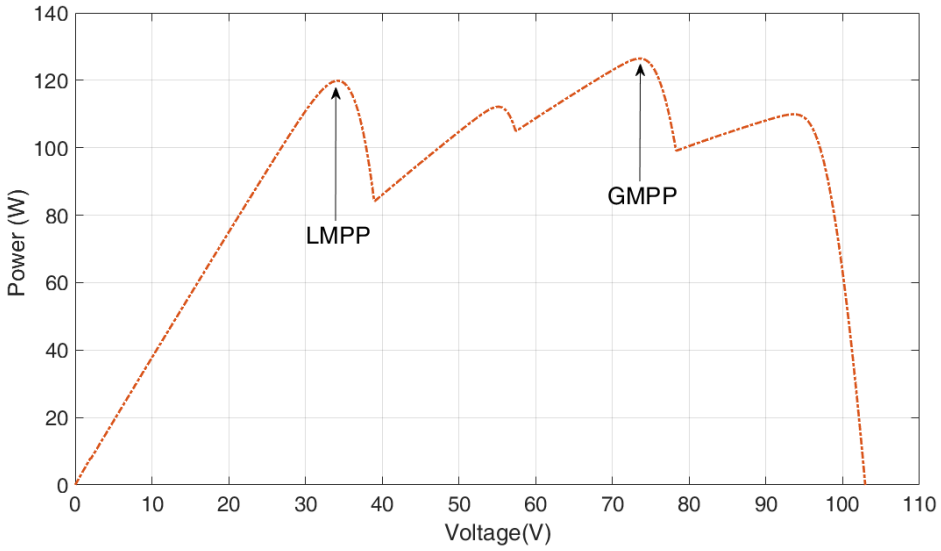

Figure 2-6: Pattern contains two clusters where the GMPP is located in the second cluster.

By looking at the behavior and the tracking process of the VWS, the explanation of this failure can be understood. It is detailed in Figure 2-7. The tracking is assumed to start at point Q. The voltage window (VW) is calculated using the power operating triangle (POT) at STC. Then the voltage of point 1 is checked, and thus V_{min1} is calculated. The algorithm increases the voltage by the global voltage step (ΔV_{GSTEP}). This latter should be inferior than V_{ocP} as suggested by [18]. Therefore, ΔV_{GSTEP} is chosen equal to 10V. After that, the value of power at Point 2 (P_2) is checked. Since $P_2 > P_Q$, the value of P_{store} is updated as : $P_{store}=P_2$. Then, point 3 is checked. Since $P_3 < P_2$, the value of V_{min2} is calculated; correspondingly, point **"*a*"** is skipped since it falls outside the new POT. Then, the reference voltage increased and point 4 is tested. Since $P_4 < P_{store}$, a new POT is calculated and a new VW is defined: [V_{min3}, V_{max}]. Then, the reference voltage is increased as follows: $V_5=V_4+\Delta V_{GSTEP}$ and point 5 is checked. However, due to the large value of ΔV_{GSTEP}, the region in which the GMPP exists is eventually skipped. Hence, the GMPP which is located between Points 4 and 5 is missed. Since $P_5 < P_{store}$, a new POT is calculated and the new VW becomes: [V_{min4}, V_{max}]. After checking point 6, the search process is stopped since V_{min5} falls outside of the VW.

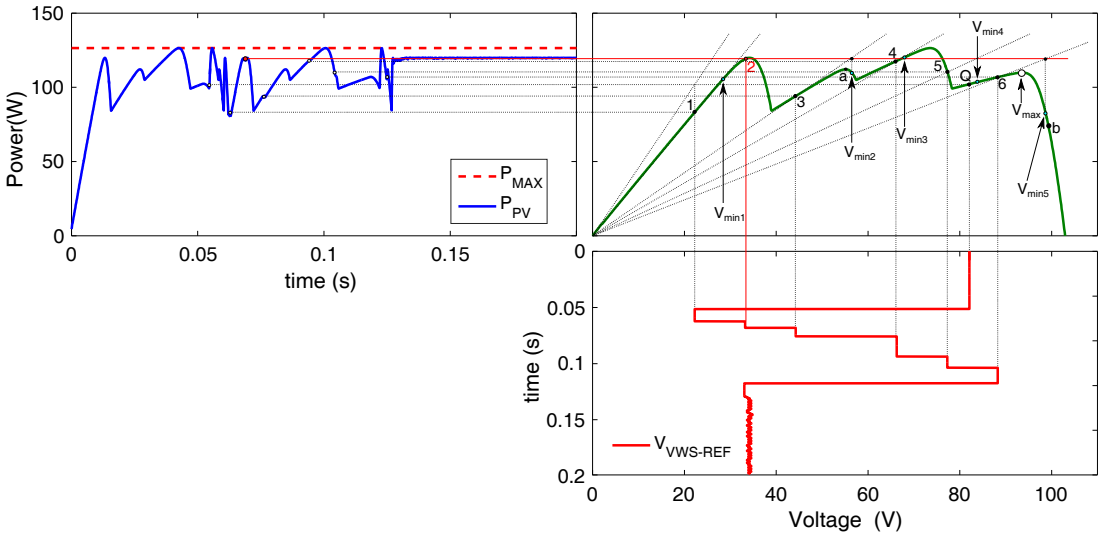

Figure 2-7: Step by step explanation of the failure of VWS in tracking the GMPP of Pattern of Figure 2-6.

2.3 Group 2: MPPT based on Soft-Computing Approach

Since the relation between the extracted power and the output voltage (*P-V*) is highly nonlinear, fuzzy logic (FL) and artificial neural networks (ANN) are a suitable solutions for the MPPT problem under uniform insolation. For PSC, several pieces of research have made attempts to realize global MPPTs by evolving different methods based mainly on meta-heuristic optimization algorithms. In evolutionary computing family, MPPT algorithms were proposed based on Genetic algorithms (GA) in [30-32] and Differential Evolution (DE) in [46–48]. In swarm intelligence family, Particle Swarm Optimization (PSO) for MPPT is preferred due to its simplicity and fast computation capability [7, 33-36] [49–53]. Furthermore, recent works have implemented MPPT methods using grey wolf optimization (GWO) [8], cuckoo search (CS) [9, 37], flashing fireflies (FF) [10], jaya algorithm (JA) [38], artificial bee colony (ABC) [13], flower pollination algorithm (FPA) [12]. These soft computing techniques capitalize on the vast power of modern computers to search for the global maximum power point (GMPP). It has one distinct advantage: it can be made to effectively scrutinizes the entire *P-V* curve search space; hence its suitability in handling partial shading conditions. However, these methods are much slower than the conventional MPPT [7, 39]. To improve the tracking speed, the modified versions of the metaheuristic algorithms are introduced. For instance, authors in [37] proposed the modified cuckoo search (MCS) that eliminates the Lévy flight term from the conventional CS equation. Similarly, in

[40], the original DE based MPPT is amended by removing the random number and skipping certain sampling intervals.

2.3.1 Fuzzy Logic (FL)

Fuzzy Logic is considered as one of the most suitable techniques for MPPT. The *P-V* curves exhibit non-linear function influenced mainly by weather conditions. FL control has several advantages; it does not require precise mathematical modeling; furthermore, it deal with imprecision inputs and it can handle non-linearity. However, prior expertise is required for the design of FL controller [43]. The digital implementation of the fuzzy controller has

Table 2-1: Summary of Fuzzy logic-based MPPT methods.

MPPT Technique	Summary	Implementation
[41] Chao et al.	A Fuzzy logic based MPPT controller was implemented using tow stage DC-DC boosting converter. The first stage is used to track the MPP while the second stage is used to supply the DC bus with the required voltage for grid connection.	Direct method (D_{ref})
		Two stages DC-DC boosting converter
		DSP TMS320F2812
[42] El Khateb et al.	A Fuzzy based MPPT controller with SEPIC converter is proposed. An experimental validation of the proposed scheme is carried out for both SEPIC DCDC and single-phase DC-AC converters.	Indirect method (V_{ref})
		SEPIC converter
		DSP TMS320F28335
[43, 44] Larbes et al.	Genetic algorithms was used to optimize the membership functions of Fuzzy logic based MPPT controller. The algorithm was implemented using FPGA chip and compared with various intelligent MPPT algorithms.	Direct method (D_{ref})
		Buck converter
		FPGA Virtex-5 Xilinx
[45] Boukenoui et al.	A scanning and storing algorithm is applied in the first stage to locate the MPP. Then, the identified MPP is tracked precisely by employing Fuzzy Logic.	Direct method (D_{ref})
		Boost converter
		Software validation

been carried out in [46, 47]. The fuzzy controller was improved by selecting the best membership functions using genetic algorithms in [43] and particle swarm optimization in [48]. Table 2-1 summarizes selected MPPT controllers based on Fuzzy Logic.

The FL block has four modules: a fuzzification stage, a rule base, an inference engine and an aggregation stage. A typical FL-based MPPT controller, which is considered for the comparative study carried out in Chapter 5, is described. It has two inputs and one output. The inputs variables are the error $E(k)$ and the change in the error $\Delta E(k)$ which are defined as follows:

$$E(k) = \frac{P(k) - P(k-1)}{V(k) - V(k-1)} \tag{2.2}$$

$$\Delta E(k) = E(k) - E(k-1) \tag{2.3}$$

k is the sampling time. $P(k)$ and $V(k)$ are respectively the instantaneous output power and voltage of the PV module. In the fuzzification step, the numerical variables are transformed into linguistic variables which can be: Negative (N), Zero (Z) and Positive (P). Figure 2-8 show the membership functions of E and ΔE. The number, the type and the range of the membership functions are chosen by previous knowledge and/or experimental data from the PV system. The accuracy of the output depends on the number of used linguistic variables. Higher number improves the output stability accuracy. However, it increases the algorithm complexity and the computing time. After fuzzification, the inference engine based on Mamdani method applies nine rules which have the form IF-THEN as expressed in Table 2-2. It should be noted that a good understanding of the system's behavior is required to establish these rules base. In the aggregation step, the output is computed using Sugeno-Type Fuzzy Inference Method. Its output provides a reference voltage for the converter in order to locate the MPP. The output function has five levels s = [NB, NS, Z, PS, PB]. Negative Big (NB), Negative Small (NS), Zero (Z), Positive Small (PS) and Positive Big (PB). The output level S_i of rule i is weighted by the firing strength $\mu_i(s_i)$. This latter is computed using the multiplication operator as follows:

$$\mu_i(s) = \mu_i(E)\mu_i(\Delta E) \tag{2.4}$$

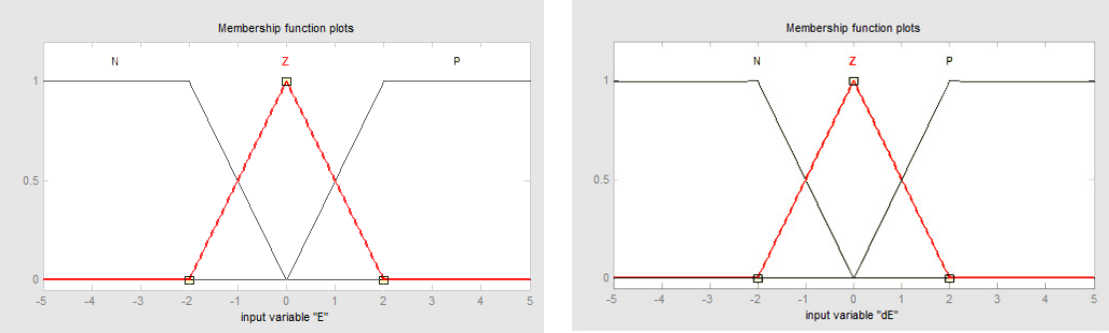

(a) (b)

Figure 2-8: (a) Membership function of the linguistic input E. (b) Membership functions of the linguistic input ΔE.

where μ_i(E) and μ_i(ΔE) are, respectively, the membership functions of E and ΔE of the rule i. The numeric output which is the weighted average for the nine rules is calculated as follows

$$V_{ref} = \frac{\sum_{i=1}^{9} \mu_i(s) s_i}{\sum_{i=1}^{9} \mu_i(s)} \tag{2.5}$$

Table 2-2: Rules base table of the FL-based MPPT controller.

dE\E	**N**	**Z**	**P**
N	NB	NS	Z
Z	NB	Z	PB
P	Z	PS	PB

2.3.2 Artificial Neural Networks (ANN)

Artificial neural networks are an alternative way to handle nonlinear problems. They can learn from examples and deal with incomplete data. Once trained, they can perform fast predictions [49]. ANN approach is proposed for MPPT control in the literature [50, 51]. The requirement of a large database for training the ANN model is the main constraint of such

controller. In [52], the database was established from measurements of irradiance, temperature and the corresponding optimal duty cycle. Authors in [53] proposed an optimization of the ANN structure using genetic algorithms. A complex approach is proposed in [54] where a fuzzy controller is used to perform the choice between many ANN models, the choice of the local model is based on the optimal performance in the operating range of temperature and irradiance. Table 2-3 summarizes selected MPPT controllers based on ANN.

Table 2-3: Summary of ANN-based MPPT methods.

MPPT Technique	Summary	Implementation
[53] Kulaksiz et al.	ANN based MPPT controller was proposed. The ANN was trained using a database obtained from experimental measurements. Then, Genetic algorithm was employed to get the ideal size of the ANN structure.	Indirect method (V_{ref}) Two level DC-AC inverter DSP ADSP-21992
[55] Mancilla-David et al.	A low cost MPPT algorithm and Irradiance sensor was proposed. The database was generated using a mathematical model of the PV cell. The trained neural network provides the MPP voltage and the irradiance value.	Indirect method (V_{ref}) - PIC18F6627 Microcontroller
[56] Jiang et al.	A hybrid MPPT controller combines ANN and P&O without irradiance sensor was proposed. ANN, which is trained off-line with several partial shading cases, is used to predict the region of MPP; then, P&O technique is employed to track the MPP.	Direct method (D_{ref}) Buck converter DSP TMF28335

A typical ANN-based MPPT is described in this section. Besides FL, it will be evaluated and compared with other SC-based MPPT controllers in Chapter 5. For each measure of irradiance and temperature, the PV module has a unique MPP; to locate this point, the voltage corresponding to the MPP V_{mp} must be applied to the output of the PV module. This ANN-based MPPT controller consists of a two-layer feed-forward network as shown in Figure 2-9. The neural network is defined according to its structure which includes number of layers, numbers of neurons in each layer, type of activation function in each layer and interconnection between layers. It should be noted that this structure is chosen after several tests in order to increase the accuracy of the obtained neural network. The input variables,

which are the irradiance and the temperature, are transmitted to the hidden layer through the two neurons of the input layer. The hidden layer is composed of five neurons whose activation function is a hyperbolic tangent function which is given by:

$$f_h(u) = \frac{2}{1+e^{-2u}} - 1 \tag{2.6}$$

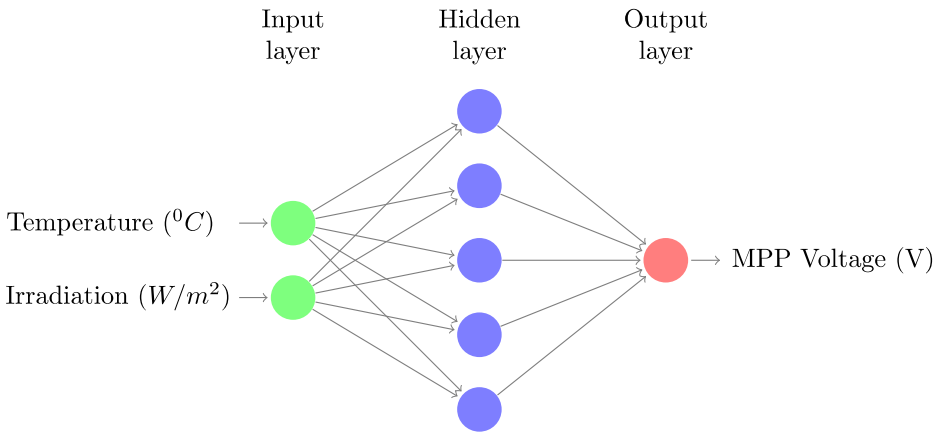

Figure 2-9: Structure of the Neural Network.

The output activation x of the hidden layer neurons are therefore computed using the following expression

$$x = f_h(W_h[G \;\; T]^T + b_h) \tag{2.7}$$

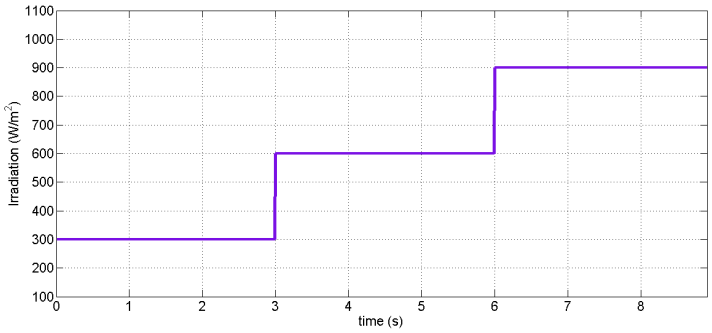

(a)

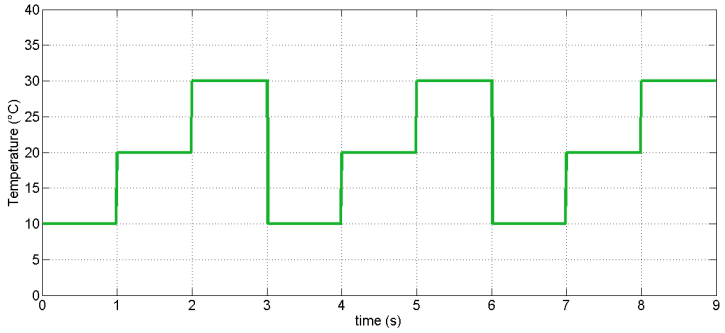

(b)

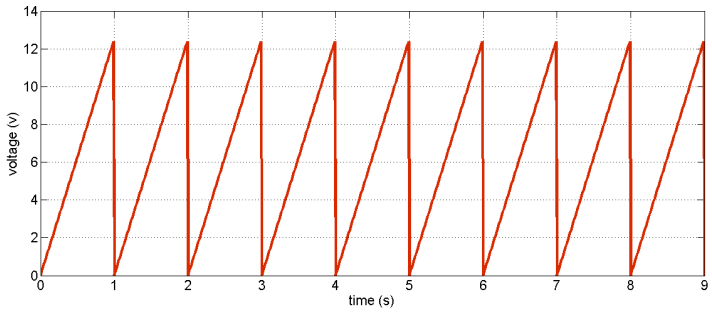

(c)

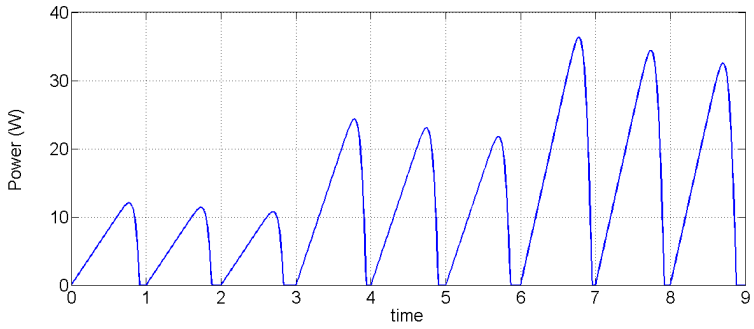

(d)

Figure 2-10: Example of a simulation to obtain nine patterns. (a) Solar irradiance values. (b) Temperature values. (c) Output voltage of the PV module. (d) Output power of the PV module.

The strengths of the neurons respectively of the hidden and output layer are represented by the weight matrix denoted respectively by W_h, W_o and the biases vector denoted respectively by b_h, b_o. The vector of the input signals contains the irradiance G and the temperature T. The output layer contains one neurons whose linear activation function is given by:

$$f_o(x) = x \tag{2.8}$$

This neuron provides the computed MPP voltage $\hat{V}_{mp}$ using the following expression

$$\hat{V}_{mp} = f_o(W_o x + b_o) \tag{2.9}$$

The database, which the neural network will be trained with, should include a wide range of measurements in order to increase the prediction accuracy. In this work, the database is established from simulation on the model of PV module shown above. Figure 2-10 shows an example used to establish nine patterns. For instance, between 4s and 5s, the irradiance value is equal to 600 W/m^2 while the temperature value is equal to 20°C as shown in Figures 2-10(a), 2-10(b). In this interval, the output voltage of the PV module is ramped in a linear fashion from zero to V_{oc} as shown in Figure 2-10(c). Figure 2-10(d) shows the output power curve in which the MPP appears clearly. For this weather condition (600 W/m^2, 20°C), the operating point of the MPP is (V_{mp}=8.89V, P_{mp}=22.02W).

Figure 2-11 represents the database obtained from simulation. It is used to train the ANN controller. This database contains 312 pattern of irradiance, temperature and the corresponding MPP voltage. It is divided into three sub-databases: 80% are used for training the neural network and the rest are used for validation and testing. Note that a controller trained with this database can only be useful for PV modules with same characteristics.

The neural network is trained off-line using Levenberg-Marquardt backpropagation algorithm which minimizes the mean square error (MSE) using the approximate Hessian matrix. This algorithm is chosen as the optimization tool because of its proven computing efficiency and good performance. The MSE is calculated as follows :

$$MSE = \frac{1}{n}\sum_{i=1}^{n}(V_{mp}(i) - \hat{V}_{mp}(i))^2 \tag{2.10}$$

where V_{mp} is the i^{th} target and $\hat{V}_{mp}$ is its estimated output. Figure 2-12 shows the evolution of the performance error for the trained ANN-baed MPPT controller. The MSE curve of validation is practically similar to that of the training, thus confirming the success of the ANN learning. The best MSE during the training process is equal to 3.29×10^{-4}.

Figure 2-13 compares the ANN computed outputs with the targets. As it can be observed, the ANN shows high prediction capability. The target output is computed with high accuracy. The max error in the validation step is equal to 0.056V. The minimum voltage is equal to 7.2 V. The relative error therefore does not exceed 0.78%. Regression value,

denoted by R, measures the correlation between the ANN outputs and the targets. Its value equals 1 for an ideal relationship.

After the training process, the ANN-based MPPT controller is expected to be able to provide the MPP voltage at any weather condition. An advantage of this controller is the fact that it does not need a high iterations number to locate the MPP. Consequently, this reduces oscillations around the MPP and improves efficiency of this controller. It should be noticed that this technique requires irradiance and temperature sensors with the introduction of a calculator.

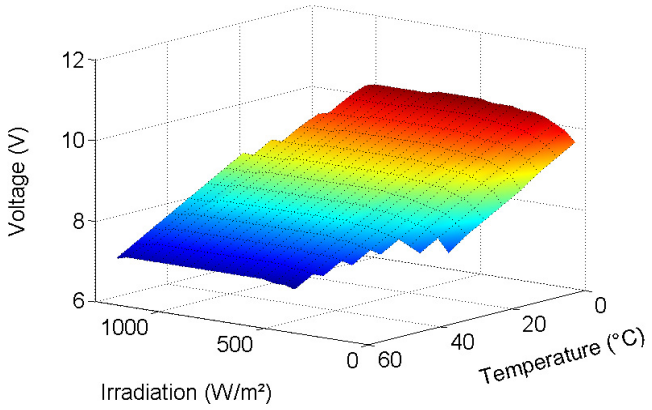

Figure 2-11: The database used to train the neural network: V_{MPP} versus different values of temperature and irradiance.

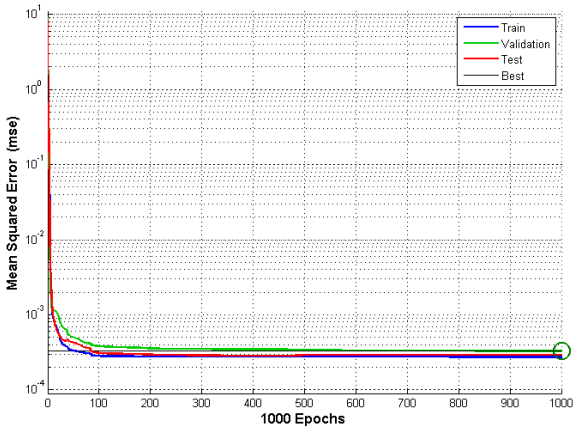

Figure 2-12: The mean square error evolution during the training process.

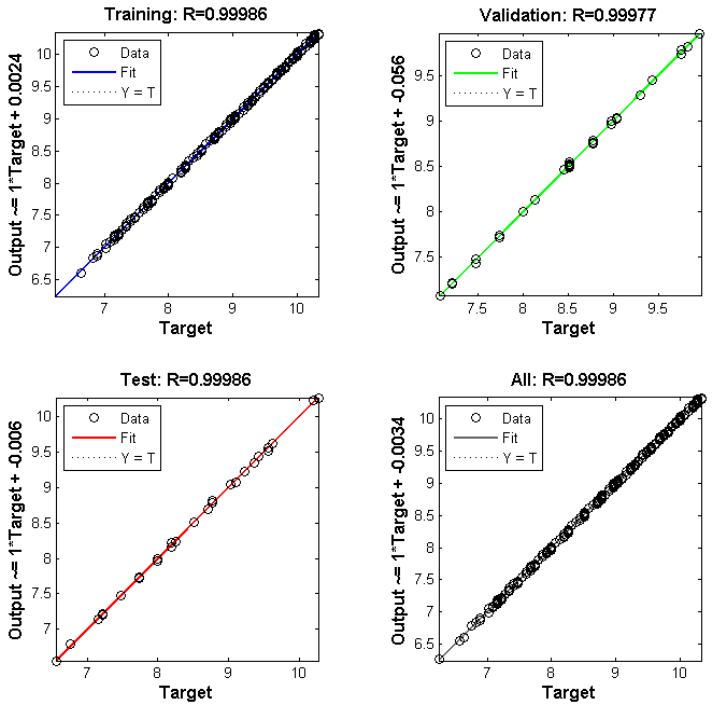

Figure 2-13: The ANN estimated outputs and targets during the training process.

2.3.3 Genetic Algorithms (GA)

Genetic Algorithms (GA) is an optimization technique based on evolution of biological systems. This algorithmic concept is based on the survival of the fittest, i.e., stronger individuals in the population have a higher probability to produce children. There is a limited published work adopted the GA to be used for the MPP tracking. In [30], Genetic Algorithms was employed directly to track the MPP. Firstly, an initial population of Duty cycles set is selected. After that, genetic operations are employed until reaching the MPP. An MPPT technique embeds P&O algorithm in genetic algorithms structure was proposed in Daraban et al [57]. GA procedure may be summarized as follows :

1. An objective function is identified to quantify the fitness of each candidate solution.
2. Generate randomly an initial population.
3. Evaluate the fitness of each individual according to the objective function.
4. Creation of new population by employing genetic operators (selection, crossover, mutation):

- Selection operator : select individuals that will be used to create the new generation according to their fitness.
- Crossover operator : create new individuals by recombining two selected parent individuals.
- Mutation operator : makes a random change of a chosen part in the new individual with very low probability.

5. Stop the algorithm when the stopping criterion is satisfied or a specified number of generations is achieved; elsewhere, the algorithm continue to generate new population.

The objective function is maximizing the power extracted from the PV module. To start, the GA requires to set the initial population. In the beginning, a search space should be definded. For MPPT, it could be a voltage range where all possible MPPs could be confined in under any is guaranteed to be within this voltage range at any enviremental conditions should be selected. The vector of initial population is chosen to cover this interval. This interval is the search space within the MPP that should be located. The initial population includes six individuals $[V_1, V_2, V_3, V_4, V_5, V_6]$. These individuals are transmitted successively as a reference voltages to the power converter. In the literature, there are two strategies: Fixed sampling time strategy (FSTS) and variable sampling time strategy (VSTS). FSTS is the most used by researchers. In this strategy, a sampling time is fixed to ensure that the system attains the steady state regime before changing the voltage reference. This leads to obtain a good reading of the PV output power. However, the main drawback of this strategy is the time wasted once the steady state regime attained in time less than the sampling time. This non-exploited time may diminish the rapidity of the MPP tracking. To avoid this problem, authors in [58] proposed an MPPT controller with VSTS. The sampling time changes according to the duty cycle perturbation. If the perturbation is small, a small sampling time is chosen and vise-versa. The ASTS is integrated by using a comparator between the reference voltage computed by the GA controller and the PV output voltage. Once the reference voltage is attained, the corresponding power is measured and stored, and the next individual is set as new reference voltage to the power converter. By means of this, the rapidity of MPPT algorithm is greatly increased. Figures 2-14 and 2-15 present a comparison of the MPP tracking between the FSTS and the proposed ASTS under similar enviremental conditions (25°C and 500 W/m^2). The tracking time of the MPP by means of the FSTS is 1.83 s; however, using ASTS, the algorithm needs only 0.23 s to achieve the

MPP. After testing all individuals of the generation, the criterion of selection is performed by elitism. The crossover step consists of combining two individuals parents to produce a child. This step is done using the following expression

$$V_i(k) = rand(1)V_i(k-1) + (1-rand(1))V_j(k-1) \tag{2.11}$$

where *j* is an integer random number between 1 and 6. The mutation step is performed with very low probability 5%. This step make a random change in individuals using the following equation

$$V_i(k) = V_{min} + rand(1)(V_{max} - V_{min}) \tag{2.12}$$

where V_{min} is the minimum voltage in the search space and V_{max} is the maximum voltage in the search space. At the vicinity of the MPP, individuals values are very close. The MPP is assumed to be found. To avoid unnecessary fluctuation caused usually by the mutation operator, the criterion 12 is met to stop the search process and to set the best solution among all generations as a reference voltage to the power converter.

$$\begin{cases} |\Delta P| \le \Delta P_{min} \\ |\Delta V| \le \Delta V_{min} \end{cases} \tag{2.13}$$

where ΔP_{min}, ΔV_{min} values are set by user. When the convergence value is satisfied, the GA operation will stop. Otherwise, the GA operation will continue by applying genetic operations until the MPP is reached. Extreme variation in the irradiance level cause a strong fluctuation in the output power. GA-based MPPT controller must re-initialize the search for the new MPP whenever it detects a change in weather conditions. Therefore, the inequality 13 must be satisfied to re-initialize the search of the new MPP.

$$\begin{cases} \dfrac{|P_{i+1}-P_i|}{P_i} \geq \Delta P_{set} \\ |V_{i+1}-V_i| \leq \Delta V_{set} \end{cases} \tag{2.14}$$

where $\Delta P_{set} = 10\%$ is predetermined percentage of power and ΔV_{set} is predetermined voltage set by user. (i +1) is the actual measured value while i is the previous measure. The operation principle of the GA-based MPPT controller is resumed in Figure 2-16.

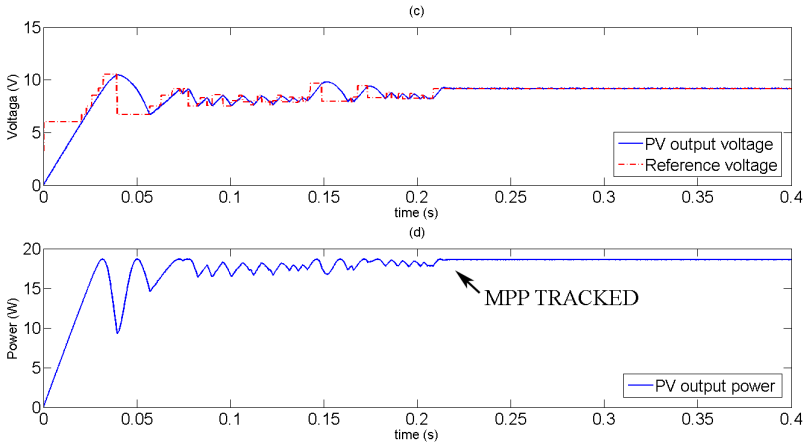

Figure 2-14: Maximum power point tracking using the proposed ASTS.

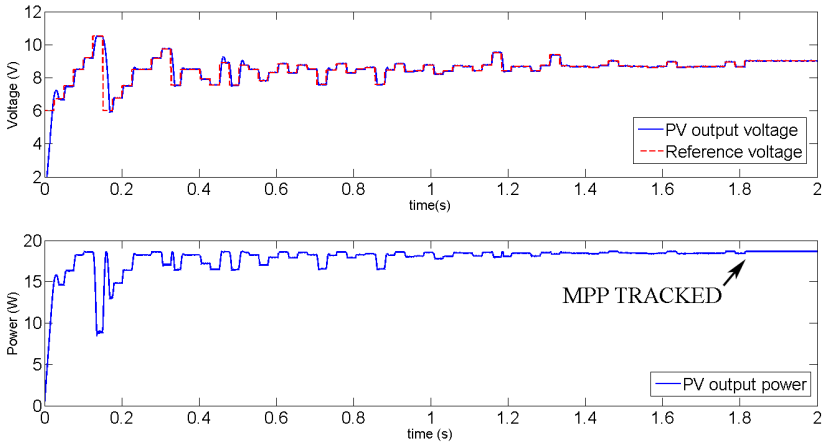

Figure 2-15: Maximum power point tracking by using the FSTS.

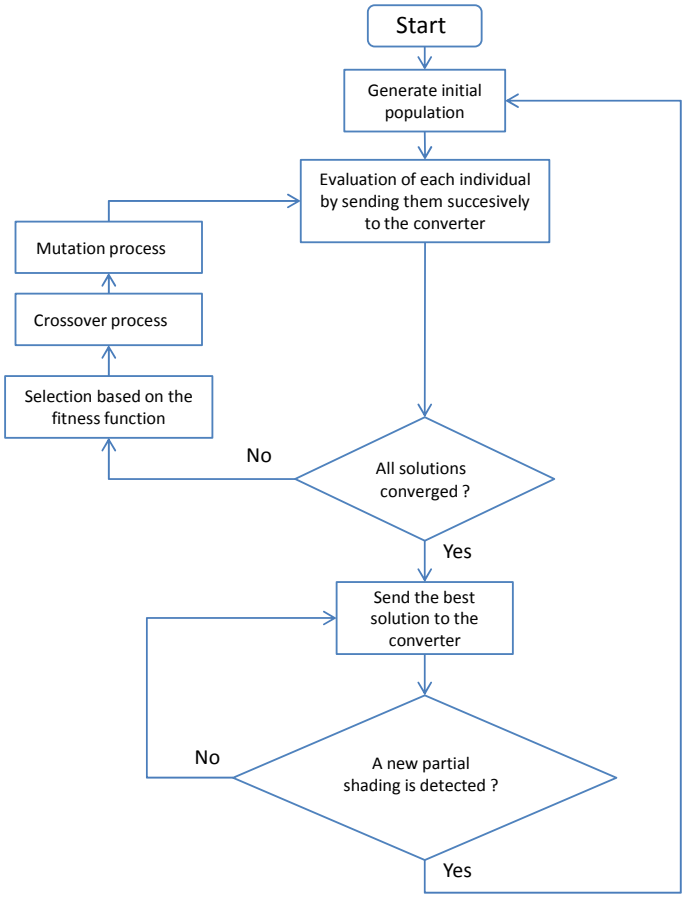

Figure 2-16: GA-based MPPT controller flowchart.

2.3.4 Particle Swarm Optimization (PSO)

PSO is meta-heuristic approach applied to solve multi-objective function optimization. The PSO algorithm works using a population (swarm) of candidate solutions called particles/agents. Their mouvement within the search space depends on simple mathematical formulas. The particle's movement is guided by its own best position, its speed and the entire swarm's best position. When a best solution is being found, this consequently will guide the future movement of the swarm towards this new position. This process is repeated until all the swarm's particles converge to the best position in the search space. Several published works has adopted the PSO algorithm for the MPP tracking. Table 2-4 summarizes selected MPPT conrtollers based on PSO.

Table 2-4: Summary of the PSO-based MPPT controllers.

MPPT Technique	Summary	Implementation
[59] Liu et al.	A modified PSO based MPPT algorithm was proposed. Unlike standard version of PSO, the parameters are defined by linearly varying functions with respect to the sampling time in order to speed up the convergence.	Indirect method (V_{ref}) Boost converter dsPIC33FJ16GS502 Microcontroller
[7, 34] Ishaque et al.	Authors introduced several improvements to the conventional MPPT PSO algorithm with using Hill climbing method when the MPP is located to improve the performance and the tracking accuracy.	Direct method (D_{ref}) Buck-Boost converter DSP TMS320F240
[28] Lian et al.	A hybrid MPPT algorithm combines P&O and PSO methods was proposed. Initially, P&O method is employed to locate the nearest local maximum. Starting from that point, the PSO method is employed to locate the MPP.	Indirect method (V_{ref}) Interleaved Boost converter DSP TMS320F28035
[60] Sundareswaran et al.	A combined PSO and P&O MPPT algorithm was proposed. In the first stage, PSO is used to locate the MPP. Then, the MPP tracking is performed using P & O method.	Direct method (D_{ref}) Boost converter PIC16F876A Microcontroller
[58] Mirhassani et al.	The PSO algorithm was implemented with variable sampling time strategy to increase the tracking speed. The sampling time selection is based on the converter current behavior.	Direct method (D_{ref}) Boost converter TMS320F335 DSP
[25] Seyedmahmoudian et al.	The proposed MPPT technique employs a hybrid evolutionary algorithm which combines PSO and DE. The proposed technique shows several advantages in the MPP tracking under partial shading conditions.	Direct method (D_{ref}) SEPIC converter Atmega328P Microcontroller

In this approach, several cooperative particles are used; each one shares information obtained in its own search process. Each particle moves in the search space with a velocity v_i^k; this movement depends on its own previous best position $p_{i_{best}}$ and the best position attained among all the particles of the swarm g_{best}. The velocity is calculated by

$$v_i^{k+1} = wv_i^k + c_1 r_1 (p_{i_{best}} - x_i^k) + c_2 r_2 (g_{best} - x_i^k) \tag{2.15}$$

where w is the inertia weight, c_1 and c_2 are positive constants representing the acceleration coefficients; r_1, r_2 are the normalized random numbers between [0, 1]. Therefore, the particle's position, xi, is updated using

$$x_i^{k+1} = x_i^k + v_i^{k+1} \tag{2.16}$$

During the optimization process, the particles spread over the search space in different directions. Figure 2-17 shows the typical movement of particles for one iteration. f is the objective function which we aim to maximize. For each iteration cycle, if $f(x_i) > f(p_{i_{best}})$, $p_{i_{best}}$ is updated by x_i. Additionally, g_{best} is updated by the best position achieved by all the particles, i.e., if $f(p_{i_{best}}) > f(g_{best})$, $g_{best} = p_{i_{best}}$. The objective function is chosen to be the output power of the PV array

$$f(x_i^k) > f(p_{i_{best}}) \tag{2.17}$$

First, an initial vector of four particles is defined as

$$x^1 = [V_1, V_2, V_3] \tag{2.18}$$

To start the optimization process, the algorithm transmits successively the particles to the power converter. By using the proposed ASTS, no sampling time is needed to ensure that the system attains steady state regime. Once the reference voltage is attained, the corresponding power is measured and stored and the next particle is called. In each iteration, the position and velocities are updated by using Eqs (2.15) and (2.16). For each iteration k, if $f(x_i^k) > f(p_{i_{best}})$, then, $p_{i_{best}}$ should be updated and replaced by x_i^k. Further, for i=1,2 and

3, if $f(p_{i_{best}}) > f(g_{best})$, g_{best} should be also updated and replaced by $p_{i_{best}}$. This process continues until the MPP is reached. At the MPP region, particles arrive with a very low velocity and the objective function can no longer improve; if the difference between them is sufficiently small, i.e., criterion (2.14) is satisfied, the MPP is assumed to be found and the searching process is stopped. When a change in environmental condition occurs, the PSO algorithm re-initializes the search for the new GP again. The flowchart represented in Figure 2-18 illustrates the proposed PSO algorithm. If *w* value is small, the particle's movement will be slow. However, if *w* takes high value, particle's movement will be very rapid; therefore, that's may cause fluctuations around the MPP when steady state regime is achieved. c_1 represents the acceleration coefficient of a particle towards its own best position $p_{i_{best}}$. While c_2 represents the acceleration coefficient of a particle towards the best position among all the swarm's particles g_{best}. Accordingly, the proposed algorithm exhibits a very good performance by selecting three particles, $w = 0.4$, $c_1 = 0.2$ and $c_2 = 0.9$. More accurate results can be achieved by increasing the number of particles. However, such operation increases the computation time. Figure 2-19 represents the MPP tracking using same previous environmental condition (25°C and 500 W/m^2). Using ASTS, PSO-based MPPT controller tracks the MPP in less than 0.06 s. Hence, PSO approach is faster than GA.

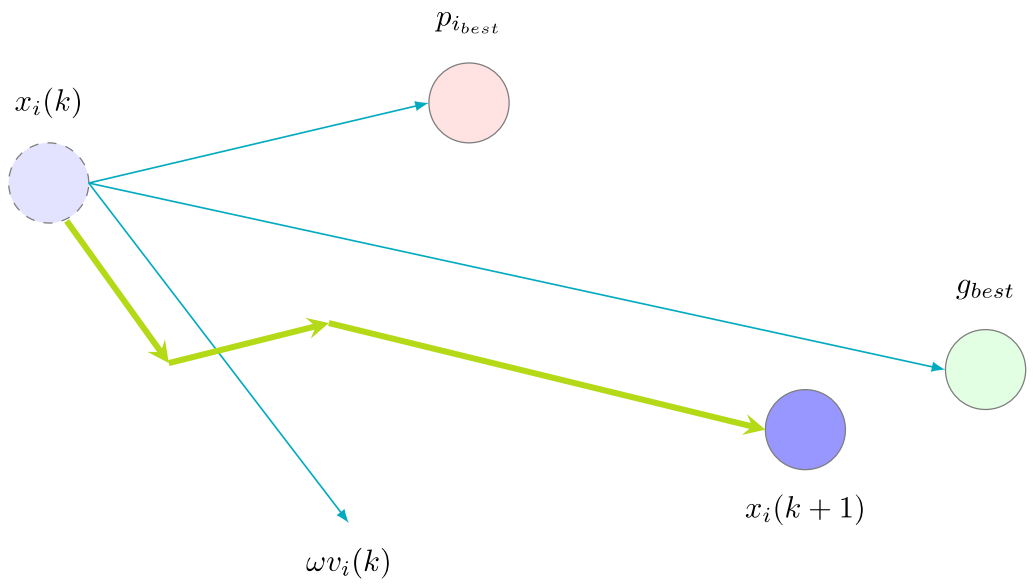

Figure 2-17: Displacement of agent in the search space.

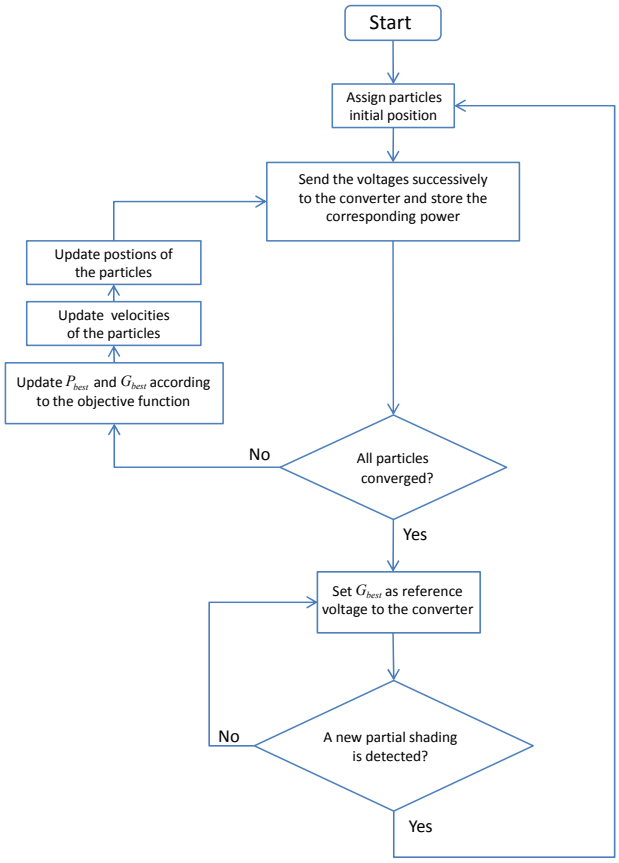

Figure 2-18: Flow chart of the PSO-based MPPT controller.

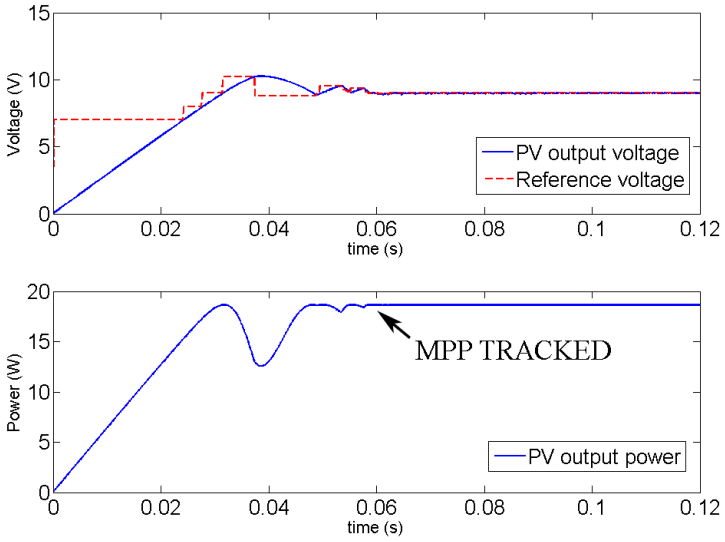

Figure 2-19: Maximum power point tracking using PSO approach.

2.4 Group 3: Hybrid Approach

In the recent literature, a new approach, known as the hybrid MPPT is gaining interest [22-28]. It is a combination of the conventional and soft-computing algorithms, with the aim of exploiting the advantages of each type and compensate of their weaknesses too. For example, ANN was used to improve the performance of P&O technique in [61]. Fuzzy logic is used to improve the performance of perturb and observe in [62] and increment of conductance in [63]. Hybrid MPPT combining PSO with P&O is proposed in several recently published works [26, 28, 60]. Since, the proposed control method contains the PSO and P&O components, these hybrid methods are described and their imperfections are highlighted. This gives a clear vision on the literature gap that this thesis aims to focus in.

2.4.1 Hybrid PSO and P&O proposed by *K. Sundareswaran et al* [60]

The algorithm proposed in [60] has a double stage of tracking. It locates the GMPP using the generic PSO. After that, a P&O algorithm is turned on to handle the small changes in the GMPP position. Although the performance demonstrated in this algorithm, there is no effort to overcome the major constraints of generic PSO reported in many research papers [7, 39], particularly its sluggishness in tracking the GMPP. Furthermore, in generic PSO, the particles share among them only the best position (G_{best}) which is a key factor in their movement. In addition to using the random numbers which slows down the tracking speed [7], most likely that one particle rescan the same region scanned before by another particle, which results in additional unnecessary iterations and increase the convergence time.

2.4.2 Hybrid PSO and P&O proposed by *K. L. Lian el al* [28]

Author in [28] proposed a hybrid method combines the P&O with the generic PSO algorithm (HPSO). During the first phase of exploration, the P&O is initialized from $0.8V_{oc}$ to track the rightmost local peak. Then, it stores the voltage of the tracked local peak as V_{LMPP}. Later in a further stage, a generic three particles PSO with w = 0.4, c_1=1.5, c_2=1.5 is initialized at the following voltages [V_{LMPP} -0.3V_{oc}, V_{LMPP} -0.15V_{oc}, V_{LMPP}] to locate the

GMPP. For validation, authors used only two simple shading patterns. Each comprises of three power peaks.

Although this hybrid method shows good tracking performance, the major constraints of generic PSO is still not properly handled, particularly its sluggishness in tracking the GMPP [7, 25, 39]. Furthermore, there is no indication that this hybrid method can work properly when subjected to a complex shading pattern, for example, *P-V* curve with more than one MHP.

After examining the HPSO by simulation, it is found that this algorithm can fails in tracking the GMPP for some partial shading cases. For instance, the HPSO fails in tracking the GMPP for the shading patterns shown in Figures 2-20 and 2-21. For the pattern of Figure 2-20, the HPSO initializes the P&O algorithm at $0.8V_{oc}$ and tracks the rightmost peak (in the first stage) and stores its corresponding voltage as V_{LMPP}. The PSO is activated to scan the voltage range [V_{LMPP} - 0.3, V_{LMPP}] in the second stage. However, in the first stage, the P&O did not converge towards the right most peak, which is the GMPP (located at $0.9V_{oc}$). Consequently, the conventional PSO scanned the incorrect voltage range and the true GMPP is missed.

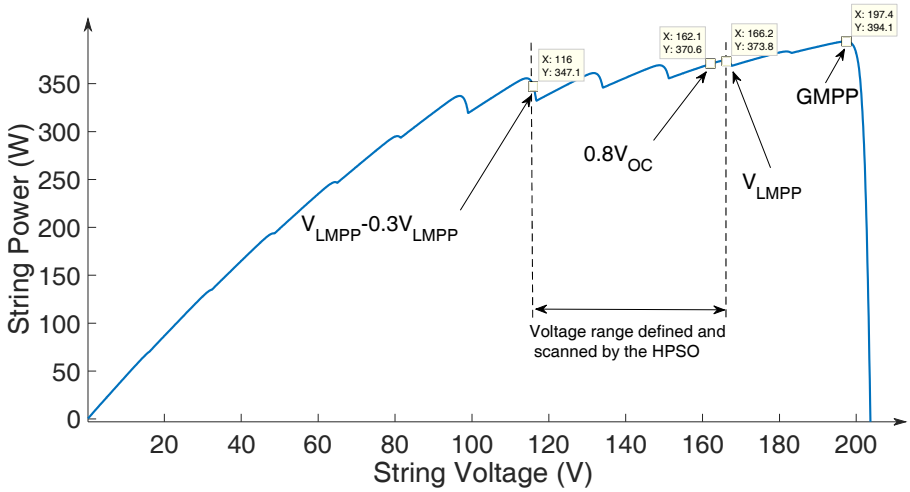

Figure 2-20: Failure of HPSO in tracking the GMPP located at the right most end of the *P-V* curve.

For the pattern of Figure 2-21, the HPSO also fails in tracking the GMPP. The identified voltage range to be scanned by the PSO, i.e., [V_{LMPP} - 0.3, V_{LMPP}], is again not the correct voltage range containing the GMPP, which is located at the left most side of the *P-V* curve. Consequently, the HPSO converged towards the LMPP, thus missing the GMPP.

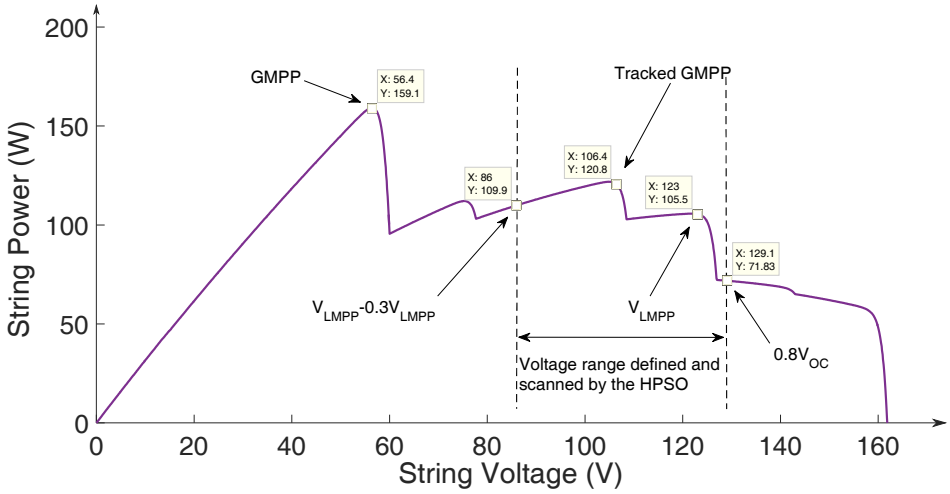

Figure 2-21: Failure of HPSO in tracking the GMPP located at the left most side of the *P-V* curve.

2.4.3 Hybrid PSO and P&O proposed by *C. Manickam et al* [26]

In *Manickam et al* [26], the partial shading occurrence is identified by observing the change in the MPP voltage. The tracked V_{LMPP} using P&O is compared to the MPP voltage under uniform irradiance. If the voltage difference between LMPPT and MPP is large, the partial shading is assumed to occur; thus, the algorithm calls the GMPPT subroutine. This latter defines analytically the voltage window at which the GMPP is expected to be inside. Then, the conventional PSO is activated to explore this voltage window and track the GMPP.

Although the search space of PSO is reduced by using a window-based search, it is uncertain if the voltage windows are always defined correctly. This is because authors of [26] formulated a general equation to calculate the lower and upper limits of the voltage windows based on the observations from only four peaks. However, it has been demonstrated in [64] that the power peaks located at the right side are right shifted towards Voc. If the shading pattern is higher than four peaks, it is very likely that the algorithm defines the wrong voltage window and, consequently, converges towards an incorrect global peak. Accordingly, the lower and upper limits of the voltage windows need to be revised carefully taking into account the issue highlighted by [64], i.e., the right shift of the LMPPs

located at the right side of the P-V curve. Furthermore, since the algorithm in [64] has been tested with only four power peaks, it is unclear if it is capable of handling the complex shading patterns that contain multiple MHP.

2.4.4 Work by *R. B. A. Koad et al* [23]

The work in [23] focused on the MPP tracking under uniform irradiance condition. The MPP area is estimated using Lagrange method after measuring four points on the *P-V* curve. Then, the generic PSO algorithm is activated using three particles near the vicinity of the MPP. The tracking speed is estimated under fast irradiance change, as well as using the EN50530 test. However, only one shading pattern (with four peaks) is used to test the algorithm. Furthermore, in case of complex shading pattern with multiple power peaks (for instance 8 peaks), the vicinity of the GMPP cannot be estimated by Lagrange using only four points in the P-V curve. In such case, the GMPP may be missed easily.

2.5 Summary

In this chapter, the most prominent MPPT methods proposed for partial shading have been reviewed. They are categorized into three major groups. First is the improved conventional MPPT. Although these MPPT methods improve the tracking efficiency and overcome the partial shading problem, they may behave slow and even fail in tracking the GMPP for some complex partial shading patterns. The second group is the Soft-Computing MPPT. These techniques scrutinize the entire search space; thus, it is very unlikely that the GMPP will be missed. However, they exhibit sluggishness in tracking the GMPP. Most of metaheuristic algorithms are suffering from the trade-off between tracking speed and the tracking accuracy (efficiency). The tracking speed can be improved by increasing the step sizes in the iteration. However, this may lead the algorithm to miss certain local maxima points and therefore traps a local maximum power point (LMPP) thus results reduction in tracking efficiency. On the other hand, reducing the step sizes in addition of using random numbers in the iteration reduces the tracking speed.

The third group is the hybrid MPPT. It is a combination of the conventional and metaheuristic approaches with the aim of exploiting the advantages of each type and overcoming their weaknesses too. Among these methods, the hybrid MPPT combining PSO and P&O are reviewed. Although these approaches demonstrated improvement in the overall tracking performance, they are still suffering due to the utilization of generic PSO. For this latter, it is very unlikely that the GMPP will be missed. However, it exhibits sluggishness in tracking the GMPP despite its effectiveness. This can be attributed to two main reasons. First, the random numbers that are embedded in the generic PSO velocity equation results in haphazard movement of the particles. If no corrective measure is taken to guide the movement, the convergence time significantly increases. For example, if a low valued random number is multiplied with the global best (G_{best}) and a high valued random number is multiplied with the personal best (P_{best}) in the velocity equation, the next iteration will direct the particle will be towards the P_{best} instead of G_{best}. In another case, if both G_{best} and P_{best} are multiplied with a lower valued random number, only a small change in the velocity is obtained; hence a small step in the particle movement. Consequently, further iterations need to be carried out. Second, there is a high possibility that a PSO particle will explore the space which has been previously scanned by other particles. This unnecessary operation is due to the lack of communication between particles, as they try to converge towards G_{best}, resulting in sluggishness in the convergence speed.

To overcome the shortcomings mentioned above, a hybrid scheme combining the PSO and P&O is proposed in this work. The main inspiration is to propose a new mechanism for the PSO particles movement and communication. The idea is to introduce a communication procedure between the PSO particles such that the regions that have been previously explored (by other particle) will not be searched again (by another particle). The hybrid structure combines 1) P&O incorporated with SSJ and 2) enhanced PSO. The PSO particles expand their scanned intervals using the P&O incorporated with SSJ. The PSO particles communicate, in addition to the (G_{best}), their scanned intervals to prevent redoing the scan process in the regions scanned previously by other particles. Furthermore, the tracking speed is not compromised due to the utilization of the SSJ mechanism in the particles movement. The former mechanism accelerates the convergence speed by avoiding scanning unnecessary regions in the *P-V* curve. The PSO scrutinized the entire search space; thus, the GMPP will not be missed. The main benefits of the proposed scheme are:

1. The unnecessary movement of particles is minimized.
2. The convergence time is reduced.
3. The GMPP tracking is guaranteed even under complex shading conditions.

CHAPTER 3

MODELING AND PRESENTATION OF THE PV SYSTEM

3.1 Introduction

Simulation performing software is a convenient way to evaluate the theoretical performance of a controller/system. The simulation conditions can be easily controlled and this allows testing a wide range of conditions in order to finally select the best solution. The PV system, which consists of a PV module, an MPP tracker and a DC load, is built in Matlab/Simulink environment. This chapter presents 1) a brief review on the PV cell modelling methods and the electrical characteristics of the equivalent circuit based-models. 2) Modeling of the buck-boost converter and proposition of an adaptive sliding mode controller of the input voltage of the converter. 3) Description of the experimental set-up used for the real tests.

3.2 Modeling of PV cells

3.2.1 Introduction

Modeling and behavioral simulation of the PV modules are still a part of the actual researches in solar energy field. The PV cell is basically a semiconductor diode whose *p-n* junction is exposed to light. Among the various modeling schemes, the artificial intelligence methods can be employed such as ANN and Neuro-Fuzzy approach [65]. However, the popular modeling approach is the equivalent electrical circuit due to its simplicity. There are two equivalent circuit models, i.e. the single-diode and two-diode model [65]. Parametric equations of these models can define the *I-V* curve for any given *G* and *T*. The shape and amplitude of the *I-V* curve, in turn, are governed by the values of the model parameters, which have to be determined.

3.2.2 The One Diode PV Model

The equivalent circuit of the one-diode model is shown in Figure 3-1. The current source simulates the photo-current (I_{PV}) which depends on the irradiance and temperature. The ideal

diode describes the cell polarization phenomena. The series resistance (R_s) is included to represent the internal cell resistance in the circuit. The shunt resistor (R_p) is included to represent losses due to the diode leakage current. The output current of the one-diode model is described by

$$I = I_{PV} - I_o\left[e^{\frac{V+IR_s}{\alpha V_T}} - 1\right] - \frac{V+IR_s}{R_p} \tag{3.1}$$

where $V_T = kT/q$ is the thermal potential, the diode current (I_D) is

$$I_D = I_o\left[e^{\frac{V+IR_s}{\alpha V_T}} - 1\right] \tag{3.2}$$

In total, the model requires the determination of five unknown parameters, i.e. I_{PV}, I_o, α, R_s, and R_p. In addition to that, the values of these parameters vary with G and T as follows

$$I_{PV} = \frac{G}{G_{STC}}\left(I_{sc,ref} + K_I\Delta T\right) \tag{3.3}$$

$$V_{oc} = V_{oc,ref} + K_V\Delta T \tag{3.4}$$

where $\Delta T = T - T_{ref}$, the subscript "*ref*" denotes the reference parameters values at STC[1].

The saturation current of the diode (I_o) is given by

$$I_o = I_{o,ref}\left(\frac{T}{T_{ref}}\right)^{\frac{3}{\alpha}} exp\left(\frac{qE_g}{\alpha k}\left(\frac{1}{T_{ref}} - \frac{1}{T}\right)\right) \tag{3.5}$$

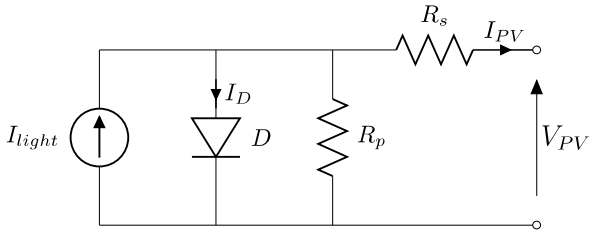

Figure 3-1: The one-diode model equivalent circuit.

[1] Standard Test Condition (STC): G = 1000 W/m^2, T = 25^{o}C.

Due to its simplicity (i.e. five parameters), the one-diode model is more popular. However, recently, the two-diode version has gained attention owing to its superior accuracy [66, 67]. The improvement is primarily due to the inclusion of an extra diode, which represents the charge recombination process that is neglected in the single-diode model [65].

3.2.3 The Two Diode PV Model

Generally, the one diode model is based on the assumption that the recombination loss in the depletion region is absent. However, the recombination represents a substantial loss that cannot be adequately modeled using a single diode. The consideration of this loss leads to a more precise model known as the two-diode model shown in Figure 3-2. This model is known to be very accurate and has been widely used by many researchers [66, 67].

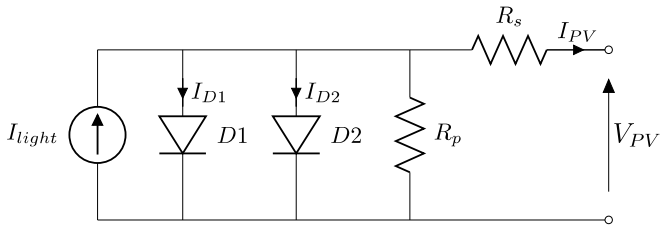

Figure 3-2: The two-diode model equivalent circuit.

The output current of the two-diode model is given by

$$I = I_{PV} - I_{o1}\left[e^{\frac{V+IR_s}{\alpha_1 V_T}} - 1\right] - I_{o2}\left[e^{\frac{V+IR_s}{\alpha_2 V_T}} - 1\right] - \frac{V+IR_s}{R_p} \tag{3.6}$$

I_{o1}, α_1 and I_{o2}, α_2 denote the saturation current, ideality factor of the first and second diode, respectively. In total, seven unknown parameters in the model are required to be determined, i.e. I_{PV}, I_{o1}, I_{o2}, α_1, α_2, R_s, and R_p.

3.2.4 Temperature Influence on *P-V* and *I-V* curves

To better illustrate the influence of the environmental conditions (G and T) on the electrical characteristics on the *P-V* module, simulation tests are carried out on a typical PV module by varying G and T. The one diode PV model is used in simulation. The main specifications of the simulated module are listed in Table 3-1. The *P-V* and *I-V* curves are plotted and discussed. Figure 3-3 shows respectively the *P-V* and *I-V* characteristics under different temperature levels between 0 and 50°C while the irradiance is kept constant at 1000 W/m^2. Figure 3-3(b) and Figure 3-3(d), represent top view of Figure 3-3(a) and Figure 3-3(c), respectively. The black dotted line represents the operating point at the MPP, i.e., maximum power P_{MPP} versus optimal voltage V_{MPP}. As observed in Figure 3-3, when the temperature rises, the PV maximum power decreases. Furthermore, open circuit voltage V_{OC} and V_{MPP} also decrease. Meanwhile, a little increase is observed in short-circuit current I_{SC}.

Table 3-1: PV module specifications.

Rated power (W)	36
MPP Current (A)	4.12
MPP Voltage, (V)	9
Short-circuit current (A)	4.38
Open-circuit voltage (V)	11.3
Number of series cells	20
Number of parallel strings	1

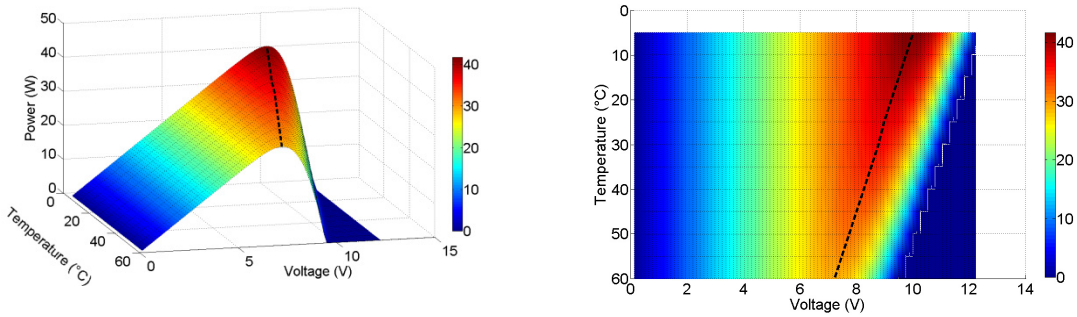

(a) (b)

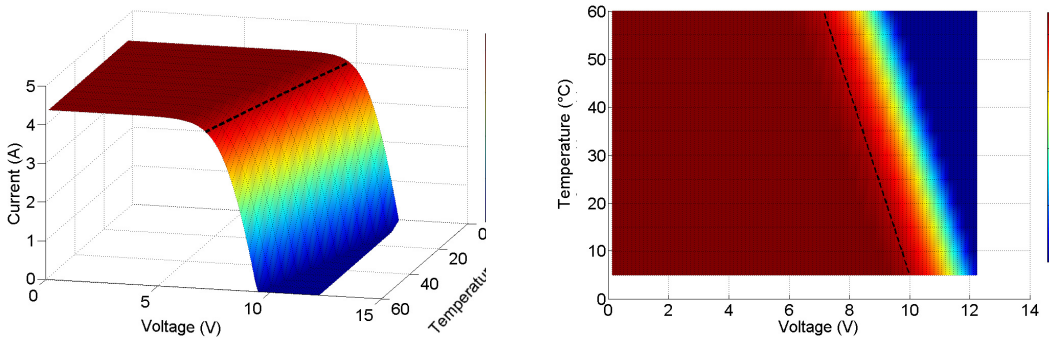

(c) (d)

Figure 3-3: Temperature effect on *P-V* and *I-V* characteristics.

3.2.5 Irradiance Influence on *P-V* and *I-V* curves

Figure 3-4 shows the electrical characteristics of the PV module under variable irradiance levels (from 0 W/m^2 to 1000 W/m^2). The temperature is fixed constant at 25 °C. When solar irradiance increases, I_{SC} and P_{MPP} increase as well. The MPP voltage V_{MPP} and open circuit voltage V_{OC} increase slightly. As shown previously, the electrical characteristics of the PV module are strongly influenced by weather conditions. *P-V* and *I-V* curves clearly exhibit nonlinear characteristics. The output power/current of PV module are depending on 1) the PV operating voltage, 2) the temperature and 3) the irradiance. The short-circuit current is directly proportional to the irradiance level, while the MPP voltage is influenced by temperature more than irradiance. Figure 3-5 shows the theoretical maximum power available with respect to changes in temperature and irradiance. It is observed that the maximum power is directly proportional to the irradiance and inversely proportional to the temperature. It is also observed that the irradiance level has a significant effect on the maximum power compared to the temperature. Hence, the maximum power available is depending on the irradiance more than the temperature.

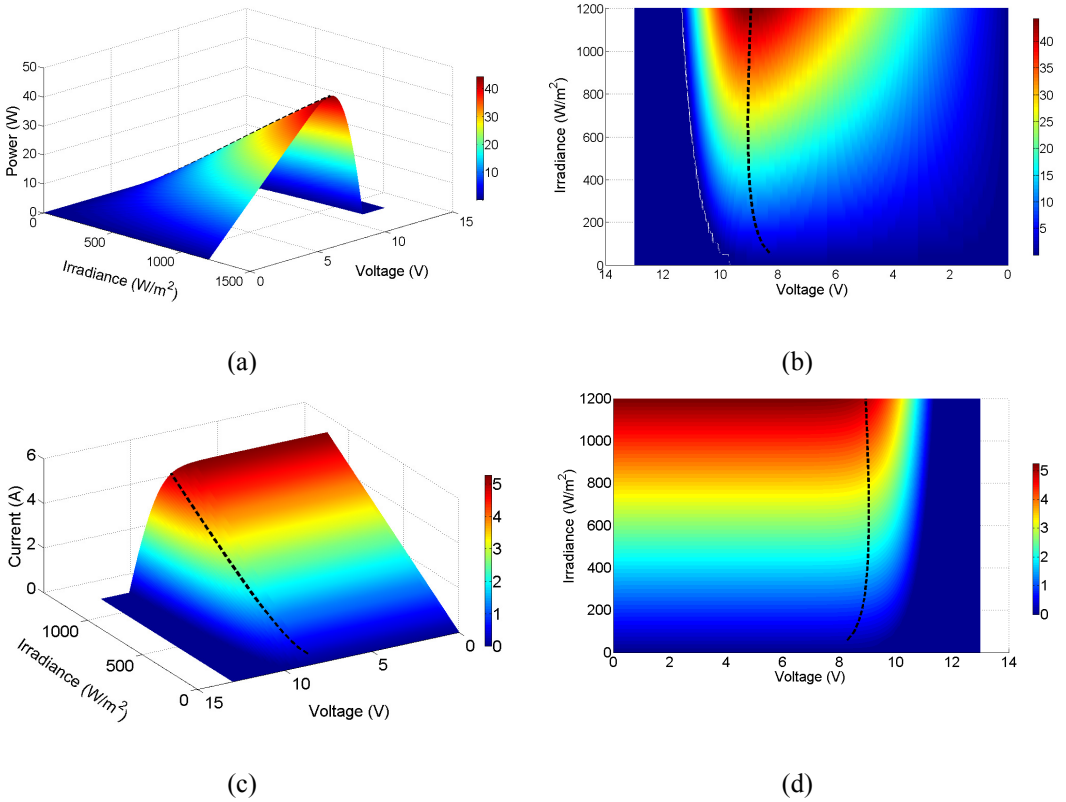

Figure 3-4: Irradiance effect on *P-V* and *I-V* characteristics.

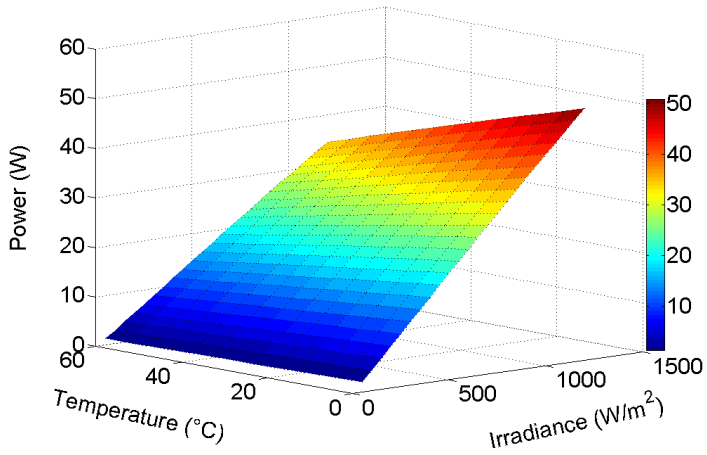

Figure 3-5: Maximum power according to changes in environmental conditions.

3.2.6 Overview of Parameters Estimation Methods used in Cell Modeling

The model parameters, when used in conjunction with the datasheet information, describes the electrical characteristics of the PV module. Therefore, the main objective of PV module modelling is to ensure that the *I-V* curves obtained by using the computed parameters closely match the measured curves provided by the manufacturer. Recently, the two-diode model has gained attention owing to its superior accuracy compared to the one-diode model. However, it increases the complexities and consequently the computational burden because of the seven parameters to be determined. Due to the presence of two exponential terms and the implicit equations, obtaining the solution for these seven parameters is very challenging. The main challenge is to estimate the accurate values of these parameters while maintaining a reasonable computational effort. The parameters are normally solved in two ways: the numerical extraction or the analytical method.

In the numerical extraction, a point-by-point fitting of the computed *I-V* values to the experimental dataset is carried out using certain mathematical algorithms. By defining an objective function, the model parameters are extracted by minimizing the error between the two [66, 68]. Despite its accuracy, the approach inherits several drawbacks. First, to do the comparison, it is mandatory that the entire experimental *I- V* dataset is available. However, this information is not always given in the module datasheets; hence, the application of the numerical extraction approach is highly situational. Second, due to the point-by-point comparison, the execution speed is very slow. This is especially true when evolutionary algorithm (EA) is utilized to optimize the curve fitting [69].

The analytical approach computes the model parameters by solving a system of equations, derived from several key points of the *I-V* curve. These points, namely the short circuit current (I_{SC}, 0), maximum power point (I_{MPP}, V_{MPP}), open circuit voltage (0, V_{oc}), temperature coefficients for short circuit current (K_i) and open circuit voltage (K_v), are commonly available in the standard datasheet. Since there is no need to analyze the entire *I-V* curve, the number of iteration is much less, leading to much faster computation. Considering speed is an important factor for simulation, the analytical method is more practical. Despite this merit, the approach always involves certain simplifications on the two-diode model. This is inevitable due to the insufficient number of equations to independently determine the seven lumped parameters. Although these approximations simplify the

computation, the solutions are compromised and at times, unrealistic approximations that cannot be physically justified are considered.

With the recent popularity of soft-computing, a new approach—known as the hybrid method is proposed to compute the model parameters. As the name suggests, it incorporates both analytical and soft-computing numerical extraction approaches. The analytical equations are employed to relate certain parameters to the variation of *G* and *T*, while the soft-computing technique is used for optimization. This approach improved significantly the accurateness and the computational speed as argued by [67, 70].

3.3 Modeling and Control of the Buck-boost Converter

3.3.1 Modeling of the Buck-boost Converter

The power electronic converter is an essential part of the PV system. It plays the role of adaptation stage between the PV module and the load. The DC/DC buck-boost converter is selected due to its ability to regulate the PV output voltage on a wide load voltage range. PV output voltage can be either greater or less than load voltage. The schematic diagram of the power converter is depicted in Figure 3-6.

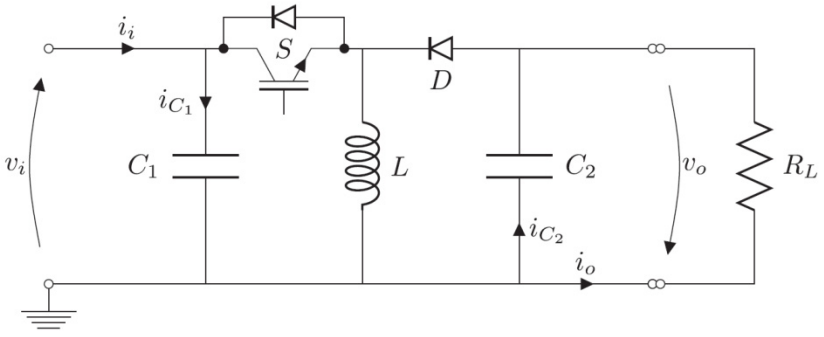

Figure 3-6: Schematic diagram of buck-boost converter.

By controlling the duty cycle, the operating point is adjusted to match the MPP in order to extract the maximum power available. The power flow is controlled by varying the duty cycle α of the switching period T_d. According to the state of the switch S, the converter operation may be subdivided in two operating states:

• S=1; t ∈ [0, αT_d]: During the On-State, the diode is reverse biased. The energy is stored in the inductance L. Applying Kirchhoff's law for each mesh in the circuit; the model of the power converter is given by the following equations:

$$\begin{cases} i_{C_1}(t) = C_1 \dfrac{dv_i(t)}{dt} = i_i(t) - i_L(t) \\ i_{C_2}(t) = C_2 \dfrac{dv_o(t)}{dt} = -i_o(t) \\ v_L(t) = L \dfrac{di_L(t)}{dt} = v_i(t) \end{cases} \tag{3.7}$$

• S=0; t ∈ [αTd, T_d]: During the Off-State, the diode D is forward biased. The stored energy is transferred from L to the capacity C_2.

$$\begin{cases} i_{C_1}(t) = C_1 \dfrac{dv_i(t)}{dt} = i_i(t) \\ i_{C_2}(t) = C_2 \dfrac{dv_o(t)}{dt} = i_L(t) - i_o(t) \\ v_L = L \dfrac{di_L(t)}{dt} = -v_o(t) \end{cases} \tag{3.8}$$

The converter model is represented by Eq (3.7) in the ON-State and by (3.8) in the OFF-State. Using (3.7) and (3.8), the average model of the converter can be written as

$$\begin{cases} C_1 \dfrac{dv_i(t)}{dt} = i_i(t) - \alpha i_L(t) \\ C_2 \dfrac{dv_o(t)}{dt} = (1-\alpha) i_L(t) - i_o(t) \\ L \dfrac{di_L(t)}{dt} = \alpha . v_i - (1-\alpha) v_o \end{cases} \tag{3.9}$$

When the converter operates in steady-state regime, the average value of $i_{C1}(t)$, $i_{C2}(t)$ and $v_L(t)$ become zero; accordingly, the following equations are obtained

$$\begin{cases} I_i - \alpha I_L = 0 \\ (1-\alpha) I_L - I_o = 0 \\ \alpha V_i - (1-\alpha) V_o = 0 \end{cases} \tag{3.10}$$

while I_i, I_L, I_o, V_i and V_o are respectively the average values during one switching period of $i_i(t)$, $i_L(t)$, $i_o(t)$, $v_i(t)$ and $v_o(t)$. Therefore, using the expression (3.10), the voltage conversion ratio of the converter can be written as follows

$$G_v = \frac{V_o}{V_i} = \frac{\alpha}{1-\alpha} \tag{3.11}$$

Figure 3-7 shows variation of the voltage conversion ratio G_v versus duty cycle.

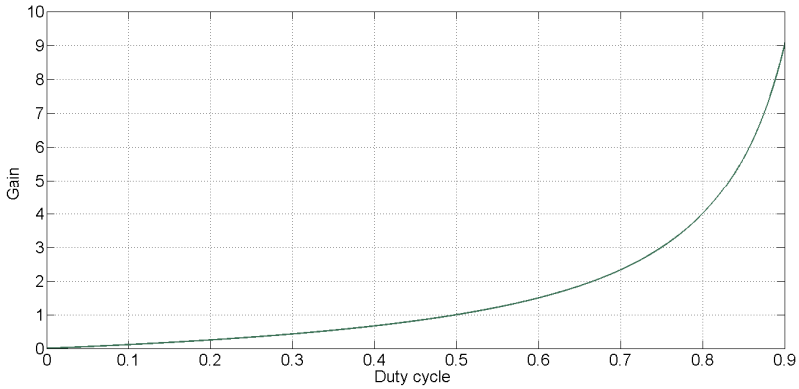

Figure 3-7: Voltage conversion ration versus duty cycle.

3.3.2 Control of the Buck-boost Converter

The aim of MPPT in PV systems is to ensure that maximum power is extracted from the PV module at any environmental condition. The proposed MPPT control structures in the literature can be divided into two categories: direct and indirect control method. The direct method is widely used in the literature. The control structure is characterized by direct computation of the duty cycle from the MPPT algorithm. This scheme reduces the computation time and simplifies the tracking structure [7]. However, it makes the operating point at the MPP sensible to the environmental condition and the load disturbance as shall be

discussed in the next section. To avoid such limitations, the indirect method which embeds a voltage controller in the MPPT tends to be more efficient.

Proposition of Sliding Mode Controller with adaptive switching gain:

Integrating a robust voltage controller can improve the overall performance of the MPPT. The sliding mode control is a powerful technique characterized by its speed and robustness against losses and parametric changes. In this section, a controller for the input voltage of the Buck-boost converter is proposed. The controller is based on sliding mode control with adaptive gain to reduce the chattering effect [71]. The average model of the Buck-boost shown in (3.9) is used for developing the controller. It can be rewritten as follows

$$\begin{cases} \dot{x}_1 = \dfrac{a_1}{a_2} - \dfrac{x_3}{a_2}u \\ \dot{x}_2 = \dfrac{x_3}{a_3} - \dfrac{a_4}{a_3} - \dfrac{x_3}{a_3}u \\ \dot{x}_3 = -\dfrac{x_2}{a_5} + \dfrac{x_1}{a_5}u + \dfrac{x_2}{a_5}u \end{cases} \tag{3.12}$$

where system states x_1, x_2 and x_3 are $v_i(t)$, $v_o(t)$ and $i_L(t)$, respectively. The variables $i_i(t)$ and $i_o(t)$ are considered constants; so the system parameters are as follows: $a_1 = i_i(t)$, $a_4 = i_o(t)$, $a_2 = C_1$, $a_3 = C_2$ and $a_5 = L$.

The objective is to develop a control law for α, denoted by $u(t)$, to annul the tracking error $e(t)$, which is defined by

$$e(t) = x_1 - x_{1,ref} \tag{3.13}$$

where $x_{1,ref}$ is the reference voltage. Consider the surface of Slotine and Li given by

$$S = (\lambda + \frac{d}{dt})^{n-1} e(t) \tag{3.14}$$

where λ is positive constant and n is the order of the system. Since $n=1$, therefore $S(t)=e(t)$. The process of sliding mode control can be divided into two phases: reaching phase and sliding phase. Therefore, two types of control laws are derived separately: the hitting control, denoted by u_{hit}, to force error $e(t)$ to lie on the sliding surface in the reaching phase. Then, the

equivalent control, denoted by u_{eq}, to move the error along the sliding surface to the origin. The global input control to be determined is

$$u(t) = u_{eq} + u_{hit} \tag{3.15}$$

Once the sliding surface has been selected, a necessary condition to remain the tracking error into the sliding surface is obtained by deriving Eq (3.11)

$$\dot{S} = 0 \tag{3.16}$$

By Assuming that $\dot{x}_{1,ref}$ =0 and substituting (3.12) in (3.16), the u_{eq} can be obtained as follows

$$u_{eq} = \frac{a_1}{x_3} \tag{3.17}$$

Since the converter is designed to operate at the continuous conduction mode (CCM), it is guaranteed that x_3 will never become zero. In the reaching phase, the existence of the sliding mode is guaranteed in the sense of the Lyapunov stability theory. The hitting control must be designed to provide convergence towards the sliding surface. For this purpose, a positive definite Lyapunov candidate function can be chosen as

$$V_1 = \frac{1}{2} S(t)^2 \tag{3.18}$$

To prove the global asymptotic stability of $S(t)$, $\dot{V}_1$ has to be a semi-definite negative function. Therefore, the reachability condition in (12) should be fulfilled

$$\dot{V}_1 = S\dot{S} < 0, S \neq 0. \tag{3.19}$$

For this reason $\dot{S}$ is selected as follows

$$\dot{S} = -k.sgn(S) \tag{3.20}$$

Using (3.12), (3.15) and (3.17), u_{hit} can be calculated as follows

$$u_{hit} = \frac{a_2}{x_3} k.\mathrm{sgn}(S(t)) \tag{3.21}$$

Thus, the final expression of $u(t)$ can be written as

$$u(t) = \frac{a_1}{x_3} + \frac{a_2}{x_3} k.\mathrm{sgn}(S(t)) \tag{3.22}$$

The final form of the expression of the duty cycle α can be given by

$$\alpha = \frac{i_i(t)}{i_L(t)} - + k \frac{C_1}{i_L(t)} sgn(v_i(t) - v_{i,ref}(t)) \tag{3.23}$$

To reduce the chattering effect, signum function is replaced with hyperbolic tangent function. Furthermore, an adaptation law for the switching gains is developed. Let's assume that for a given switching gain k, the reachability condition is satisfied. The gain to be estimated $\hat{k}$ is given by

$$\hat{k} = k - \tilde{k} \tag{3.24}$$

$\tilde{k}$ is the estimation error which shall be zeroed. Therefore, a Lyapunov candidate function is defined

$$V_1 = \frac{1}{2} S^2 + \frac{1}{2\gamma} \tilde{k}^2 \tag{3.25}$$

where γ defines the learning coefficients. By substituting (3.24) in the derivative of (3.25) and after simplification, the adaptation law for $\hat{k}$ is obtained as follows

$$\hat{k} = \int \gamma |S| .dt \tag{3.26}$$

3.4 Description of the Set-up used for the Experimental Validation

The proposed MPPT is verified experimentally using an in-house PV array simulator (PVAS) [72]. The PVAS emulates the electrical behavior of a PV array by utilizing dc voltage controlled-current sources. The latter is characterized by the *I-V* curve of a specific shading pattern. The algorithm is implemented on a low power (250 W) buck-boost converter with the following specifications: L=1 mH, C_1=470 µF and C_2=220 µF. Its output drives the ITECH IT 8816B dc electronic load. The switches are driven by PWM at switching frequency (f) of 50 kHz. The MPPT codes are programmed into the dSPACE DS1104 controller board, which is built around the TMS320F240 DSP [73]. The overall

experimental set-up is shown in Figure 3-8 while the power electronics devices used are depicted in Figure 3-9.

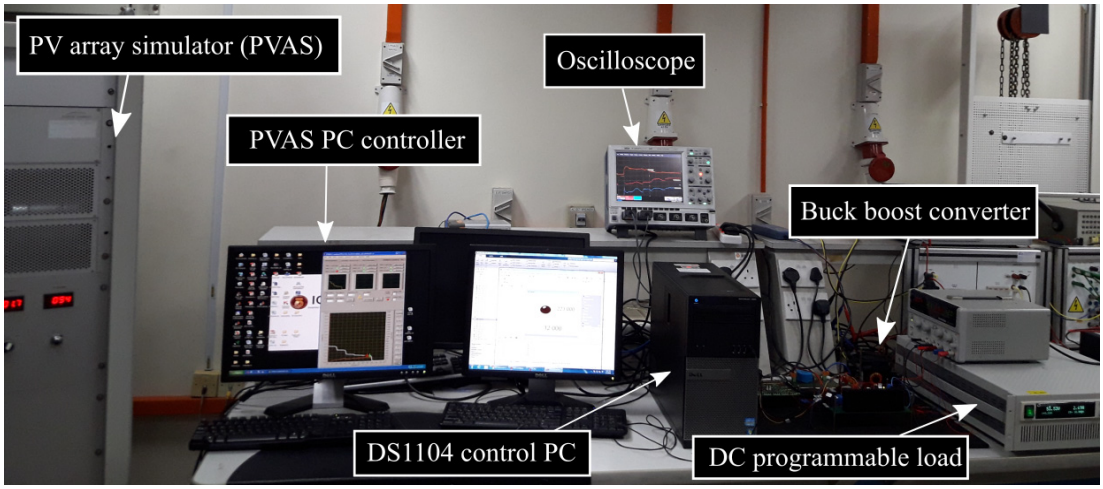

Figure 3-8: Set-up used for the Experimental Validation

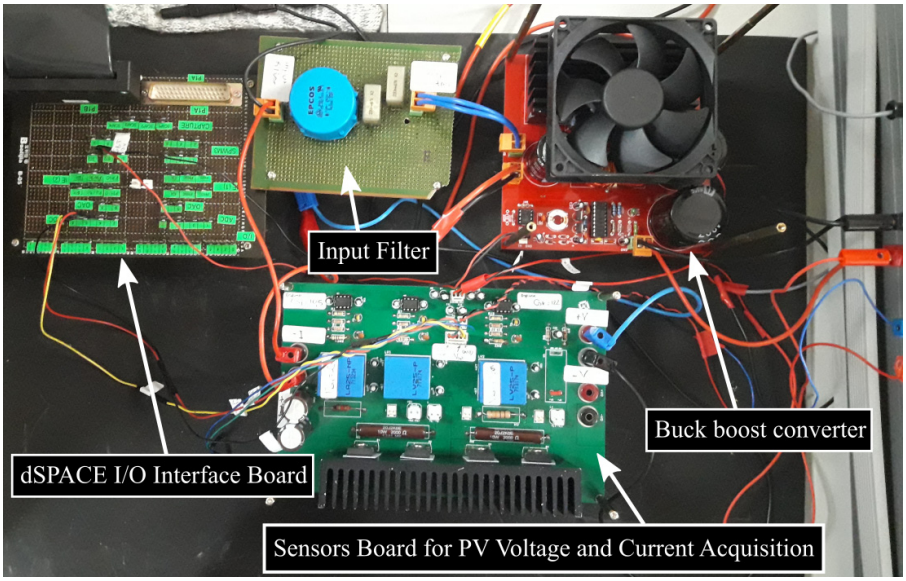

Figure 3-9: Power electronics device used in the experimental set-up.

The tool chain used is Matlab/Simulink/Stateflow from the MathWorks Inc for the controller development and TargetLink from dSPACE GmbH for the code generation. To produce highly efficient C code in the target hardware, the modelling guidelines for production code using TargetLink [74] are taken into consideration during the controller development phase. Afterwards, the developed controller is revised using Simulink Model Advisor to meet with the MAAB (MathWorks Automotive Advisory Board) guidelines [75] before the implementation phase. The MPPT controller is depicted in Figure 3-10. It is a

model-based controller built under Simulink/Stateflow environment then loaded to the dSPACE board. The controller comprises of a filtering unit (for signal conditioning), the MPPT algorithm and a voltage controller. The feedback signals are obtained from the LV25-P (voltage) and LA25-NP (current) sensors. These signals are conditioned using a first order discrete filter. In the voltage control loop, a digital PI controller is used to matches the reference voltage that emerges from the MPPT algorithm. The sampling time is 20 ms.

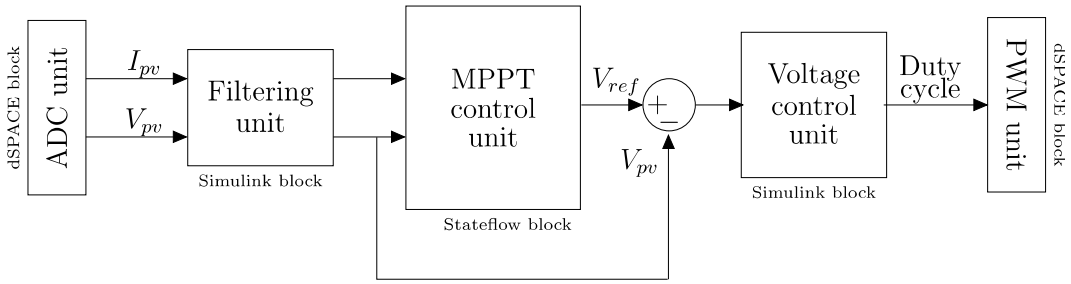

Figure 3-10: Diagram of the (Simulink mobel)-based MPPT controller loaded to the DSP.

3.5 Summary

In this chapter, the material used thoroughly in this thesis have been described. Modeling of the PV cell and the buck-boost is presented. Thereafter, an adaptive sliding mode controller of the input voltage of the converter, which will be used in the rest of the thesis, is proposed. Finally, the set-up used for the experimental validation is described.

CHAPTER 4

PERFORMANCE ASSESSMENT OF DIRECT AND INDIRECT CONTROL METHODS

4.1 Introduction

One of the important consideration for MPPT designers of PV system is the choice of an appropriate control method in conjunction with the MPPT algorithm. Typically, the MPPT is implemented using either one of the two methods. First is the direct control; in literature it is also known as the duty cycle based MPPT. In this configuration, the MPPT computes the duty cycle (D) and directly transmits this value to the dc-dc converter. There is no additional process, i.e. another control loop in between the MPPT block and the converter. In other words, the MPPT algorithm itself decides the optimum duty cycle (D_{MPP}) so that the system achieves the maximum power point (MPP). The second approach is the indirect control, also known as the voltage based MPPT. Here, the MPPT only generates a reference voltage (V_{ref}); then a voltage controller is designed to adjust D so that the converter input voltage (V_{PV}) follows the former. Figure 4-1 shows the general block diagram of the direct and indirect MPPT control for a general converter.

Structural-wise, the direct method is simpler than its counterpart because the MPPT updates D without an intermediate operator. However, since the direct method is based on the power versus duty cycle (P-D) characteristic, the value of D_{MPP} can vary widely with respect to the changes in G. This is because a small change in G forces D_{MPP} (in the P-D curve) to shift its position significantly. In addition to that, the direct method exhibits considerable transient fluctuations when the load varies. The problem can be traced to the fact that the P-D curve is dependent on the converter topology and thus is sensitive to the load variation [76, 77]. This situation is crucial for stand-alone PV system, where the converter is directly connected to the load. It is also equally important for grid-connected system because the load variation is reflected as a disturbances at the dc link. This in turn deviates the PV voltage from V_{MPP} [78]. On the other hand, the indirect method is characterized by the P-V curve. It is less affected by the rapid fluctuations in G due to the fact that the V_{MPP} is restricted within a much narrower boundary, compared to D_{MPP}. Consequently, a change in G results a smaller variation in V_{MPP}. Furthermore, since the P-V curve depends only on G and T, the V_{MPP} is not influenced by the converter topology. Thus, if any change in the load or any disturbance in the dc link takes place, V_{MPP} remains almost constant as the voltage controller forces the operating point to be near the vicinity of V_{MPP}. This allows for a more efficient tracking during load variation.

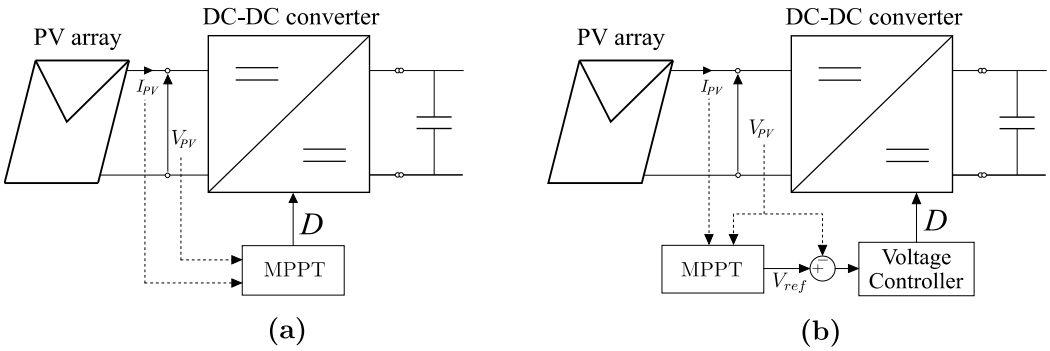

Figure 4-1: DC-DC converter connected to PV array. (a) Direct (duty cycle–based) control structure. (b) Indirect (voltage-based) control structure.

The simpler control structure is the obvious reason why numerous researchers, for example [7, 15, 16, 20, 22, 24, 26, 27, 40, 77, 79, 80] preferred the direct method. This is in contrast to the indirect control, in which a voltage controller, such as a PI or a PID is required [14, 19, 29, 35, 37, 81-83]. However, apart from the simplicity, the proponents of the direct method did not provide other justification for their choice. None has considered the influence of converter topology, load changes and rapid change in G on the tracking performance. Only authors in [76] are aware of the fact that the direct control is inferior in handling the load variation. Accordingly, they proposed a modified version of incremental conductance to reduce the power loss due to the inefficient tracking. Similarly, the proponents of the indirect method did not clarify their reasons too. They only commented on its general advantages, without providing any evidence on the underlying principles that make it superior to the direct method.

Thus far, there is no definitive effort to evaluate and compare both controllers in systematic manner [84, 85]. Based on this literature gap, an attempt is made in this chapter to objectively assess the performance of both control methods by computing the MPPT efficiency during the steady state oscillation, under rapid changes in the irradiance and in presence of load disturbances. A comprehensive analysis is provided to show the variation of the D_{MPP} position (in P-D curve) with respect to changes in both of irradiance and load value. For convenience, the controllers are used in conjunction with perturb and observe (P&O). The choice is deliberate—considering the fact that P&O is the most widely used MPPT for uniform insolation as well as partial shading conditions. The analysis is verified by MATLAB/Simulink simulation and validated by experimental work using the same parameters and the same tests scenario. It is envisaged that this work will be able to provide a useful insight on the conclusive choice of the appropriate control structure for MPPT controller design.

4.2 Analysis of (PV-Converter) System Characteristics

To show the dependency of the duty cycle under varying irradiance and load, the combined characteristics of the PV module and its dc-dc converter are analyzed. The general system is shown in Figure 4-2. The string comprises of three series-connected MSX60 [25] PV modules with the specifications shown in Table 4-1. The dc-dc converter block represents the three basic converter topologies, i.e. the buck-boost, buck and boost converter connected to a variable resistive load.

Table 4-1: The MSX60 PV module Specifications.

Short Circuit current (I_{SC})	3.8 A
Open circuit voltage (V_{OC})	21.1 V
Current at P_{MPPT} (I_{MPPT})	3.5 A
Voltage at P_{MPPT} (V_{MPPT})	17.1 V
Maximum power (P_{MPPT})	59.85 W
Temperature coefficient of V_{OC} (K_V)	-0.08 V/ºC
Temperature coefficient of I_{SC} (K_I)	$3e^{-3}$ A/ºC
Number of cell in series per module	36

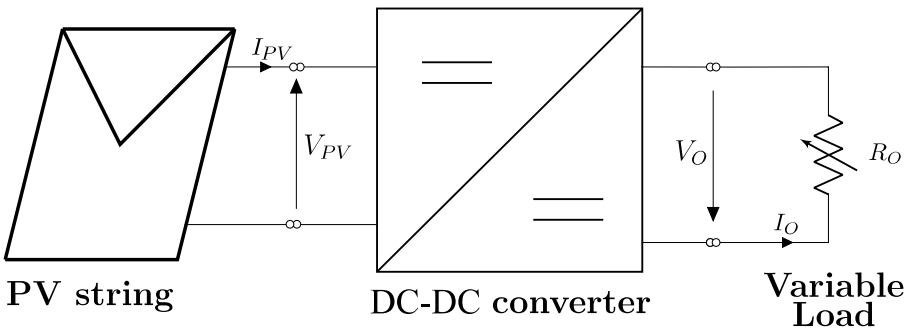

Figure 4-2: Typical PV-converter system used for the analysis.

4.2.1 Effects of Irradiance

The combined electrical characteristics of the module and the converter can be established by deriving the relationship between V_{PV} and D. Neglecting the effect of parasitic resistor, the input-output gain transfer of a buck-boost converter at steady state is given as

$$V_O = \frac{D}{1-D} V_{PV} \tag{4.1}$$

$$I_{PV} = \frac{D}{1-D} I_O \tag{4.2}$$

Since $V_O=R_O I_O$, the equation that represents the load line seen by the PV generator can be written as

$$I_{PV} = \frac{1}{R_O}\left(\frac{D}{1-D}\right)^2 V_{PV} \tag{4.3}$$

Using similar derivation, for buck converter

$$I_{PV} = \frac{D^2}{R_O} V_{PV} \tag{4.4}$$

while for boost converter,

$$I_{PV} = \frac{1}{R_O}\left(\frac{1}{1-D}\right)^2 V_{PV} \tag{4.5}$$

Consider the ideal one-diode PV model equation given by [65]

$$\begin{aligned} I_{PV} &= I_{SC} - I_0\left[\exp\left(\frac{V}{\alpha V_T}\right) - 1\right] \\ I_{PV} &= I_{SC} - I_0\left[\exp\left(\frac{V_{PV}}{\alpha V_T}\right) - 1\right] \end{aligned} \tag{4.6}$$

where V_T is the thermal potential, I_{SC} is the short circuit photo-current, I_0 is the saturation current and α denotes the ideality factor of the diode. Replacing (4.6) in (4.3), the combined equation for the PV-buck-boost system can be written as

$$I_{SC} - I_0\left[\exp\left(\frac{V_{PV}}{\alpha V_T}\right) - 1\right] - \left(\frac{D}{1-D}\right)^2 \frac{V_{PV}}{R_O} = 0 \tag{4.7}$$

Similarly, replacing (4.6) in (4.4) for the PV-buck system,

$$I_{SC} - I_0\left[\exp\left(\frac{V_{PV}}{\alpha V_T}\right)\right] - \frac{D^2}{R_O}V_{PV} = 0 \tag{4.8}$$

and replacing (4.6) in (4.5) for the PV-boost system

$$I_{SC} - I_0\left[\exp\left(\frac{V_{PV}}{\alpha V_T}\right)\right] - \frac{1}{R_O\left(1-D\right)^2}V_{PV} = 0 \tag{4.9}$$

Figure 4-3 illustrated power, voltage and duty cycle characteristics of the PV system using the three converter topologies. The G level is varied, while R_O is fixed at 25 Ω. Note that, the change in T is not considered because its variation is much slower than G; consequently, its effect on the MPP tracking is almost negligible. Thus, T is fixed at STC, i.e. 25°C. From the duty cycle characteristics, it can be observed that the *P-D* and *V-D* curves vary from one topology to another. Furthermore, for PV-buck and PV-boost systems, there exist "non-operational" regions, where the theoretical value of D_{MPP} is beyond unity or less than zero, respectively. For example, for G = 800 and 1000 W/m^2, the MPP for the PV-buck system is located at $D_{MPP} > 1$. Similarly, for the PV-boost system, for G = 100, 300 and 500 W/m^2, $D_{MPP} < 0$. In practice, this condition is impossible to achieve and thus the converter cannot operate at these points. On the other hand, for the PV-buck-boost system, the MPP always lies within $0 < D_{MPP} < 1$. This indicates the suitability of buck-boost for MPPT implementation.

Another important observation is the fact that the MPP position in the *P-D* curve shifts significantly with respect to G. This is in contrast to the *P-V* curve, where the shift of V_{MPP} is more restricted. For example, for the PV-buck-boost, as G is varied from 100 to 1000 W/m^2, the V_{MPP} is confined within a narrow range [48V to 55V], i.e. approximately 11% of the global voltage span [0 to 63V]. This range is indicated in the *P-V* curve shown in Figure 4-3(a). For its corresponding *P-D* curve shown in Figure 4-3(c), the D_{MPP} is spread over a wider range [0.3 to 0.52], i.e. or 32% from the global duty cycle span [0 to 1]. As shall be shown later, the larger variation in D_{MPP} with respect to G makes the direct method more sensitive to the changes in the irradiance.

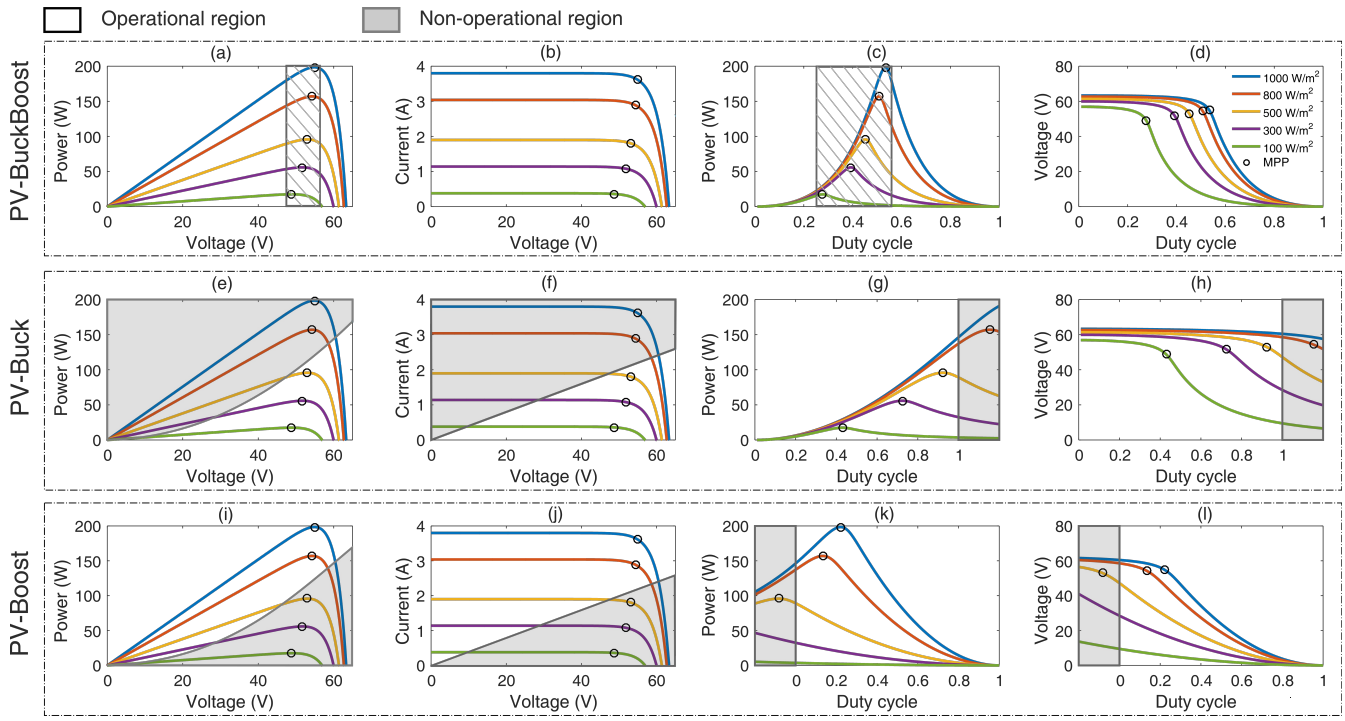

Figure 4-3: Electrical characteristics under multiple irradiance values and fixed load value at 25Ω. The *P-V* and *I-V* characteristics are shown in Figure 4-3 (a) and (b), (e) and (f), (i) and (j), for the PV-buck-boost, PV-buck, PV-boost system, respectively. The *P-D* and *V-D* characteristics at different irradiance levels are shown in Figure 4-3 (c) and (d), (g) and (h), (k) and (l), for the PV-buck-boost, PV-buck, PV-boost system, respectively.

4.2.2 Effects of Load

Returning to (4.3), the equivalent resistance (R_{PV}) seen by the array can be written as

$$R_{PV} = R_O\left(\frac{1-D}{D}\right)^2 \tag{4.10}$$

For a PV system, the operating point is defined as the point at which the load line intersects the *I-V* curve. Eq (4.10) indicates that for a particular value of D, R_{PV} is indeed the slope of the load line. In the direct control, the MPPT role is to adjust this load line by manipulating D. Furthermore, Eq (4.10) indicates that the load line also depends on R_O. Therefore, when a sudden change in R_O occurs, the load line alters its trajectory. In addition, the load line shifting reflects an entire change of the *P-D* curve. Thus, it will take a certain amount of time for the MPPT to track the new MPP.

To better illustrate this scenario, (4.7), (4.8) and (4.9) are revisited and the *P-D* characteristics for PV-buck-boost, PV-buck and PV-boost system are plotted as in Figure 4-4(a), (b) and (c), respectively. In each case, the load is varied from 20 to 100 Ω, while *G* is fixed at 300 W/m^2. For the buck-boost shown in Figure 4-4(a), the MPP moves to the right as R_O increases. Clearly, it is always possible to operate the converter at the MPP regardless of the R_O value. On the other hand, for the buck, when R_O > 60 Ω, the MPP enters the non-operational region, as observed in Figure 4-4(b). A similar situation can be seen for the PV-boost when R_O < 40 Ω, as illustrated by Figure 4-4(c).

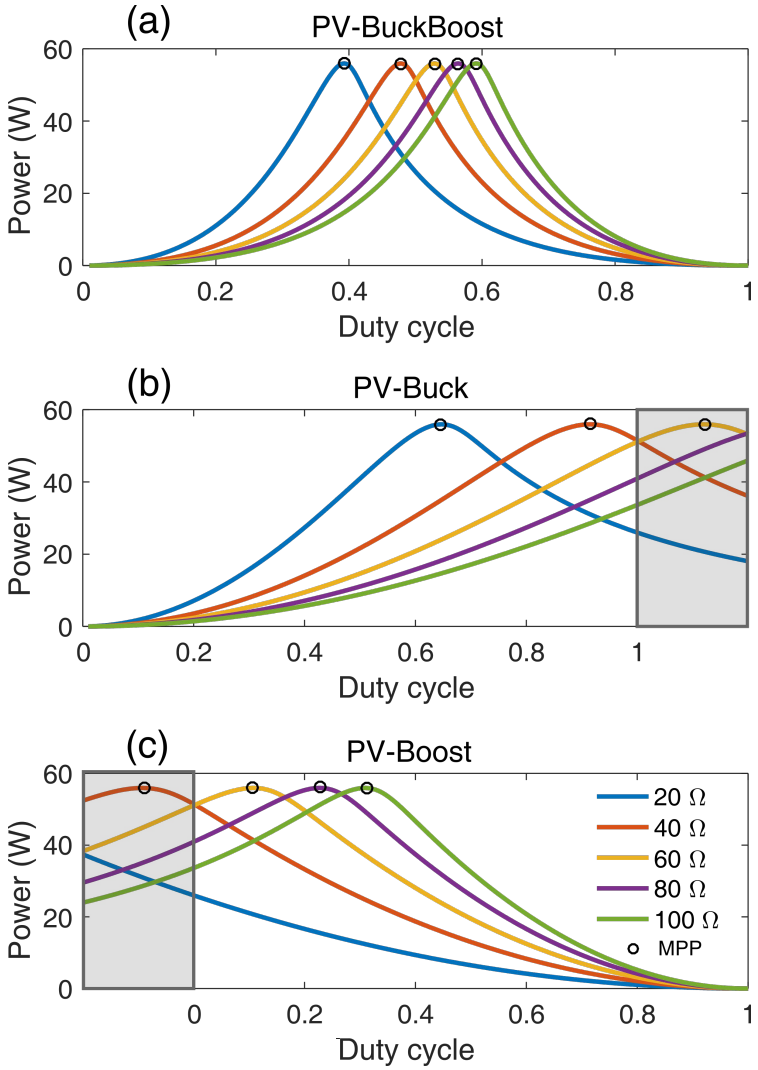

Figure 4-4: *P-D* characteristics at 300 W/m^2 at different R_O values: (a) PV-buck-boost (b) PV-buck and (c) PV-boost system.

4.3 Performance Evaluation of Both Control Methods

The standard P&O MPPT is chosen to evaluate the performance of the control methods. Due to the presence of non-operational regions for PV-buck and PV-boost, only the PV-buck-boost system is considered for implementation. For consistency, the parameters used in the model of Figure 4-2 are retained. The flowcharts of the P&O for direct and indirect control are shown in Figure 4-5(a) and (b), respectively. For the former, the operating point is adjusted by periodically updating the reference duty cycle (D_{ref}). On the other hand, for the latter, the P&O computes the reference voltage (V_{ref}) and the voltage controller adjusts D to ensure PV output voltage matches V_{ref}. The change in power (ΔP) and voltage (ΔV) at each perturbation is calculated as follows

$$\Delta P = P_{act} - P_{pre}$$
$$\Delta V = V_{act} - V_{pre} \tag{4.11}$$

where P_{act} and V_{act} are the actual measured output power and voltage of the string, respectively. Similarly, P_{pre} and V_{pre} denote the previous value for power and voltage. The perturbation in duty cycle and voltage for the direct and indirect control are, respectively, given as

$$D_{ref} = D_{ref} - \Phi_D \times sign(\Delta P.\Delta V) \tag{4.12}$$

$$V_{ref} = V_{ref} + \Phi_V \times sign(\Delta P.\Delta V) \tag{4.13}$$

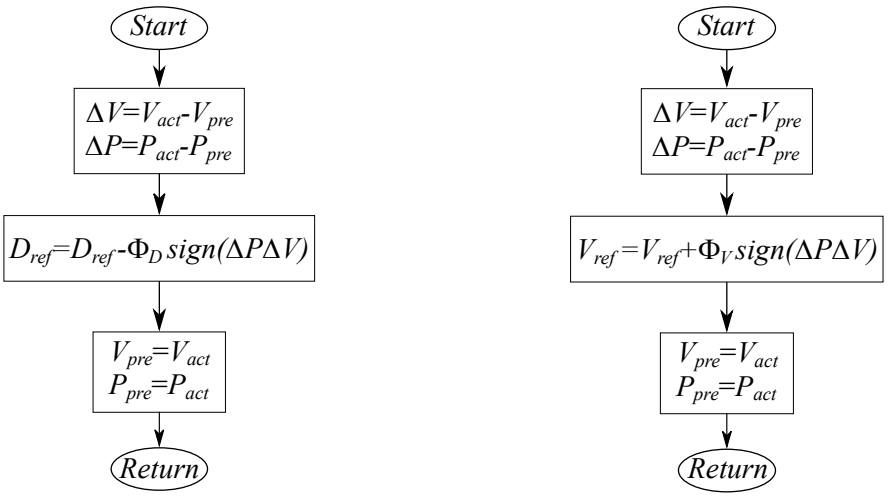

Figure 4-5: The P&O flowchart. (a) Direct and (b) Indirect methods used in conjunction with the buck-boost converter.

For a fair assessment, the duty cycle perturbation Φ_D (for the direct control) should be chosen carefully, so that the resulting voltage variation is equivalent to the voltage perturbation Φ_V (for the indirect method). Figure 4-6 shows the transfer *V-D* curve for the PV-buck-boost system. As can be seen, the function between D and V_{PV} is not linear. The voltage variation with respect to Φ_D is negligible when D is near the extremes (i.e. 0 and 1). However, it is significant at the MPP region (i.e. when D is at the vicinity of 0.52). Therefore, Φ_D should be selected by taking into account the tradeoff between the significant voltage variation at the vicinity of the MPP and the negligible voltage variation at the extremities of the *V-D* curve. To do this, the area around MPP in the *V-D* curve is linearized within the interval $0.2 < D < 0.9$, as shown in Figure 4-6.

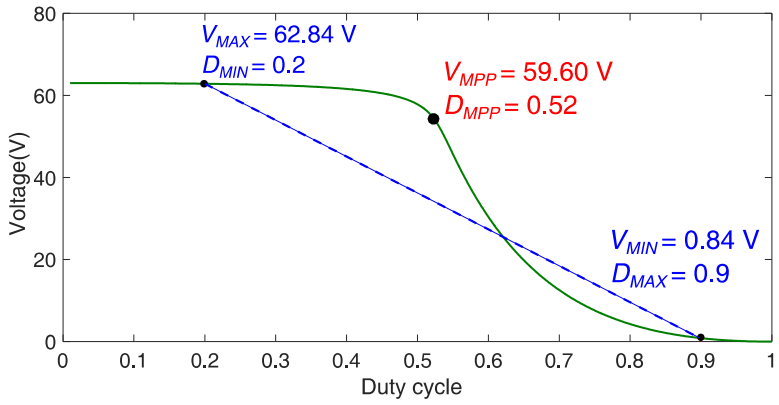

Figure 4-6: The linearized *V-D* curve of the PV buck-boost system: G=900 W/m^2 and R_O = 50 Ω.

Thus, the lower and upper boundaries of the linearized *V-D* curve are fixed to D_{MIN} = 0.2 and D_{MAX} = 0.9, respectively. Correspondingly, the lower and upper boundaries of the PV voltage are V_{MAX}=62.84 V and V_{MIN}=0.84 V, as depicted in Figure 4-6. Assuming Φ_V is set to be 2% of V_{oc} (which is typical for P&O) [29], its value is 1.3 V (for V_{oc}=63 V). Therefore, the number of operating points (n_{pts}) within [V_{MIN}, V_{MAX}] can be computed as

$$n_{pts} = \frac{V_{MAX} - V_{MIN}}{\Phi_V} \tag{4.14}$$

Using (4.14), the voltage range [V_{MIN}, V_{MAX}] in the *P-V* curve can be segmented to n_{pts} = 47 possible operating point. Correspondingly, for the direct method, the number of operating points within [D_{MIN}, D_{MAX}] must be the same i.e. 47. Thus, Φ_D is deduced as follows

$$\Phi_D = \frac{D_{MAX} - D_{MIN}}{n_{pts}} \tag{4.15}$$

4.3.1 Description of the Simulation Model

Both control structures are investigated by MATLAB/ Simulink simulation and experiment. The simulation model is shown in Figure 4-7(a). The array comprises three series connected MSX60 modules [86], feeding a buck-boost converter with a variable R_O. The converter is designed for continuous conduction mode with the following specifications: inductor (L) =1 mH, capacitors: C_1=470 μF, C_2=220 μF. The PWM switching frequency (f) is set to 50 kHz. Figure 4-7(b) and (c) show the block diagram of the direct and indirect control structures, respectively. The latter is a cascaded structure where the outer loop (MPPT) is slower than the inner loop (PI controller) [87].

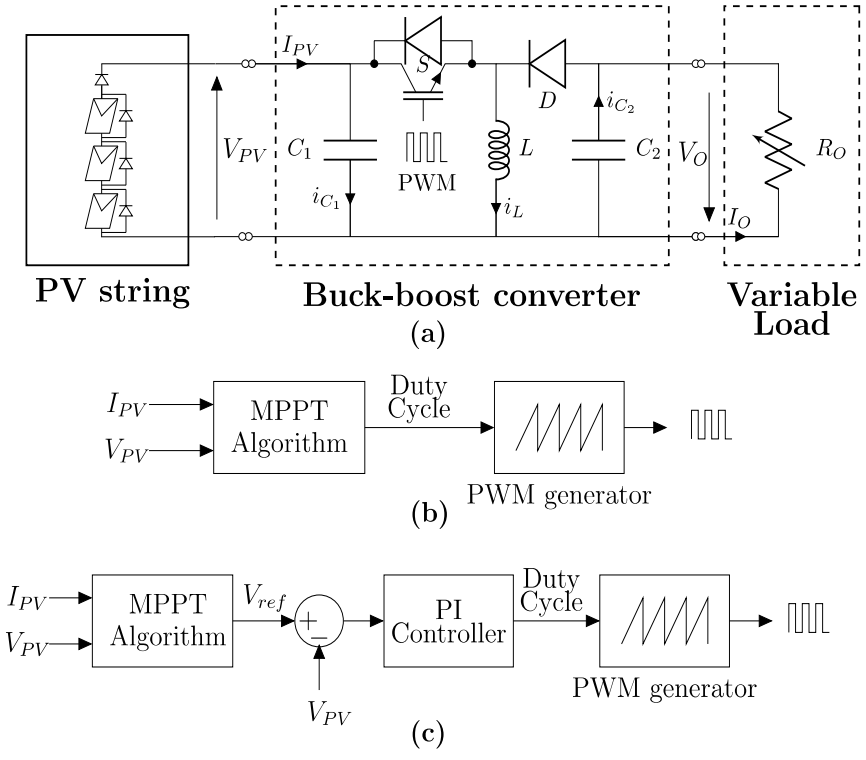

Figure 4-7: (a) The simulation model. Block diagram of [(b) direct, (c) indirect] control method.

4.4 Comparative Assessments

To assess the performances of the controllers, the MPPT efficiency at steady state and transient are computed. For the transient efficiency, the evaluation is done under fast irradiance changes and load disturbances. The efficiency (η) is calculated using

$$\eta = \frac{\int_{T_i}^{T_f}(P(t))dt}{\int_{T_i}^{T_f}(P_{max}(t))dt} \times 100 \tag{4.16}$$

where T_i and T_f are the lower and upper interval considered for the efficiency computation.

4.4.1 Steady-state Efficiency

In P&O, the drop in steady state efficiency is caused by the oscillation of the operating point as it moves forward and backward around the MPP. For this test, both control methods are analysed at G= 900 W/m^2 and T=25ºC. The resulting voltage (*I-V, P-V*) and duty cycle (*V-D, P-D*) characteristic curves are shown in Figure 4-8(a) and (b), respectively.

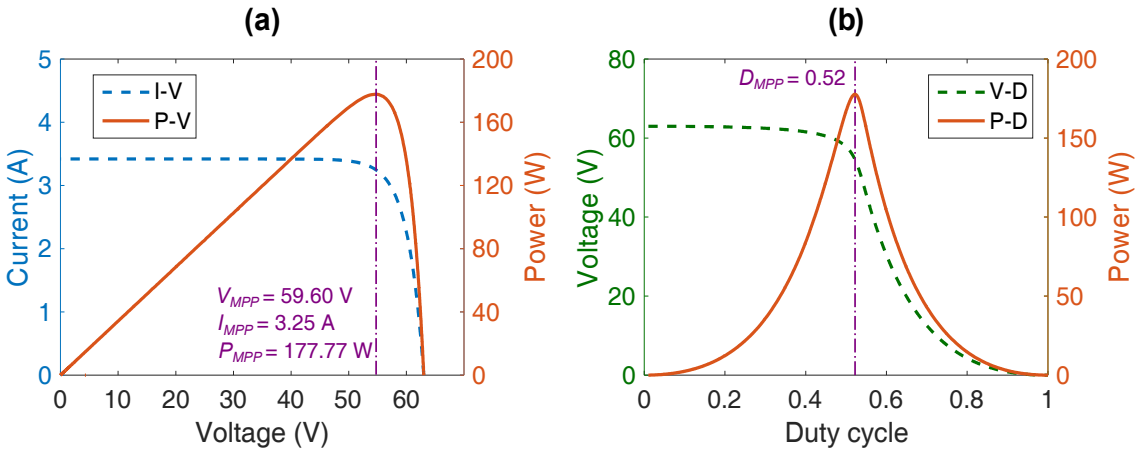

Figure 4-8: (a) *P-V, I-V* curve of the PV string and (b) *P-D*, *V-D* curve of the string at G= 900 W/m^2.

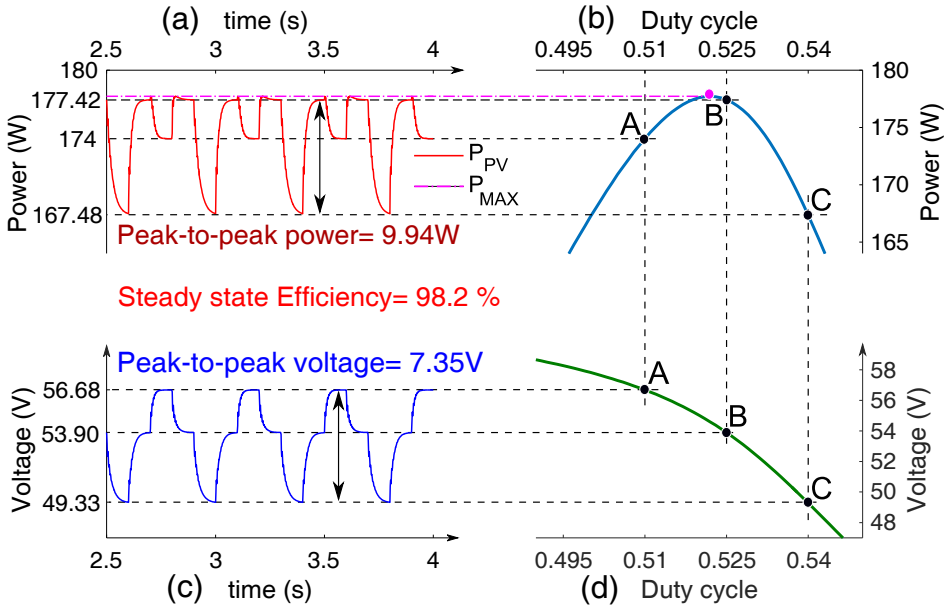

Figure 4-9: Steady state oscillation around the MPP using the direct control structure. (a) Power versus time. (b) PV power versus PV voltage. (c) Voltage versus time. (d) PV voltage versus duty cycle.

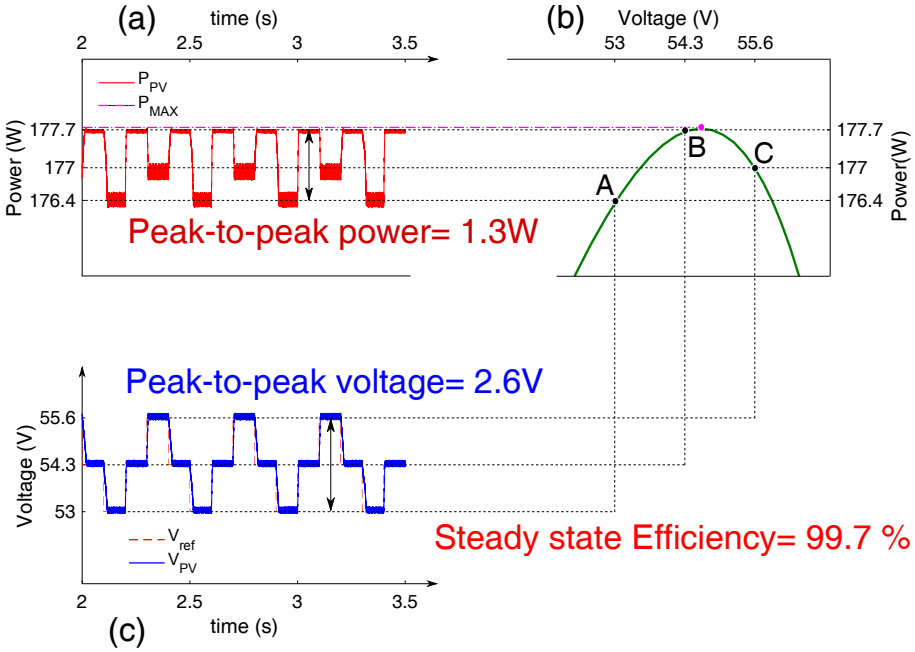

Figure 4-10: Steady state oscillation around the MPP using the indirect control structure. (a) Power versus time. (b) PV power versus duty cycle. (c) Voltage versus time.

For clarity, the time and duty cycle profiles (around MPP) of the direct method are enlarged, as shown in Figure 4-9. As can be seen from the *P-V* curve in Figure 4-9(b), the operating point oscillates around three distinct points, i.e. A (56.7 V), B (53.9 V) and C (49.3

V). Note that the duty cycle perturbation (Φ_D) between points A and B (written as AB) and BC is the same. However, from Figure 4-9(c), the corresponding voltage perturbation (Φ_V) is not. The absolute difference in voltage between AB is 2.7 V, while for BC is 7.3 V. Correspondingly, the peak-to-peak power oscillation between AB and BC is 3.4 W and 9.9 W, respectively. The drop-in voltage at point C results in significant drop in power, as seen in Figure 4-9(a)—thus contributing to the power loss at steady state. By integrating the waveform in Figure 4-9(a) using Eq (4.16) over 16 s time interval, the resulting η is 98.2%. Figure 4-10 shows the zoomed portion of the oscillation for the indirect method. From Figure 4-10(b), the operating point oscillates around A (53.0 V), B (53.3 V) and C (54.6 V). The voltage controller ensures the PV voltage operation at different V_{ref} updated by the MPPT algorithm. Since the voltage perturbation is equally spaced (Φ_V=1.3 V), the absolute difference between AB and BC equals 1.3 V. From Figure 4-10(a), the corresponding absolute power difference for AB is 1.3 W, while for BC is 0.7 W. Using Eq (16), η is 99.7%.

For experimental verification, the *P-V* and *I-V* curves in simulation of Figure 4-8(a) are loaded into the PVAS. The oscillograms obtained for both direct and indirect method are illustrated in Figure 4-11 and 4-12, respectively. For the former, the voltage and power oscillation is 8 V and 11 W, respectively. On the other hand, for the indirect method, the voltage oscillation is recorded as 3 V, while the power oscillation is 3 W. For comparison, the simulation and experimental results are shown in Table 4-2. In general, they match quite well. The most likely source for the difference between the simulation and experimental measurements is the noisy signals and wiring loss in the hardware.

For efficiency calculation, the measured signals are analysed by the PVAS post-processing software. The algorithm logged the voltage and current values at every sampling instant. Then, the data is integrated over a number of cycles. Despite this slight difference between the simulated and experimental efficiency, it is clear that the indirect control method is superior at steady state.

Table 4-2: Steady state Efficiency.

	Power Oscillation (W)		Voltage Oscillation (V)		Steady State Efficiency (%)	
	Direct method	Indirect method	Direct method	Indirect method	Direct method	Indirect method
Simulation	10.0	1.3	7.4	2.6	98.20	99.70
Experiment	11.0	3.0	8.0	3	97.79	99.24

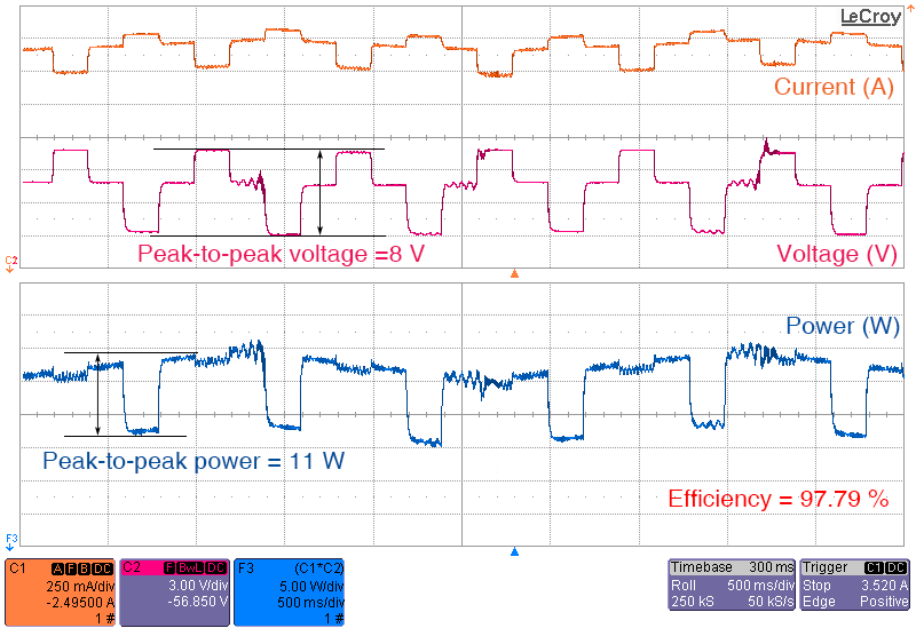

Figure 4-11: Experimental waveforms of the steady state oscillation using the direct control method.

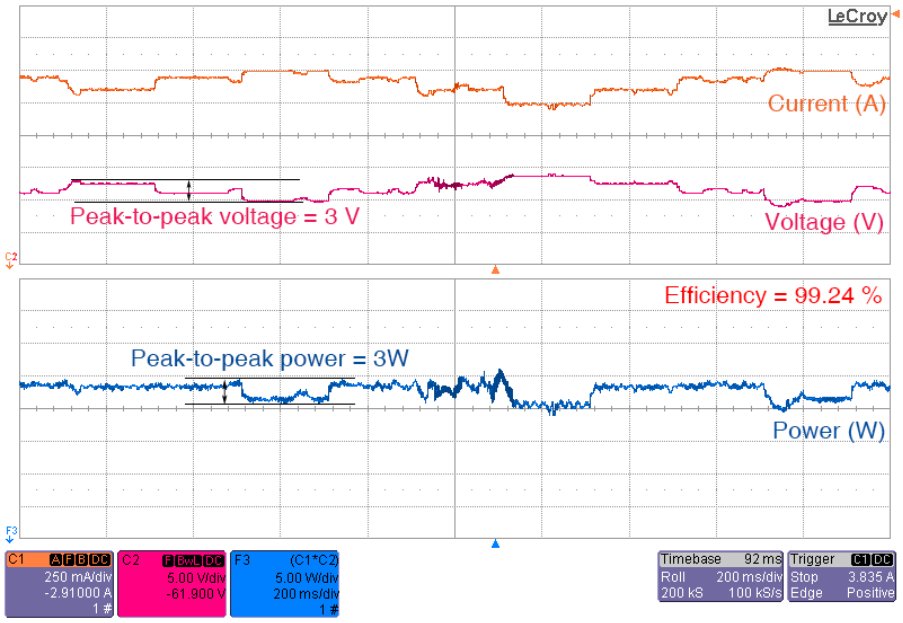

Figure 4-12: Experimental waveforms of the steady state oscillation using the indirect control method.

4.4.2 Step Change in Irradiance

When *G* changes rapidly with time, the P&O tends to diverge from the tracking locus [29, 77, 82]. For these cases, the MPPT tests are based on the EN 50530 dynamic efficiency [88], with a maximum irradiance change of 100 W/m^2/s. However, due to the utilization of PV in applications such as car mounted PV and wearable technology (backpack PV), the systems could be subjected to very rapid irradiance change, i.e. up to 100 W/m^2/ms [89]. For that reason, the MPPT performance is tested under very fast irradiance change, i.e. step waveform.

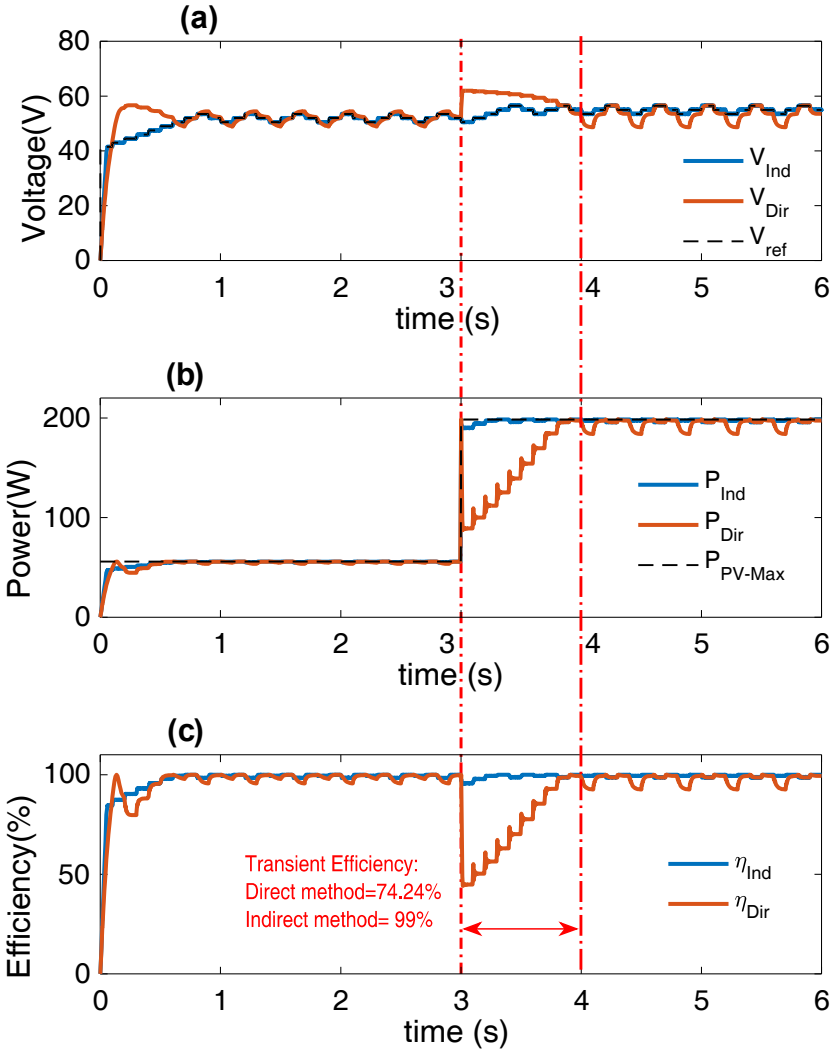

Figure 4-13: Tracking performance of both control structures in case of step change in the irradiance value at t=3s (From 300 W/m^2 to 1000 W/m^2). (a) PV voltage versus time. (b) PV power versus time. (c) Instantaneous efficiencies for both methods.

In this test, the initial G is set to 300 W/m^2. Then, at 3 s, it is stepped to 1000 W/m^2. Simulation in Figure 4-13(b) shows that the direct method results in the divergence, i.e. the MPPT is not able to track fast rising slope. On the other hand, for the indirect method, the operating point remains at MPP despite the step change in G. It follows the tracking locus almost perfectly. The direct method requires eight duty cycle perturbations (Φ_D) before it recovers to MPP; the sluggishness results in the loss of transient efficiency, as shown in Figure 4-13(c). Its computed average transient efficiency is 74%. For the indirect control, it is 99%.

The reason for the divergence of the direct method can be clarified from the magnified P-D and P-V curves shown Figure 4-14. Prior to the step change, G =300W/m^2, the system operates at MPP1. When the step change to 1000 W/m^2 takes place at t = 3 s, the operating point shifted to point A on the V-D and P-D curve, as seen in Figure 4-14(b) and (d), respectively. Consequently, the MPPT algorithm needs to perform eight successive Φ_D perturbations in order to reach the new MPP (MPP2). In other words, in the process of climbing to MPP, it takes eight increments of duty cycle, i.e. $D_{MPP2}=D_{MPP1}+8\Phi_D$. This can be observed in Figure 4-14(a) and (c), respectively. During the transition from D_{MPP1} to D_{MPP2}, power is lost.

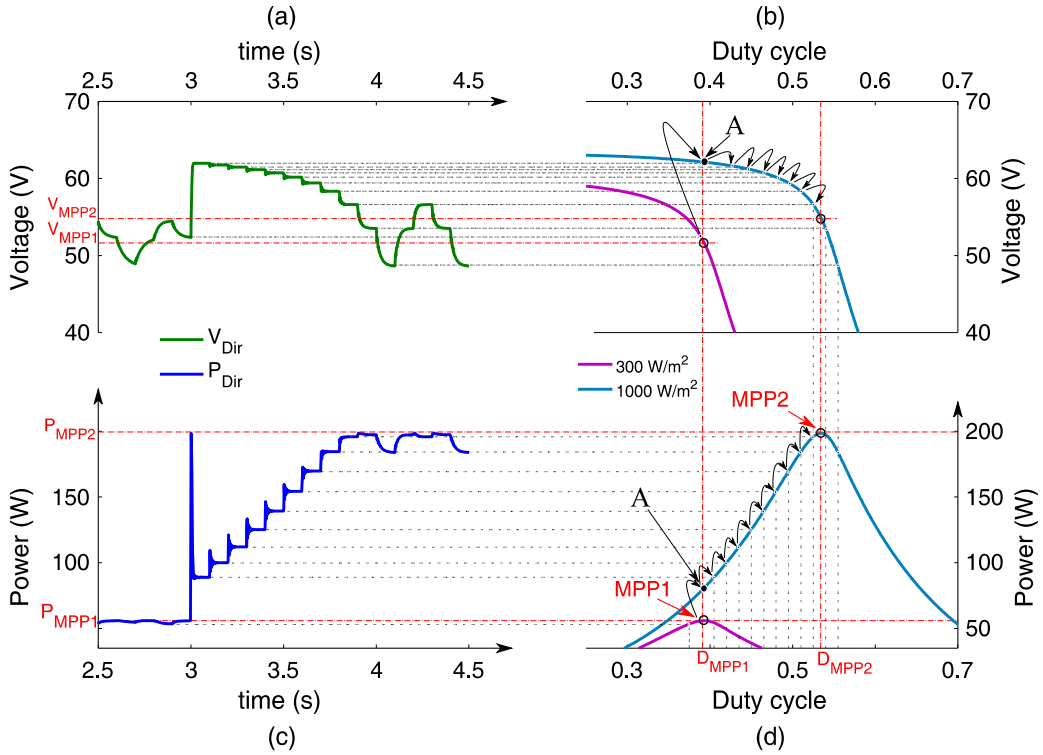

Figure 4-14: Transient explanation in case of rapid change in the irradiance using the direct method. (a) Voltage versus time. (b) Voltage versus duty cycle. (c) Power versus

time. (d) Power versus duty cycle.

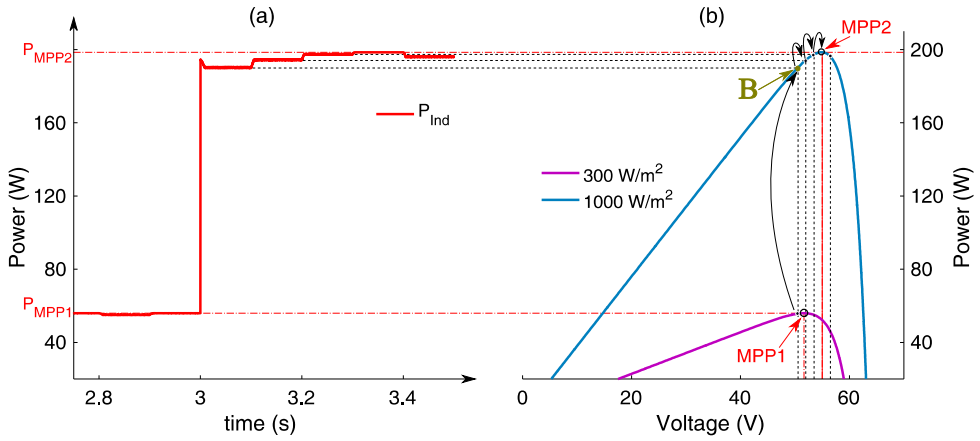

Figure 4-15: Only 2 perturbations are needed to reach MPP2 when the irradiance is changed. (a) PV power versus time. (b) PV power versus voltage.

On the other hand, for the indirect method, when G changes from 300 to 1000 W/m^2, the operating point on the P-V curve shifts from MPP1 to point B, as shown in Figure 4-15(b). However, unlike the case of the direct method, point B is located near MPP2; in this case, only two voltage perturbations ($2\Phi_V$) are needed to reach MPP2. This explains the rapid MPP tracking seen in Figure 4-15(a).

To validate this finding, an experiment is carried out using the same environmental test condition used in simulation. Using the PVAS, the irradiance step change is triggered at t = 3 s. The resulting waveforms for the direct and indirect control methods are presented in Figure 4-16 and 4-17, respectively. It can be observed that the direct method requires 2 s to re-track the new MPP. On the contrary, the indirect method is significantly faster, i.e. 400 ms. Accordingly, the measured transient efficiency is from 64% and 94.6%, respectively. The superiority of the indirect method during transients is numerically summarized in Table 4-3.

Table 4-3: Transient Efficiency under Rapid Change in G.

	Transient Efficiency (%)		**Transient Time (ms)**	
	Direct	Indirect	Direct	Indirect
Simulation	74.24	99.00	1000	200
Experiment	63.93	94.62	2000	400

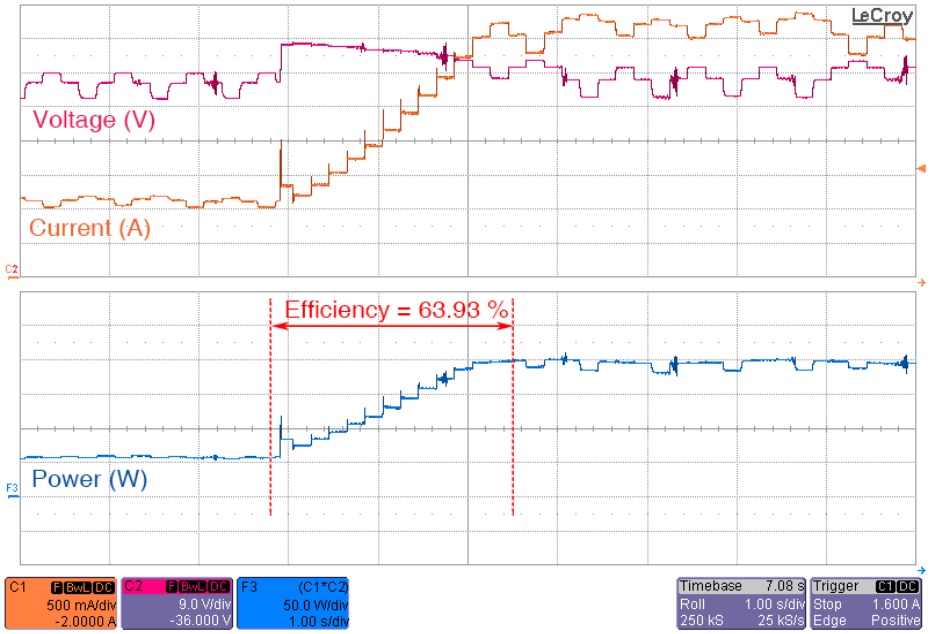

Figure 4-16: Experimental waveforms for the direct method when subjected to a step change in the irradiance at t = 3 s.

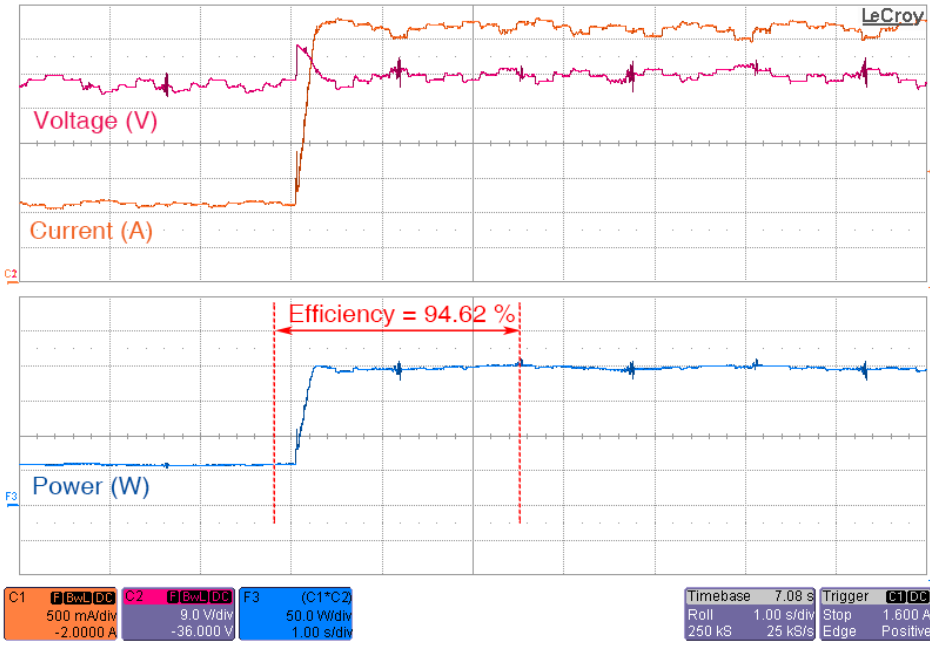

Figure 4-17: Experimental waveforms of the indirect method when subjected to a step change in the irradiance at t = 3 s.

4.4.3 Step Change in Load

To analyze the effect of load variations on the MPPT, a step change in R_O (from 20Ω to 80Ω) is introduced at t = 3 s. The response of the direct and indirect control methods are shown in Figure 4-18(a) and (b), respectively. During the transient, the efficiency of the former drops to 67%. On the other hand, the efficiency of the indirect method remains considerable, i.e. 99.7%.

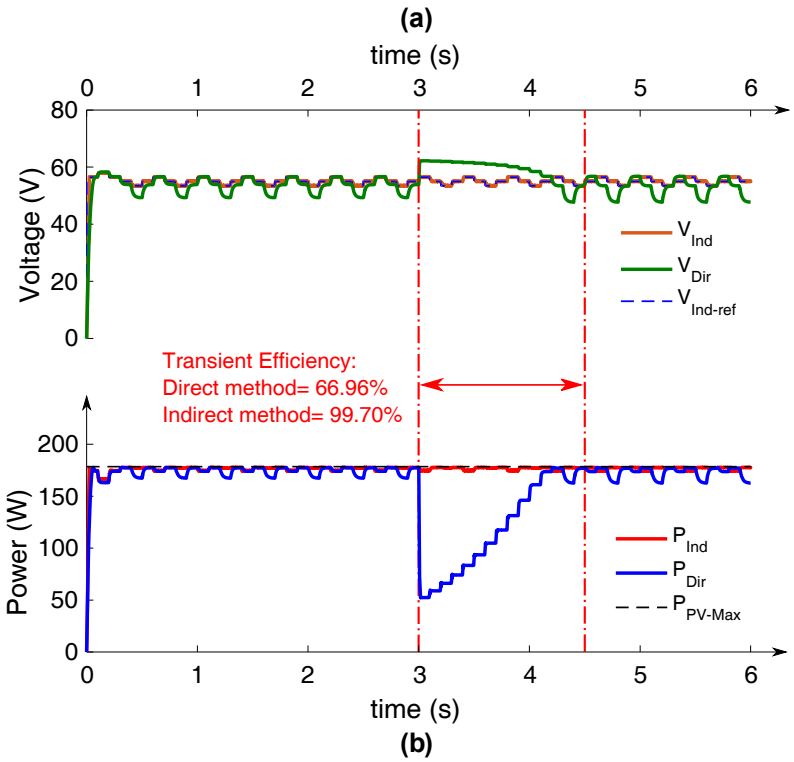

Figure 4-18: Tracking performance of both control methods in case of step change in R_O at t=3 s (From 20 Ω to 80 Ω). (a) PV voltage versus time. (b) PV power versus time.

To understand the reason for the large drop in the efficiency of the direct method, the transient portion of Figure 4-18 (2.5 < t < 4.5 s) is enlarged as in Figure 4-19(a) and (d). When a sudden change in R_O takes place, the *I-D* curve suddenly migrated from the dashed to solid lines, as observed in Figure 4-19(c). Further, the slope of the load line changes suddenly from *load line* 1 to *load line* 2 in the *I-V* curve. This is illustrated in Figure 4-19(b). As a result, the operating point on the *P-V* curve shifts from MPP to point C, as shown in Figure 4-19(e). By virtue of the P&O algorithm, the operating point starts to climb towards MPP again. To achieve this, the duty cycle needs to be updated from D_1 to D_2 as illustrated

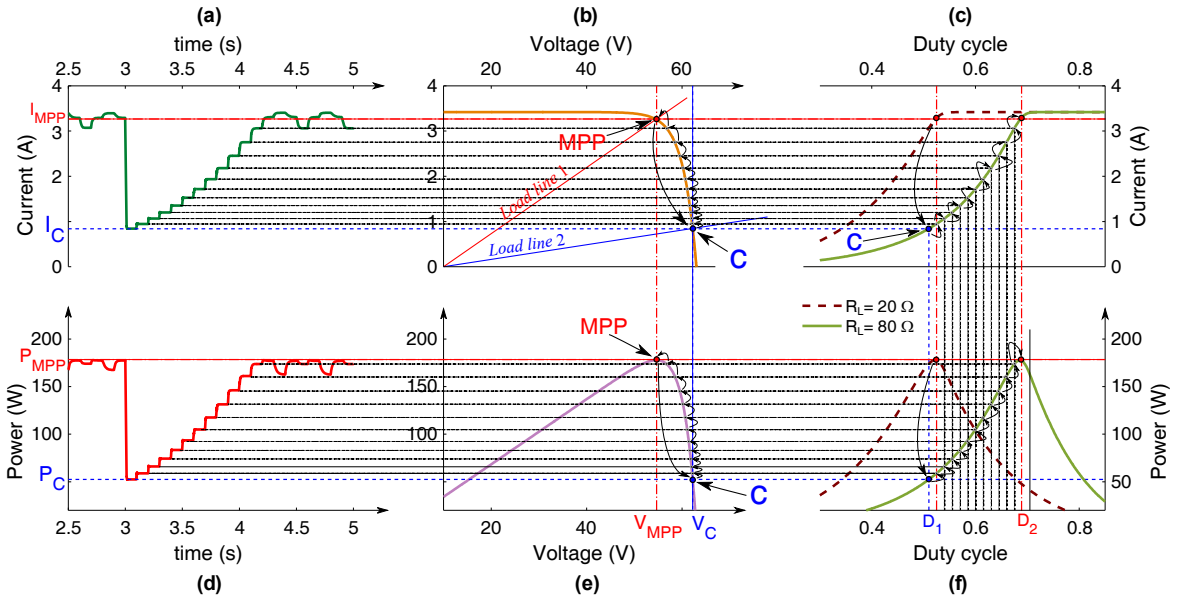

Figure 4-19: Transient analysis of the direct method. (a) PV current versus time. (b) *I-V* characteristics: operating point shifted from MPP to C when a sudden change in the load has occurred. (c) *I-D* characteristic changed due to the load change and the MPPT resumes the tracking from point C in the new *I-D* curve. (d) PV power versus time. (e) Constant *P-V* characteristics: operating point shifted from MPP to C when a sudden change in the load has occurred. (f) *P-D* characteristic changed due to the load change and the MPPT resumes the tracking from point C in the new *P-D* curve.

by the *P-D* curves in Figure 4-19(f). The process requires twelve MPPT perturbations. During this transition, the power is lost. Effectively, the load disturbance slows down the tracking of the direct method, causing the transient efficiency drop. On the other hand, the shift in the operating point does not occur for the indirect control. When the load line changes, PI controller re-tracks the MPP voltage very quickly by changing *D*. Thus, the PI controller always maintain the operating voltage at V_{MPP} regardless of the fluctuations in the load. Furthermore, since the dynamics of the PI controller is much faster than that of the MPPT, the V_{MPP} is re-tracked by the former without any interference from the MPPT controller. Due to these reasons, the indirect control method is more efficient in dealing with sudden load changes.

The experimental load disturbance test is carried out by stepping R_O from 10 to 50 Ω at t =2 s. Then, it is stepped again from 50 to 10 Ω at t = 7 s. The resulting waveforms are shown in Figure 4-20 and 4-21 for the direct and indirect method, respectively. As expected, the direct method diverges from the MPP position at 2 and 7 s. It takes approximately 2 s to recover again. Comparatively, the MPP is tracked by the indirect method within a shorter time interval, i.e. 100 ms. The measured transient efficiencies and tracking time are illustrated in Table 4-4.

Table 4-4: Transient Efficiency for both Control Methods under Load Disturbances.

	Transient Efficiency (%)		Transient Time (ms)	
	Direct	Indirect	Direct	Indirect
At t=2s	70.15	96.42	2200	200
At t=7s	73.73	98.81	2000	100

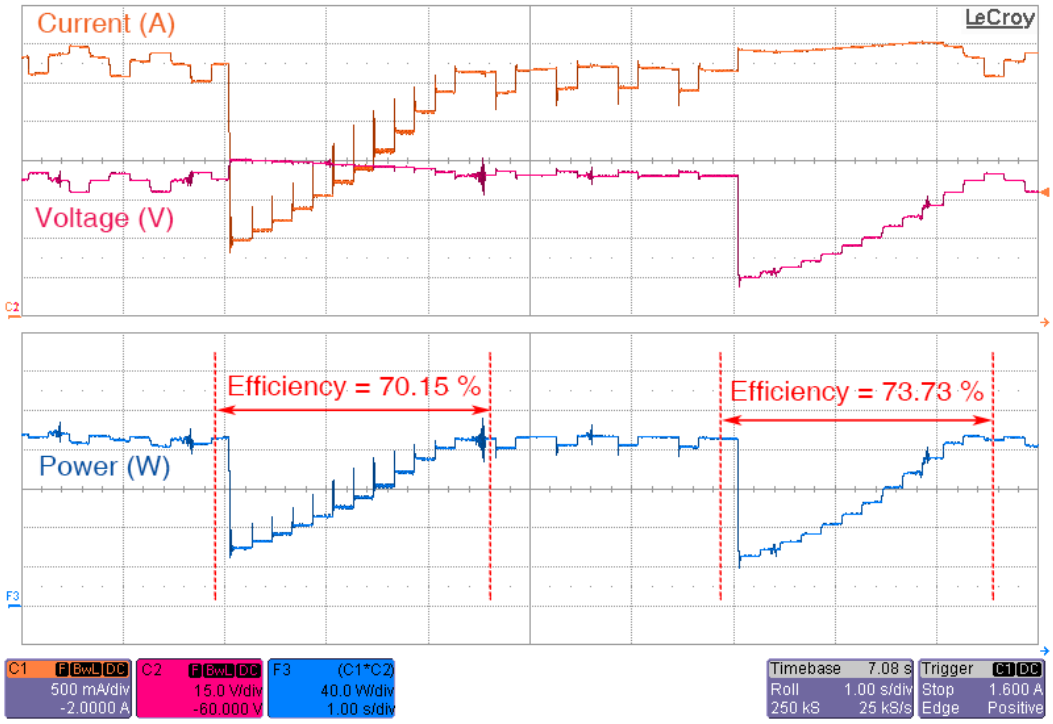

Figure 4-20: Experimental waveforms using the direct method. The PV system is subjected to load disturbances at t=2 s (From 10 Ω to 50 Ω) and at t=7 s (From 50 Ω to 10 Ω).

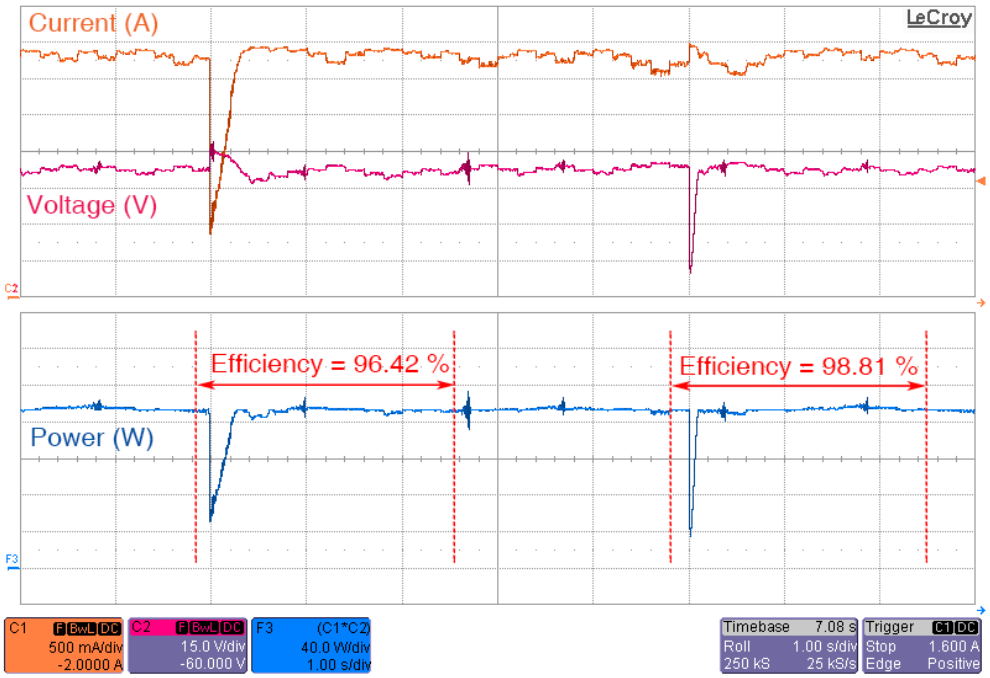

Figure 4-21: Experimental waveforms of the indirect method. The PV system is subjected to load disturbances at t=2 s (From 10 Ω to 50 Ω) and at t=7 s (From 50 Ω to 10 Ω).

4.5 Summary

In this chapter, the performance of the direct and indirect control methods for MPPT were evaluated under various environmental test conditions and load disturbances. From the results, it can be concluded that the steady-state oscillation for direct method is higher; thus, it results in higher power losses. In addition, during the rapid change in the irradiance, its efficiency is reduced due to larger transients. Furthermore, the direct method is dependent on the converter topology. Consequently, it is more sensitive against the load disturbances. Based on these findings, it is envisaged that the indirect method is more suitable to be used in conjunction with the MPPT. Despite these advantages, the indirect method requires additional design processes for the voltage controller. However, that should not pose a problem because its implementation requires only few additional lines of code and tuning of controller parameters.

CHAPTER 5

COMPARATIVE STUDY FOR MPPT BASED ON ARTIFICIAL INTELLIGENCE UNDER UNIFORM INSOLATION CONDITIONS

5.1 Introduction

There are quite a number of MPPT techniques published over the decade, each with its own merits and disadvantages. It is difficult to evaluate/compare all the proposed MPPT techniques in a general way. This is due to the fact that those MPPT techniques are implemented on different PV systems and tested under different weather conditions. In this chapter, an attempt is made to give a comprehensive comparative study between four selected AI-based MPPT techniques namely: fuzzy logic (FL), artificial neural networks (ANN), particle swarm optimization (PSO) and genetic algorithms (GA). A PID-based MPPT technique, similar to the conventional methods such as P&O and IncCond, is included and compared to the other AI-based MPPT. The competing MPPT techniques are extensively described in the literature review chapter. The competing techniques are evaluated by simulation under identical operating conditions, i.e., tests are carried out on the same PV system under the same weather profile. The tracking performance of the competing techniques is evaluated based on the obtained results of simulation. Furthermore, the robustness of competing techniques against ageing of PV modules is verified to show the dependency on PV characteristics. Thereafter, basing on the simulation results and according to the software and hardware requirements, a comparative study is made to highlight the advantages/ inconvenient of each technique. At the end of this chapter, a general recommendations for each MPPT technique are given as conclusion hoping to be a useful material for the MPPT designers and working researchers in this area.

5.2 The PV System Considered for Simulation

To simulate the behavior of the competing MPPT controllers, a block diagram of the PV controlled system developed under Matlab/Simulink is depicted in Figure 5-1. It consists of a PV module, an MPP tracker and a DC load. The MPP tracker is a device composed of power converter associated with an MPPT control unit which generally uses a processor. The converter maintains continuously the PV operating point at the MPP in order to extract the maximum power available regardless the environmental changes.

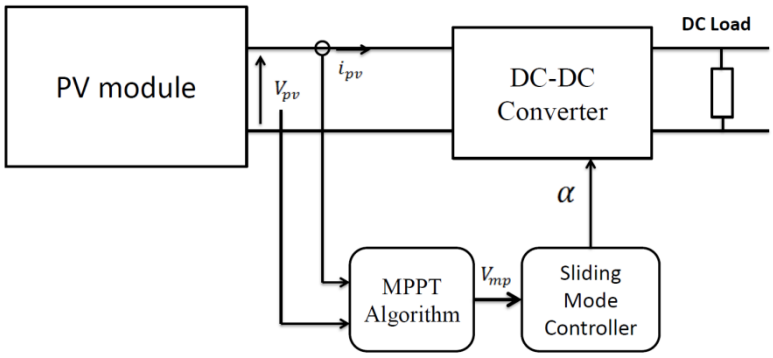

Figure 5-1: The complete PV system with the MPPT control unit [90].

5.3 Evaluation of the MPPT Controllers

To evaluate the performance of the competing controllers, the simulated system is subjected to a theoretical weather profiles that cover major expected scenarios. This test profile is subdivided into three intervals: In the first interval (t∈[0,3] s), the PV module is subjected to a constant environmental condition (32°C and 800 W/m^2). The second interval (t∈[3,20] s) contains fast and extreme variations in both irradiance and temperature levels. Figure 5-2(a) shows the performance tracking of the competing MPPT controllers. Along the simulation period, all controllers exhibit good tracking of the MPP at any weather condition. Figure 5-2(b) shows the MPP tracking at steady state of temperature and irradiance (30°C and 600W/m^2). Figures 5-2(c) and (d) show respectively the MPP tracking at fast and extreme changes in the solar irradiance (from 850W/m^2 to 600W/m^2) with a constant temperature value (32 °C). As shown in the simulation results presented above, all the competing controllers provide an accurate MPP tracking with very small fluctuations. But in fact, there is a slight difference between them. To better highlight this difference, a complete comparative study is presented taking into account: 1) the performance criteria; 2) the robustness against parameter changes in the PV system; 3) the implementation requirements and the global cost.

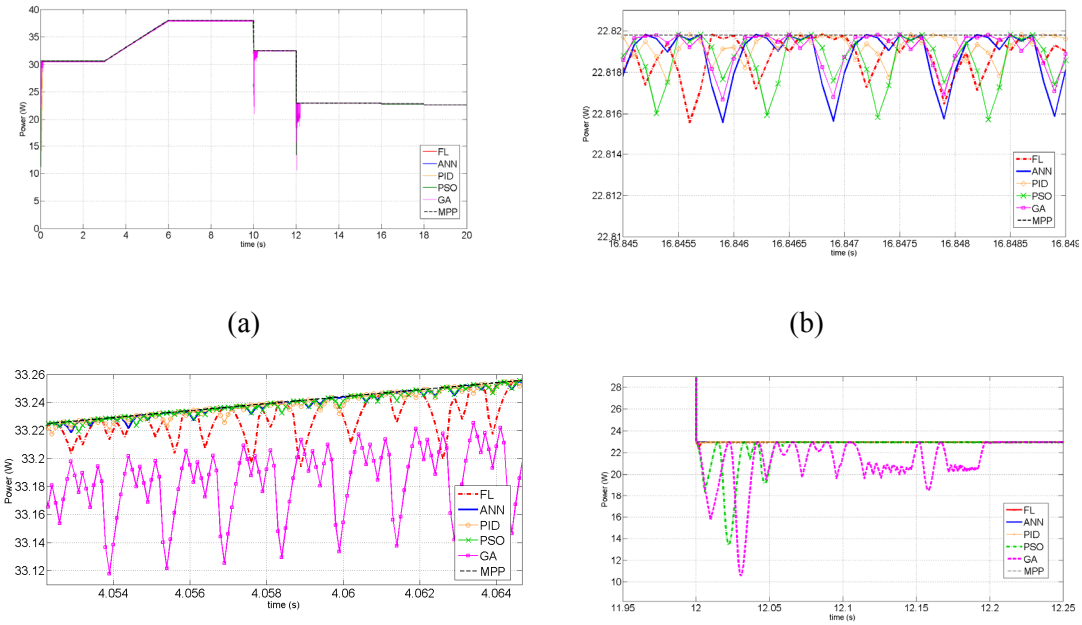

Figure 5-2: Performance tracking of the competing MPPT controllers under variable weather changes. (a) MPP tracking during the 20-s test profile. (b) MPP tracking at steady state weather conditions (30°C and 600 W/m^2). The MPP tracking under (c) fast and (d) sudden change in the solar irradiance

5.3.1 Performance Evaluation of the Competing MPPT Controllers

Basing on the simulation results presented above, a comparative analysis has been carried out to classify the competing controllers according to the performance criteria. This latter consists of four parameters: 1- the tracking speed, 2- the tracking error, 3- the variance and 4- the efficiency. Figure 5-3 shows the transient response of the MPP tracking during a step increase of the MPP. It is clear to show that all the competing MPPT controllers exhibit fast tracking response. The MPP is reached by all the competing MPPT controllers in less than 140 ms. The tracking error $e_m(t)$ is defined as the difference between the theoretical maximum power $P_{max}(t)$ and the power extracted by the MPPT technique $P(t)$. Therefore, the tracking error is given by:

$$e_m(t) = P_{max}(t) - P(t) \tag{5.1}$$

The average value of the tracking error denoted by E_m is calculated by

$$\int_0^{20} \frac{e_m(t)}{20} dt \tag{5.2}$$

The variance V_m may provide information about the oscillation around the MPP. The variance measures how far the function $e_m(t)$ is spread out. A small variance indicates that the function tends to be very close to the mean, which means that there is less oscillation; while a high variance indicates that the function is very spread out around the mean, which means that there is a significant oscillation. The variance V_m is calculated by

$$\int_0^{20} \frac{e_m(t)^2}{20} dt \tag{5.3}$$

The efficiency (η) is calculated as follows

$$\eta = \frac{\int_0^{20} (P(t))dt}{\int_0^{20} (P_{max}(t))dt} \times 100 \tag{5.4}$$

In this analysis, the performance of the competing MPPT controllers is evaluated using the previous equations. Table 5-1 summarizes the response time, the average tracking error, the variance and the efficiency of the competing MPPT controllers. All techniques exhibit very good performance. FL and ANN-based MPPT controllers outperform the others. The MPP is tracked very rapidly with high accuracy and few oscillations. PSO and GA-based MPPT controllers need the re-initialize the search of the new MPP when a change in the environmental conditions is detected. This is performed at the expense of more computational time thus resulting to efficiency drop and sluggishness in the MPP tracking. Nevertheless, PSO shows very good tracking speed and accuracy compared to GA-based MPPT controller. PID based MPPT controller exhibits very good results in term of precision and efficiency with low tracking speed.

Table 5-1: Performance of the Competing MPPT Controllers.

MPPT	Tracking Time (ms)	E_m	V_m	η (%)
PID	131.5	0.0518	0.922	99.83
FL	27	0.0188	0.39	99.94
ANN	27	0.0160	0.3168	99.95
GA	139.2	0.0945	0.5214	99.68
PSO	47.2	0.0352	0.3763	99.88

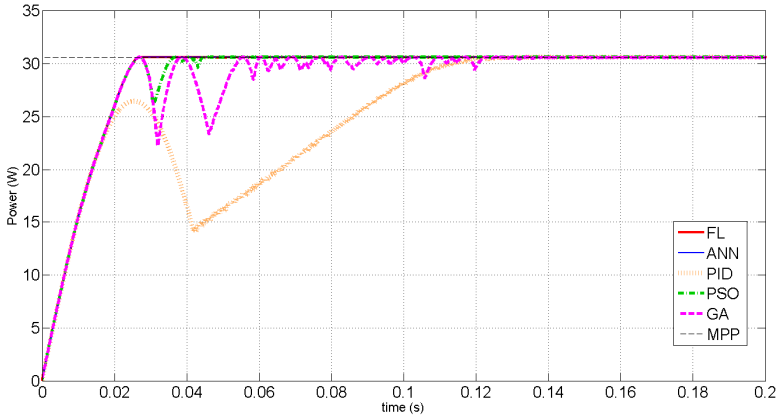

Figure 5-3: Controllers speed at the start-up period of tracking.

5.3.2 Robustness against Parameter Changes

Authors in [91, 92] classified the MPPT strategy to be either direct or indirect. Indirect strategy uses some prior knowledge of PV characteristics or uses databases that include data for different weather conditions or empirical mathematical formulas to estimate the MPP. Direct strategy seeks the MPP directly without any prior knowledge of PV characteristics. The MPP is tracked by gathering the past and the present information of the measured power and voltage. In the present comparative study, ANN-based MPPT can be classified as indirect strategy, while FL, PSO, GA and PID-based MPPT control are classified in the direct strategy group. Simulation is carried out to test the robustness of the competing MPPT controllers against parameter changes of the PV module. In fact, parameters changes are mainly related to the aging of the cells constituting the PV module [93]. The aging of PV module may be modeled by introducing modifications on the electrical equivalent circuit model [94]. A test is carried out to show the behavior of both strategies against aging of the PV modules. In fact, the PV module parameters change over the years. To simulate this phenomenon in software, the aging is simulated within short period by step increases in the series resistance as shown in Figure 5-4. Figure 5-5 shows the MPP tracking according to the changes in the series resistance shown above. From this simulation, it can be concluded that aging decreases considerably the performance of PV modules. Furthermore, all the competing MPPT controllers track correctly the new MPP and deal with parameters changes except the ANN-based MPPT controller. This latter losses robustness when parameters changes occur in the PV module. Hence, direct MPPT has the advantage of the MPP tracking

independently from the PV module parameters. The correct working of MPPT controllers based on indirect strategy needs parameters updating according to the state of the PV module.

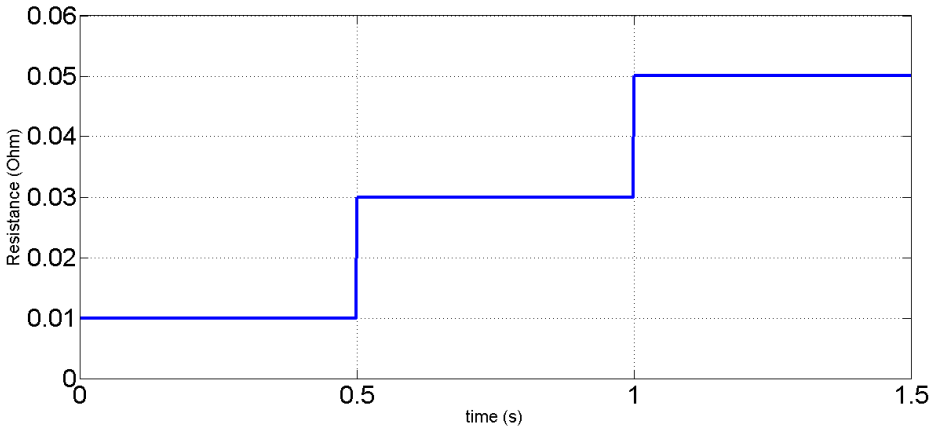

Figure 5-4: Emulating the PV aging: step increases in the series resistance of the PV module.

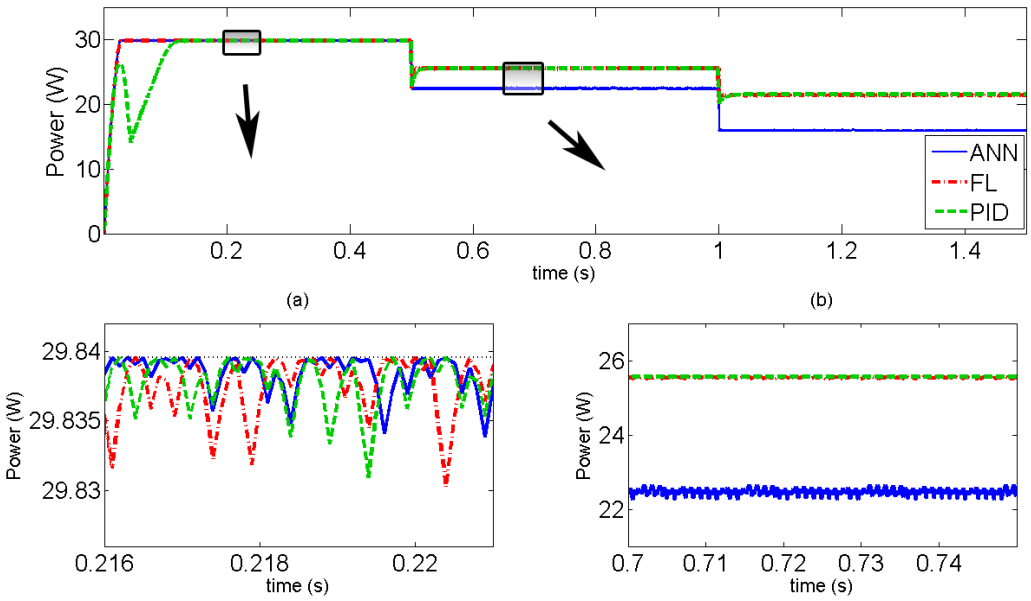

Figure 5-5: Robustness of the MPPT controllers against parameter changes.

5.3.3 Cost of Software and Hardware Requirements

An attempt to classify the competing MPPT controllers according to the implementation cost is made in this section. The implementation cost is estimated based on the

manufacturing requirements, i.e., the type of used sensors, type of circuitry, software level complexity. The type of the required sensors depends on the variables needed to be measured such as: voltage, current, temperature and irradiance. Voltage and current sensors are cheap and easy to implement while the temperature sensor is usually more expensive. The irradiance sensor is very expensive and still quite rare. The type of circuitry can be either analog or digital. Analog circuit uses continuous time voltages and currents while digital circuit uses states in discrete time. Generally, analog circuits are simpler and cheaper than a digital implementation which requires an advanced level of programming knowledge [95]. Expensive applications use advanced techniques and complex circuitry. Considering the above factors, classification of the competing MPPT controllers with an estimation of the total cost is summarized in Table 5-2.

Table 5-2: Classification of the Competing MPPT Controllers.

MPPT technique	**PID**	**FL**	**ANN**	**GA**	**PSO**
Required Sensors	Current, voltage	Current, voltage	Temperature, irradiance	Current, voltage	Current, voltage
Hardware Implementation	Analog or Digital	Digital	Digital	Digital	Digital
Software Complexity	Low	High	Medium	High	High
Total Cost	Low	Medium	High	Medium	Medium

PID-based MPPT controller is simple and easy to implement since only a reduced number of sensors is required. The implementation is possible in both analog and digital circuit. FL, PSO, GA and ANN-based MPPT controllers are more complex and require the obligatory use of a calculator which can be a low cost microcontroller, Digital Signal Processor (DSP) or a Field Programmable Gate Array (FPGA) chip [96, 97]. ANN-based MPPT controller requires irradiance and temperature sensors; this in turn increases the cost of its implementation. As shown from Tables 5-1 and 5-2, there is a trade-off between performance and cost of implementation. This latter increases when a high performance MPPT controller is required and vice-versa.

5.4 Summary

This chapter has presented a comprehensive comparative study between four Artificial Intelligence-based MPPT controllers. The competing controllers are evaluated by simulation under variable environmental condition. A comparative analysis with a classification according to the manufacturing cost has been provided for controllers' evaluation. The comparative study showed that the implementation cost increases when a high performance MPPT controller is required. With respect to the results presented in this study, the following recommendations can be made:

- PID-based MPPT controller is relatively low-cost, easy and simple to implement, offers a good compromise between transient state speed and steady state precision with a robustness against parameter changes. It offers also a very good compromise between performance and implementation cost. The use of this controller is strongly suggested for the non-expensive applications such as pumping irrigation or street lighting systems.

- ANN is a perfect choice when a high efficiency MPPT is needed. It shows high performance and gives better results thus outperforming all other controllers. The major drawback of this controller is the additional cost of temperature and irradiance sensors. In addition, this controller suffers from loss of robustness against aging of PV modules. Basing on the above facts, such controller is not suggested to be used in MPPT systems under uniform insolation conditions.

- FL-based MPPT controller shows high performance and gives very good results. Furthermore, FL controller does not require exact knowledge of PV characteristics and needs only two low cost sensors: voltage and current. Although its implementation needs a calculator and high level programming knowledge, the use of FL-based MPPT controller is suggested to the expensive application which needs a high tracking accuracy such as satellite space, solar vehicle applications.

- PSO and GA-based MPPT controllers provide a very good MPP tracking and show very good performance. However, those techniques require the obligatory use of calculator with very high level programming knowledge. It should be noted that the implementation of GA is slightly complex than the PSO technique. It has been noted

also that these controllers need several iterations to locate the MPP thus sluggish the tracking speed. Furthermore, these controllers are not able to follow new MPP when a slight change in the MPP location is occurred. As shown above, these facts diminish their performance. Using these techniques when the PV array is small and receives always uniform insolation is not suggested. On the other hand, their use in BIPV is crucial especially since a significant power is being lost due to partial shading effect.

CHAPTER 6

PROPOSED HYBRID METHOD FOR THE GMPP TRACKING

UNDER COMPLEX PARTIAL SHADING CONDITIONS

6.1 Introduction

One major aspect of photovoltaic system utilization is the enhancement its maximum power point tracking capability. Although conventional MPPT such as perturb and observe (P&O), incremental conductance (IC) and hill climbing (HC) perform efficiently under uniform irradiance, they tend to fail when subjected to partial shading. These algorithm frequently traps at a local peak—resulting in considerable power loss. To overcome this limitation, soft computing techniques such as particle swarm optimization (PSO) [7], grey wolf optimization (GWO) [8], cuckoo search (CS) [9], flashing fireflies (FF) [10], jaya algorithm (JA) [38], differential evolution (DE) [11], genetic algorithm (GA) and artificial bee colony (ABC) [13] are proposed for MPPT. The metaheuristic approach capitalizes on the vast power of modern computers to search for the global maximum power point (GMPP). It has one distinct advantage: it can be made to effectively scrutinizes the entire *P-V* curve search space; hence its suitability in handling partial shading conditions. However, these methods are much slower than the conventional MPPT [7, 39]. To improve the tracking speed, the modified versions of the metaheuristic algorithms are introduced. For instance, authors in [37] proposed the modified cuckoo search (MCS) that eliminates the Lévy flight term from the conventional CS equation. Similarly, in [40], the original DE based MPPT is amended by removing the random number and skipping certain sampling intervals.

In recent work, additional intelligence are incorporated into the conventional MPPT to increase their performance [14-20]. Recently the *hybrid* MPPT—which combines the conventional and metaheuristic approaches, is gaining interest [22-28, 37]. In [28], the authors proposed a hybrid PSO (HPSO) that combines the conventional P&O with the standard PSO. Since the metaheuristic technique scrutinizes the entire search space, it is very unlikely that the GMPP will be missed (for the case of multiple MHP). Despite its effectiveness, the HPSO is sluggish because the random numbers (embedded in the PSO velocity equation) results in haphazard movement of the particles [7, 39]. Without a corrective measure to guide this movement, the convergence time is significantly increased [7]. Moreover, there is a high possibility that a PSO particle will explore the space which has been previously scanned by other particles.

Based on the shortcomings mentioned above, a hybrid MPPT is proposed in the present Chapter. It incorporates several features which leads improving its performance. First, the search time is minimized by integrating the SSJ into the algorithm [15]. Second, communication between the particles are established to ensure that any region that has been searched by one particle is not explored by another particle. As a result, the unnecessary movements of the PSO particles are reduced. In addition, the P&O is made to be adaptive; this allows the algorithm to climb to the nearby peak quickly, while maintaining low oscillation at steady state. In effect, the MPPT is able to perform rapid and consistent tracking of the GMPP; the convergence is guaranteed, even under complex partial shading patterns, which includes the *P-V* curve with multiple MHP.

6.2 The Proposed Improved Hybrid MPPT

The proposed hybrid MPPT [98] combines the modified P&O and PSO. For the latter, three particles are used; this choice is well optimized and gives the best result, as argued by [7, 39]. The modified P&O has an adaptive feature that allows the algorithm to climb to the nearby power peak rapidly, while at the same time it maintains low oscillation at the steady state. Furthermore, the P&O is incorporated with the SSJ scheme to reduce the tracking speed [15]. When combined with the PSO, the MPPT guarantees that the GMPP is tracked under any shading condition.

6.2.1 Initialization

The flowchart of the proposed MPPT is shown in Figure 6-1. Three PSO particles, namely $P(1)$, $P(2)$ and $P(3)$ are invoked successively at each PSO iteration. The V_{start} indicates the lowest point of the search space. It is chosen slightly lower than the voltage of the left-most power peak, i.e. $0.7\times V_{oc\_mod}$. The upper bound of the search space, labeled by V_{end}, is set to $0.9\times V_{oc\_str}$[18]. Then, $P(1)$, $P(2)$ and $P(3)$ are initialized at three distinct regions within [V_{start}, V_{end}], namely the left, middle and the right side of the *P-V* curve. At the beginning, the initial point of each particle is stored in its respective V_{Pref}, which denotes the reference voltage of the invoked particle. Consequently, $P(1)$ is initialized at V_{start}, i.e.

$$V_{\mathrm{Pr}ef}(1) = 0.7V_{oc\_\mathrm{mod}} \tag{6.1}$$

Then, $P(2)$ is initialized at the middle of the search space, i.e.

$$V_{\mathrm{Pr}ef}(2) = V_{start} + \frac{V_{end} - V_{start}}{2} \tag{6.2}$$

Finally, $P(3)$ is initialized at the right-most section of the P-V curve. Based on the work by [15], the $V_{\mathrm{P}ref}$ of $P(3)$ is suggested as

$$V_{\mathrm{Pr}ef}(3) = (n_{mod} - 1)V_{oc\_\mathrm{mod}} + 0.7V_{oc\_\mathrm{mod}} \tag{6.3}$$

6.2.2 Expanding of Particle's Scanned Interval

6.2.2.1 Perturb & Observe

After initialization, each particle climbs to its nearest local MPP (LMPP) using the P&O. Since the P&O is adaptive, the initial step size multiplier (K) is chosen to be relatively large to ensure fast convergence. Based on [29], K is set to 2% of V_{oc_str}. The reference voltage $V_{\mathrm{P}ref}(n)$ of particle n (n =1, 2 or 3) at each P&O perturbation is updated as follows

$$V_{\mathrm{Pr}ef}(n) = V_{pre} + K \times sign(\Delta P \Delta V) \tag{6.4}$$

with

$$\begin{aligned} \Delta P &= P_{act} - P_{pre} \\ \Delta V &= V_{act} - V_{pre} \end{aligned} \tag{6.5}$$

where P_{act} and V_{act} are the actual measured output power and voltage of the string, respectively. Similarly, P_{pre} and V_{pre} denote the previous power and voltage values. At this moment, the currently found LMPP is considered as the best position (P_{best}) for the particle $P(n)$. Its voltage and power values are stored in $V_{Pbest}(n)$ and $P_{Pbest}(n)$, respectively. Thereafter, the SSJ scheme is activated to skip the search within unnecessary voltage intervals.

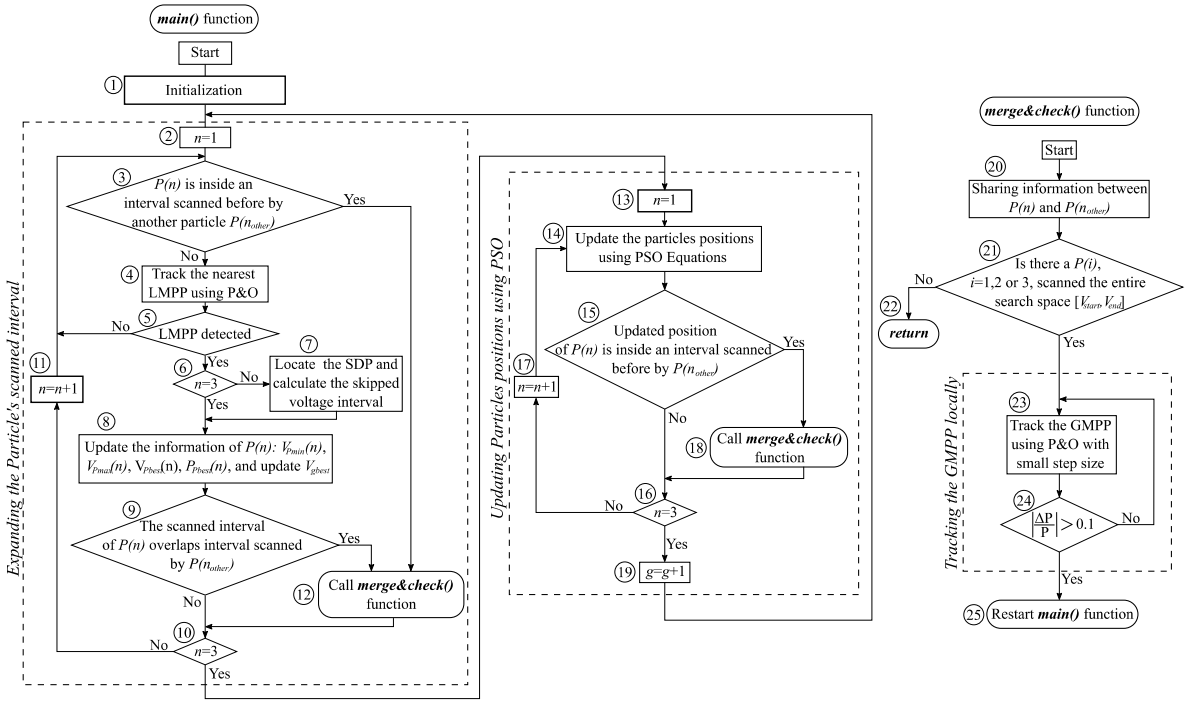

Figure 6-1: Flowchart of the proposed MPPT method. Each numbered block represents a "process".

6.2.2.2 Minimizing the Searched Region Using SSJ

Once the first LMPP is detected, the SSJ scheme is activated. The objective is to minimize the search region by identifying the voltage sections where the search can be omitted. As mentioned earlier in Section 2.2.1, the nearest LMPP is determined by P&O. Then, the corresponding SDP is calculated.

The skipped interval is determined by the following procedure: after the initialization, $P(n)$ climbs to the nearest peak [See Figure 2-1] using P&O. It records $P_{Pbest}(n)$, $V_{Pbest}(n)$. To accelerate the SDP search, the approximate value of SDP (labeled as the Predicted SDP) is calculated by shifting the operating point to the right of the peak using the following expression

$$V_{\Pr ef}(n) = V_{Pbest}(n) + 0.1V_{oc\_\mathrm{mod}} \tag{6.6}$$

The factor 0.1 is carefully chosen after observations from several shading cases. In general, the voltage interval from any LMPP and its corresponding SDP can be calculated by: V_{SDP} -V_{LMPP}. An extensive simulation demonstrated that this voltage interval is always

confined between $0.07V_{oc\_mod}$ and $0.3V_{oc\_mod}$. Hence the factor (0.1) is chosen. Examples of *P-V* curve for several shading patterns that show this condition are illustrated in Figure 6-2.

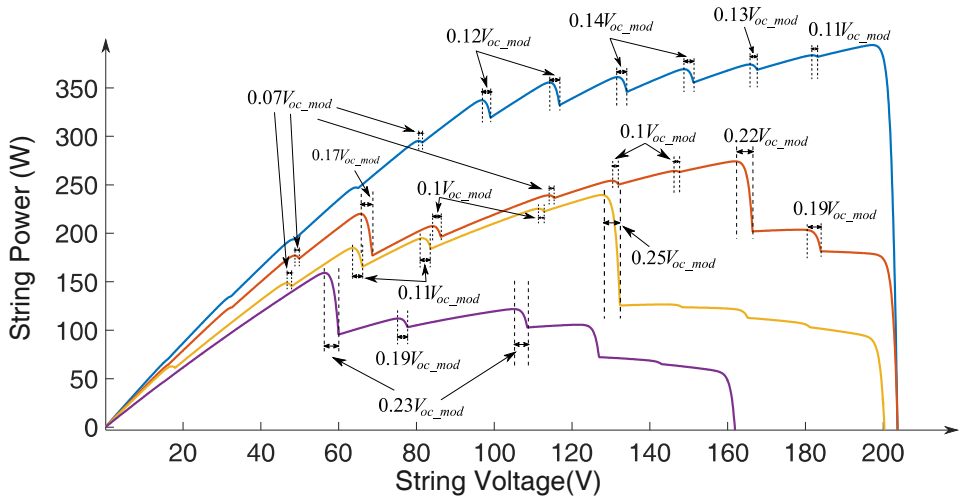

Figure 6-2: distances of voltage intervals between the LMPPs and their corresponding SDPs.

The reverse P&O initiated from the predicted SDP to locate the exact SDP rapidly. By starting the reverse P&O using Eq. (6.6), the search for SDP is accelerated. In the reverse-P&O, the following expression is used

$$V_{\mathrm{Pr}ef}(n) = V_{pre} - K \times sign(\Delta P \Delta V) \tag{6.7}$$

The reverse-P&O is similar to the normal P&O, but it locates the local minimum, instead of maximum. Note that when the operating voltage V_{PV} is on the right side of V_{SDP}, the string current I_{PV} is always lower than I_{SDP}. Therefore, within the voltage interval [V_{SDP}, V_{skip}], the operating power is always lower than the straight line P_{SDP} [See Figure 2-1]. Clearly, in this condition, P_{Pbest} is guaranteed to be the highest within that interval. Hence, since: P_{Pbest}=$P_{SDP}|_{\mathrm{at}\ Vskip}$, the upper bound of the skipped voltage interval V_{skip} can be deduced as

$$V_{skip} = \frac{P_{Pbest}(n)}{I_{SDP}} \tag{6.8}$$

Since, it is guaranteed that no other peak higher than P_{Pbest}, the interval [V_{SDP}, V_{skip}] can exempted from being explored. Thus, the unnecessary scanning is reduced, which leads to a faster convergence.

6.2.3 Avoiding Multiple Scanning of Regions by PSO

The PSO equations are modified and customized to work with the modified P&O and SSJ mechanism. Each particle $P(n)$ has a designated voltage interval that has been scanned, i.e. $[V_{Pmin}(n), V_{Pmax}(n)]$, where $V_{Pmin}(n)$ and $V_{Pmax}(n)$ are the lower and the higher voltage bounds, respectively. Within this interval, the best local position that yields the highest power $P_{Pbest}(n)$ is stored in $V_{Pbest}(n)$. Among these three best positions, the voltage with the highest power value is stored in V_{gbest}. Thereafter, the particles positions $V_{Pref}(n)$ are updated using the modified PSO equations

$$\begin{aligned} v_P^{g+1}(n) &= w.v_P^g(n) + c_1(V_{gbest} - V_{Pbest}(n)) \\ V_{Pref}(n) &= V_{Pbest}(n) + v_P^{g+1}(n) \end{aligned} \tag{6.9}$$

where $v_P(n)$ is the velocity and g is the PSO iteration number, while w is the inertia weight. The coefficient c_1 is the acceleration factor which must be chosen carefully; if c_1 is too high, the particle perturbation is too large and the GMPP may be missed. On the other hand, a small value slows down the tracking speed. All particles are directed to converge towards V_{gbest}. When the invoked particle $P(n)$ scans a certain interval, there is a possibility that this interval has been scanned by one of the other two particles, i.e. $P(n_{other})$. The possible cases are:

1. $P(n)$ overlaps the interval scanned by $P(n_{other})$ during its movement in the search space using P&O.
2. $P(n)$ overlaps the interval scanned by $P(n_{other})$ when the upper bound of its skipped interval is located inside the interval scanned by $P(n_{other})$.
3. $P(n)$ overlaps the interval scanned by $P(n_{other})$ when its updated position using PSO is inside the interval of $P(n_{other})$.

Clearly, there is no sense for $P(n)$ to keep on exploring the region that has been previously scanned by $P(n_{other})$. Thus, once $P(n)$ overlaps an interval scanned by $P(n_{other})$, the *merge&check*() function is called to share the following information

$$\begin{aligned} V_{Pmax}(n) &= max(V_{Pmax}(n), V_{Pmax}(n_{other})) \\ V_{Pmax}(n_{other}) &= max(V_{Pmax}(n), V_{Pmax}(n_{other})) \end{aligned} \tag{6.10}$$

where $V_{Pmax}(n)$, $V_{Pmax}(n_{other})$ are the higher voltage bounds of the scanned intervals by $P(n)$ and $P(n_{other})$, respectively. Similarly, for the lower voltage bounds

$$\begin{aligned} V_{Pmin}(n) &= min(V_{Pmin}(n), V_{Pmin}(n_{other})) \\ V_{Pmin}(n_{other}) &= min(V_{Pmin}(n), V_{Pmin}(n_{other})) \end{aligned} \tag{6.11}$$

The best local positions of $P(n)$, $P(n_{other})$ are updated, i.e.

$$\begin{aligned} V_{Pbest}(n) &= best(V_{Pbest}(n), V_{Pbest}(n_{other})) \\ V_{Pbest}(n_{other}) &= best(V_{Pbest}(n), V_{Pbest}(n_{other})) \end{aligned} \tag{6.12}$$

where *best*() is a function that returns the voltage that yields the highest power value. Similarly, the best global position is determined using

$$V_{gbest} = best(V_{Pbest}(1), V_{Pbest}(2), V_{Pbest}(3)) \tag{6.13}$$

Consequently, the intervals scanned by $P(n)$ and $P(n_{other})$ are merged and combined in one interval, i.e. $[min(V_{Pmin}(n), V_{Pmin}(n_{other})), max(V_{Pmax}(n), V_{Pmax}(n_{other}))]$. Thereafter, this newly determined interval is checked; if it equals the entire search space, i.e. $[V_{start}, V_{end}]$, the GMPP is assumed to be found at V_{gbest}.

6.2.4 Local Tracking of the GMPP

Once the GMPP is determined, the perturbation size of the P&O is reduced to ensure that a small change in irradiance and a slow change of temperature do not displace the operating voltage from the GMPP. In addition to that, the oscillation and thus the power loss is reduced. Accordingly, the step size (K) chosen to be 0.5% of V_{oc_str} [29]. Meanwhile, the sudden change in the power level, i.e. $\left|\frac{\Delta P}{P}\right| > 0.1$, is continuously checked to detect if new partial shading has occurred [99].

6.3 Illustrative Example

To understand the intricacies of the proposed MPPT, an illustrative example that corroborates the flowchart in Figure 6-1 is given. The objective is to describe how the PSO complements the P&O to achieve GMPP convergence of an arbitrary shading pattern. To aid the discussion, each block is sequentially numbered as "Process" (in circle). The flowchart is linked to the actual movement of particles within the search space, as shown in Figure 6-3.

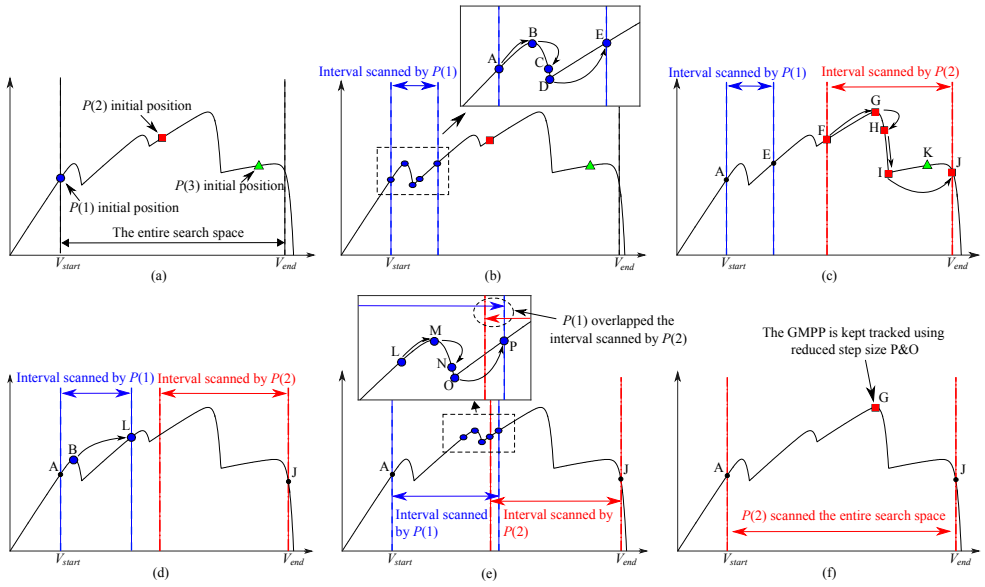

Figure 6-3: (a) Initialization of the three particles in the search space. (b) Movement of $P(1)$ in the search space. (c) Movement of $P(2)$ in the search space. The initial position of $P(3)$ is within the interval scanned by $P(2)$. (d) $P(1)$ jumps towards the GMPP after updating its position using PSO. (e) $P(1)$ during expanding its scanned interval osculates the interval scanned by $P(2)$. (f) $P(2)$ scanned the entire search space and the GMPP is tracked by P&O with reduced step size.

***Step* 1:** In the beginning, the three particles, i.e. $P(1)$, $P(2)$ and $P(3)$ are initialized respectively at the left-most, middle and right-most side of the search space as shown in Figure 6-3(a) (Process 1). These particles correspond to the blue dot, red square and green triangle. $P(1)$ is the first particle to be invoked (Process 2). As shown in Figure 6-3(b), it climbs the nearest LMPP using the P&O and finds the peak at point B (Process 4 and 5). This point is considered as the best position of $P(1)$; thus its voltage value is stored in $V_{Pbest}(1)$. Then, using Eq. (6.6), $P(1)$ jumps to the Predicted SDP, which is Point C. Thereafter, the reverse-P&O is activated to determine the exact SDP, i.e. Point D. Using the power value recorded from Point B and the current recorded from Point D, the upper boundary of the skipped voltage interval V_{skip} is calculated using Eq. (6.8). Thus the "skipped

interval" (from Point D to E) is defined, and is exempted from being explored by $P(1)$. This is done in Process 7. In addition, Point E is investigated to check the possibility of skipping another interval. At the end of Process 8, the interval that has been scanned by $P(1)$ is $[V_{Pmin}(1), V_{Pmax}(1)]$; it ranges from A to E, as shown in Figure 6-3(b). The best power recorded is at Point B, i.e. $V_{Pbest}(1)$.

***Step* 2:** Next, $P(2)$ is invoked by incrementing the counter n (Process 11). As mentioned, $P(2)$ is initialized in the middle of the search space. Its initial position is checked in Process 3; if it falls inside the interval scanned by $P(1)$, there is no need to search for the peak. Otherwise, $P(2)$ climbs the nearest LMPP from Point F onwards, using the P&O (Process 4). From Figure 6-3(c), it can be seen that the peak is located at Point G. Therefore, the voltage of Point G is considered as the best position for $P(2)$. Its value is stored in $V_{Pbest}(2)$. By virtue of the reverse-P&O (Process 7), the corresponding SDP is located at Point I. Then, V_{skip} is calculated using Eq. (6.8). However, for this case, $V_{skip}>V_{end}$, as shown in Figure 6-3(c). Thus, the interval from Point F to J is considered scanned by $P(2)$. The search region is now narrowed from Point E to F only.

***Step* 3:** When $P(3)$ is invoked, its initial position (Point K) is already inside the interval scanned previously by $P(2)$. This is shown in Figure 6-3(c). Therefore, there is no need for $P(3)$ to search for the LMPP. In other words, within the common interval, the information obtained by $P(2)$ is shared by $P(3)$ using the *merge&check*() function (Process 12). Consequently, in Process 20, $V_{Pmin}(3)=V_{Pmin}(2)$ (Point F), $V_{Pmax}(3) =V_{Pmax}(2)$ (Point J) and $V_{Pbest}(3) =V_{Pbest}(2)$ (Point G). Since none of the particle scans the entire space (Process 21), the algorithm returns to the main function (Process 10).

***Step* 4:** In the first PSO iteration, the three particles are yet to locate the GMPP. Thus, further iteration is carried out to update the positions of $P(1)$, $P(2)$ and $P(3)$ (Process 13). As the position recorded by $P(2)$ and $P(3)$ (i.e. voltage of Point G) is the best among all the positions, $P(1)$ has to converge towards the same point using Eqs. (6.9) (Process 14). Thereby, $P(1)$ jumps from Point B to L. This operation accomplishes the scanning of interval from A to L, as shown in Figure 6-3(d).

***Step* 5:** Thereafter, $P(1)$ starts to explore a new area (Process 4). A new LMPP and its corresponding SDP (Process 7) are recorded at M and O, respectively, as shown in Figure 6-3(e). In Process 8, since the power at Point M is higher than B, the voltage at the former is stored in $V_{Pbest}(1)$. Furthermore, a new skipped voltage interval (from O to P) is determined; thus, the scanned interval of $P(1)$ is now expanded from Point A until P. However, after the test in Process 9, $P(1)$ overlaps the interval scanned by $P(2)$ as shown in Figure 6-3(e). Thus, the *merge&check()*function is called (Process 12); $P(1)$ and $P(2)$ share their information

(Process 20) as follows: $V_{Pmin}(2)=V_{Pmin}(1)$ (Point A), $V_{Pmax}(1)=V_{Pmax}(2)$ (Point J), and $V_{Pbest}(1)=V_{Pbest}(2)$ (Point G). Hence, $P(1)$ and $P(2)$ have successfully scanned the region from A to J, which is the entire search space [V_{start}, V_{end}].

***Step* 6:** Since the PSO particles have found the GMPP at V_{gbest} (Point G), the P&O is re-activated. However, the step size is minimized to ensure that any change in the environmental condition will not affect the GMPP position (Process 23). This is shown in Figure 6-3(f). Furthermore, if a sudden change in the irradiance occurs—indicating that a new partial shading condition has taken place (Process 24), the program is re-initialized (Process 1). The whole process to locate the new GMPP is repeated. As illustrated by this example, the scheme scrutinizes the entire [V_{start}, V_{end}] in the search for GMPP. This operation guarantees that the GMPP will not be missed even if the PV array is subjected to a complex shading condition. Due to the SSJ, a large region of the search space has been exempted, namely B-C, D-E, G-H, I-J, M-N and O-P. In the case mentioned above, only A-B, C-D, F-G, H-I, L-M, N-O need to be scanned. By narrowing the search space, the task of locating the GMPP is greatly accelerated.

6.4 Implementation of the Proposed Method using Stateflow

6.4.1 Stateflow Environment

The above-mentioned SSJ and P&O techniques combined with PSO have to be scheduled and executed sequentially. An extended finite state machine (FSM), i.e., state chart, is designed to schedule the execution of the different functionalities of the proposed method. This state chart is implemented using Stateflow diagram as shown in Figure 6-4. Stateflow is an environment integrated in Matlab/Simulink for modeling and simulation of event-driven systems [100]. Stateflow chart is a set of finite states —rounded rectangles inside the chart— that represents the possible operating modes of a model-based system/controller. The states can be arranged hierarchically, i.e., a parent state can embed a sub-chart composed of child states (sub-states) [101]. The chart operating mode is updated when a triggering event is occurred which can be a system input or an internal event. The new activated state depends on the triggering event and the past configuration of the chart. To activate the target state and deactivate the source state, a valid transition —curved arrows connect the states—

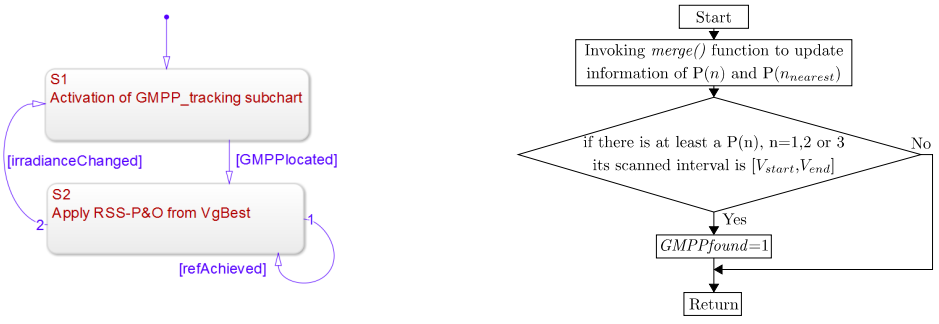

(a) (b)

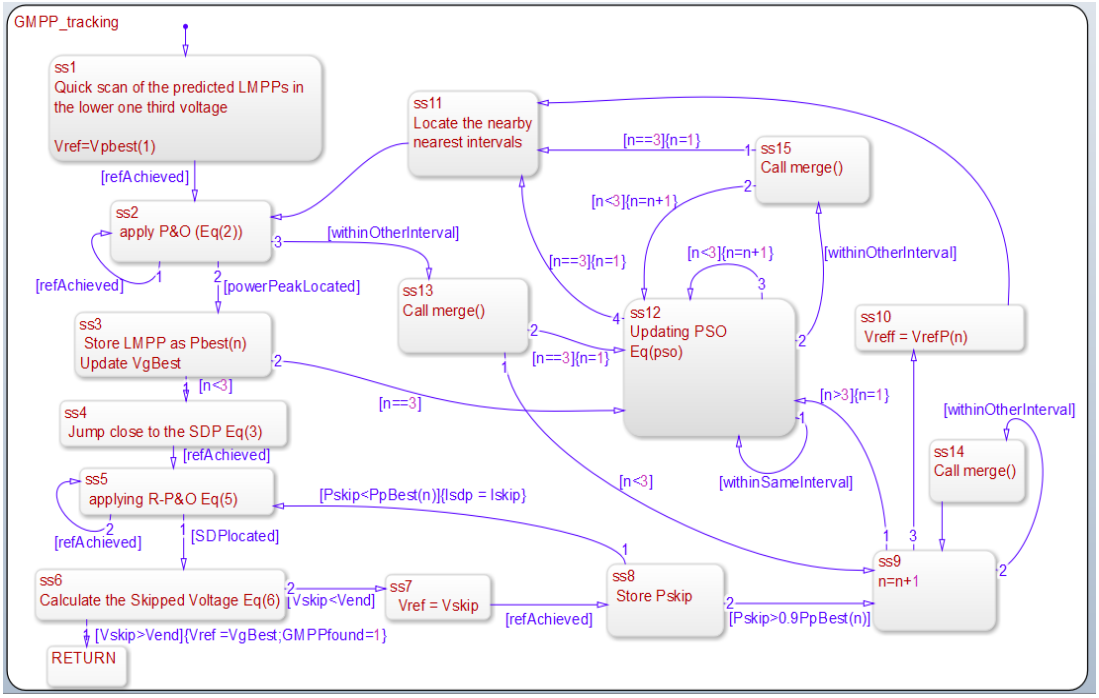

(c)

Figure 6-4: Stateflow chart of the proposed MPPT algorithm. (a) Main chart. (b) Flowchart of *merge&check*() function. (c) Sub-chart of the GMPP tracking.

path is needed, i.e., the condition associated to this transition must be true. In the case where the state is linked through more than one transition, their associated conditions are tested by priority, i.e., the lower transition number has the higher priority to be tested. A condition action can be executed during testing when a transition condition is true. The transition segment is labeled with this format: [*transition condition*]{*transition action*}. Actions can be attached also to the states, i.e., they can be executed 1) when the state is activated, 2) during the state activation and 3) when the state is deactivated. Figure 6-4 represents the Stateflow diagram of the proposed MPPT algorithm. The Stateflow chart is implemented using the OR decomposition (serial decomposition) in which only one sub-state is activated at each time. The main Stateflow chart is represented in Figure 6-4(a). The default transition initially

activates the state S1, which invokes the ***GMPP_tracking*** sub-chart, represented in Figure 6-4(c) to locate the GMPP. Once this latter is found, a ***GMPPlocated*** flag is set thus activates the state S2. During S2 activation, the GMPP is tracked using P&O algorithm to handle any slow environmental changes that may displace the GMPP from its initial location. The reduced step size K equals to 0.5% of V_{oc_str}. The P&O keeps tracking the GMPP until detecting a sudden change in the irradiance level, i.e., $\left|\frac{\Delta P}{P}\right| > 0.1$. If this is the case, the ***irradianceChanged*** flag is set and the ***GMPP_tracking*** sub-chart is re-invoked (state S1) to locate the new GMPP.

6.4.2 Description of the State-Chart for the GMPP Tracking

6.4.2.1 Exploring the Search Space Mechanism

The algorithm invokes the particles to take place in the search space one by one. Initially, $P(1)$ starts exploring the search space (sub-states ss1 and ss2) from V_{start}=0.7V_{oc_mod} which is chosen slightly lower than the minimum voltage expected of the leftmost power peak at any weather condition. Then, the LMPP voltage located by $P(1)$ is considered the best position recorded by $P(1)$. After storing this latter in $V_{Pbest}(1)$ (sub-state ss3), its corresponding SDP is predicted (sub-state ss4) using Eq (6.7). Once the predicted SDP voltage is attained, the reverse-P&O is turned on (sub-state ss5) to locate precisely the SDP. If the best LMPP found is the GMPP, $P(1)$ will skip the entire search space by repeating the contour ss5-ss6-ss7-ss8-ss5 until $V_{skip} > V_{end}$. Thus, the scanned interval of $P(1)$ becomes [V_{start}, V_{end}] and hence ***GMPPfound*** flag is set (transition 1 of ss6 is valid). Thereby, the state (S1) is deactivated and the GMPP is tracked using P&O (S2). Otherwise, i.e., $V_{skip} < V_{end}$ (transition 2 of ss8 is valid), the skipping process is stopped and the scanned interval by $P(1)$ is [V_{start}, V_{skip}] and $V_{Pbest}(1)$ is the best LMPP voltage found within this interval. Then, $P(2)$ is invoked to take place in the searching process (ss9-ss10-ss11). From the initial position of $P(2)$, which is given in Eq.(6.2), the P&O is turned on to locate the nearest LMPP. If $P(2)$ is within the interval scanned by $P(1)$ previously [V_{start}, V_{skip}], a ***withinOtherInterval*** flag is set (transition 2 of ss9 becomes valid) thus invokes the *merge&check*() function (ss14) to permit $P(2)$ sharing information obtained by $P(1)$. Thus, $P(2)$ is exempted from being invoked and $P(3)$ takes place in the searching process (ss14-ss9-ss10-ss11-ss2). Otherwise, $P(2)$ starts

searching the nearest power peak using P&O (ss9-ss10-ss11-ss2) after determining the nearest intervals scanned by the other particles (ss11). Once $P(2)$ finds the nearest LMPP (transition 2 of ss2 is valid), the reverse P&O is turned on to locate the corresponding SDP (ss3-ss4-ss5) and V_{skip} is calculated (ss6); if $V_{skip} > V_{end}$, the scanned interval by $P(2)$ is $[V_{Pinit}(2), V_{end}]$ and $V_{Pbest}(2)$ is the voltage of the higher peak found within this interval; where V_{Pinit} denotes the initial position of the particle. In this case, $P(3)$ will be exempted from being invoked in the searching process since its initial position is located at the rightmost side of the *P-V* curve within the interval scanned by $P(2)$ (***withinOtherInterval*** flag is set to 1). Hence, $P(3)$ shares the information obtained by $P(2)$ when *merge&check*() function is invoked (ss14). Thereafter, a new iteration using PSO takes place to update the particle's positions (ss12). Otherwise, i.e., the scanned interval by $P(2)$ is $[V_{Pinit}(2), V_{skip}]$, $P(3)$ is invoked to take place in the search space (ss10-ss11-ss2). During its movement, there is a possibility to osculate the interval scanned by $P(2)$. If this happens, i.e., ***withinOtherInterval*** flag is set (transition 3 of ss2 is valid), $P(3)$ and $P(2)$ will share their information and their scanned intervals will be merged (ss13) and a new iteration using PSO takes place to update the particles position (transition 2 of ss13 is valid). Otherwise, P&O is kept turned on (ss2) until finding the nearby LMPP (***powerPeakLocated*** flag is set to 1, transition 2 of ss2 true). If $V_{Pbest}(3)$ of the LMPP found is superior than $V_{Pinit}(3)$, the scanned interval defined by $P(3)$ is $[V_{Pinit}(3), V_{end}]$; if not, i.e., $V_{Pbest}(3)$ is inferior than $V_{Pinit}(3)$, it is defined by $[V_{Pbest}(3), V_{end}]$. Thereafter, a new iteration using PSO takes place to update the particle's position (transition 2 of ss3 is valid).

6.4.2.2 Updating the Particle's Positions using PSO

The best position of an invoked particle *n* (V_{Pbest}(n)) and the best particle yields the higher power among all particles (V_{gbest}) are updated when (ss3) is activated. In case of another PSO iteration is needed to take place, the particle's positions V_{Pref}(n) are updated (ss12) using Eq. (6.9). Thus, all the other particles will be directed to converge towards V_{gbest}. After updating each particle's position (ss12), their new positions will not be out from these three cases:

- The particle's position is still within its scanned interval, a ***withinSameInterval*** flag is set to 1 (transition 1 of ss12 true), thus moves the particle another step with its velocity until it finds itself outside its scanned interval.

- The particle finds itself within an interval scanned previously by another particle, ***withinOtherInterval*** flag is set to 1 (transition 2 of ss12 true), the two particles share their information and their scanned intervals are merged after invoking the *merge&check*() function (ss15).

- If all positions of particles are updated and the GMPP is not located yet (transition 4 of ss12 is valid), a new PSO iteration has to be performed in the searching process.

6.4.2.3 Sharing Information between Particles and Merging Intervals:

Figure 6-4(b) shows the flowchart of the *merge&check*() function. Each particle expands its scanned interval using the above-mentioned SSJ and P&O methods. Supposing that a moving particle $P(n)$ osculates an interval scanned by another particle $P(n_{other})$. It has no sense if $P(n)$ keeps exploring areas that has been previously scanned by $P(n_{other})$. Hence, the two particles have to be communicated in such a way to prevent re-scanning the scanned areas. To do so, once $P(n)$ osculates an interval scanned by $P(n_{other})$, a *merge&check*() function is invoked to update the particles information using Eqs.(6.10-6.13). The searching process may be stopped after each invokation of *merge&check*() function; if there is at least one particle its scanned interval is $[V_{start}, V_{end}]$, the flag ***GMPPfound*** is set and thus the GMPP is assumed to be found.

6.5 Performance Evaluation by Simulation

6.5.1 Simulation Set-up

Figure 6-5 shows the simulated PV system. The system is based on a string of twelve series-connected modules. For the simulation, the MSX60 [86] module is used; its specifications are shown in Table 4-1. The total power rating is 720 W at STC. The string feeds a variable dc load (R_L) through a buck-boost converter. The converter is designed to operate in continuous conduction mode, with the following specifications: L =1 mH, C_1=470 μF, C_2=220 μF. The switches are driven at a switching frequency (f) of 50 kHz. For the MATLAB/Simulink simulation, the two diodes model is used [66]. The proportional-integral

(PI) voltage controller is embedded in the control loop to match the voltage perturbation computed by the MPPT algorithm. The entire loop can be seen as a cascaded structure, where the outer control loop (MPPT algorithm) is much slower than the inner loop (PI controller) [87].

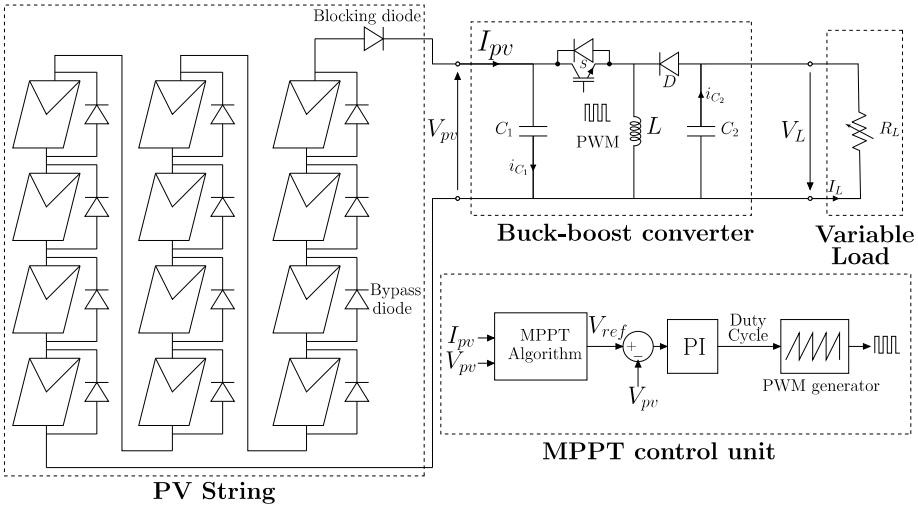

Figure 6-5: The structure of the PV system used in simulation.

A graphical-user interface (GUI) program is developed to observe the variations in the *P-V* characteristics curve versus irradiance levels. By doing so, the shape of the *P-V* curve is easily checked by manually sliding the value of the irradiance level of each module, as shown in Figure 6-6.

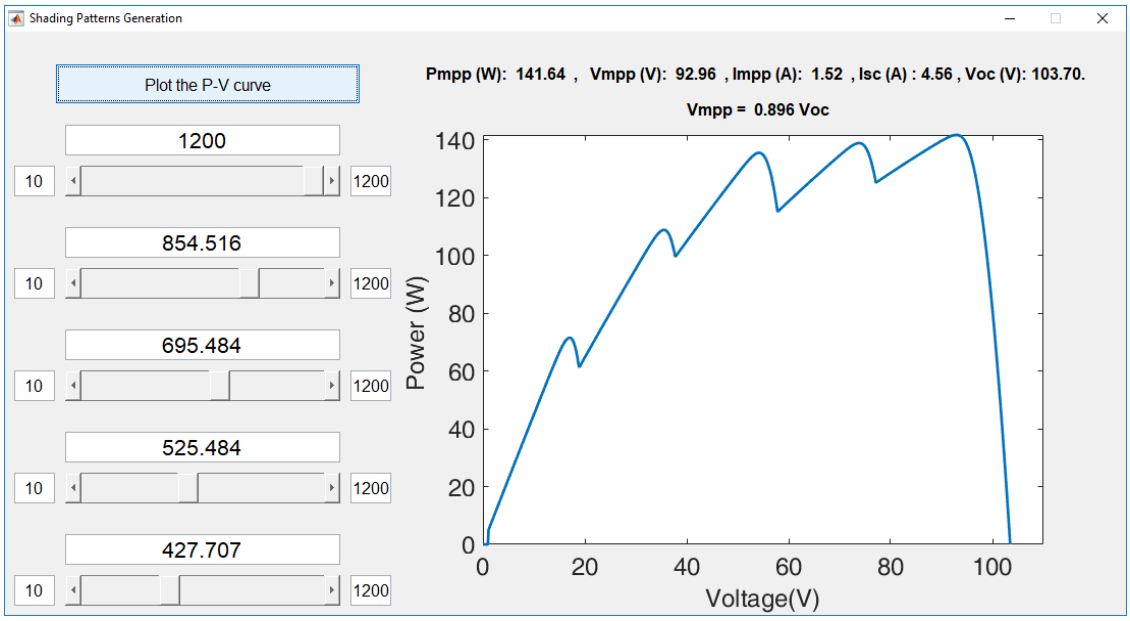

Figure 6-6: The graphical-user interface used for the *P-V* curves generation.

The complex shading patterns generated using this GUI are shown in Figure 6-7. These patterns are obtained by subjecting the string to twelve different irradiance levels. The shadings are carefully selected to include all the possible regions where the GMPP can occur, i.e. at the leftmost, middle and rightmost side of the *P-V* curve. For example, for Pattern 1, the GMPP is deliberately positioned at the extreme end [18]. The multiple cluster conditions (that leads to multiple MHP) are represented by Patterns 2 and 4. These two cases demonstrate the tracking response where the GMPP is located inside the right and the left cluster, respectively. Using these patterns, the competing MPPT algorithms are examined and evaluated.

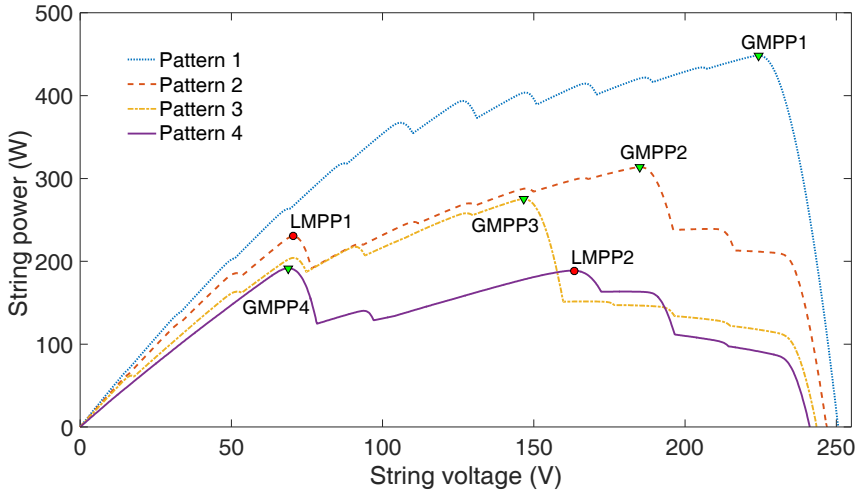

Figure 6-7: Partial shading patterns used in simulation: Pattern 1: GMPP is at the right-most side; Pattern 2: With two MHP and the GMPP is located at the right side of the curve. Pattern 3: the GMPP is at the middle of the curve. Pattern 4: With two MHP and the GMPP is located at the left side of the curve.

6.5.2 Performance Evaluation

The proposed algorithm is evaluated against the MIC [16], original version of SSJ [15], HPSO [28] and MCS [37] methods. The HPSO is a hybrid MPPT that combines the P&O with the PSO. On the other hand, the MCS is a modified version of the cuckoo search. It is a metaheuristic algorithm. The voltage and power transients during the initial search for the GMPP are shown in Figure 6-8. From these transient profiles, the performance of the

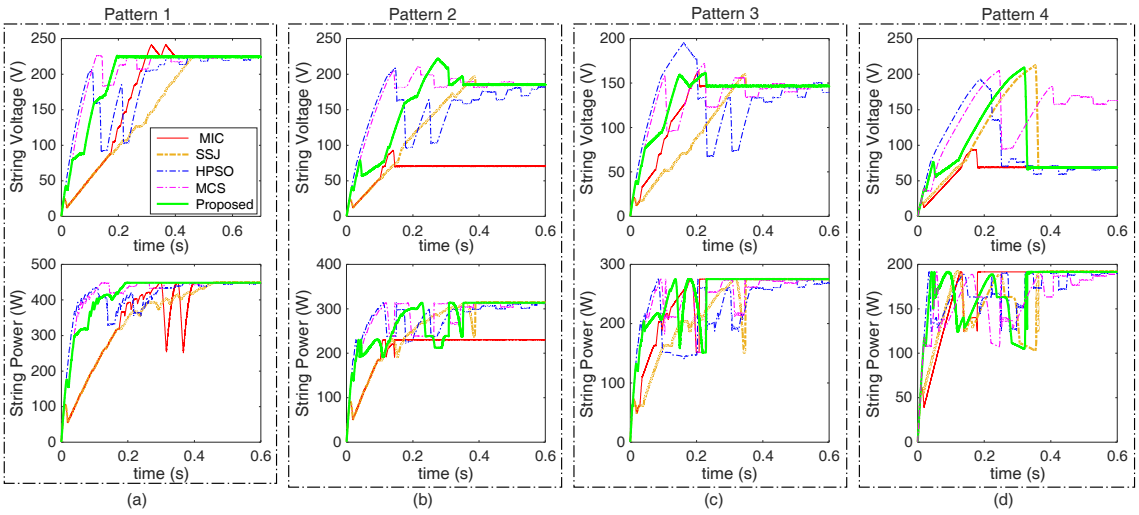

Figure 6-8: The voltage and power fluctuations of the MIC, SSJ, HPSO, MCS and proposed MPPT under the partial shading patterns shown in Figure 6-7: (a) for Pattern 1, (b) for Pattern 2, (c) for Pattern 3, (d) for Pattern 4.

competing MPPT methods are analyzed based on four assessment criteria: 1) the ability to track GMPP correctly, 2) the required number of computation cycles (or iteration), 3) the percentage of scanned interval within the search space and 4) the tracking time.

6.5.2.1 Tracking the Correct GMPP

As shown in Figure 6-11, for Patterns 1, 3 and 4, all methods successfully tracked their corresponding global peak, i.e. GMPP1, GMPP3 and GMPP4, respectively. However, for Pattern 2, the MIC fails to track GMPP2. As highlighted earlier, the failure is due to the fact that the MIC can only handle the pattern that exhibits a unique MHP. To confirm this condition, Pattern 2 reproduced as Figure 6-9. There are two clusters, each with its own MHP—labeled LMPP2 and GMPP2. The MIC starts the search from the lower end of the curve; it identifies the first three peaks and forms Cluster 1. Then the comparison is made, since the middle peak (LMPP2) is higher than the two accompanying peaks (on its left and right side), the algorithm assumes LMPP2 is the GMPP and stops the search prematurely. However, the true global peak is GMPP2. Thus, the tracking fails to locate the correct GMPP and consequently, the output power is reduced by 26 %.

Figure 6-10 illustrates the reason for the failure of MCS to locate GMPP4. Following the initialization procedures [37], three particles, i.e. $P(1)$, $P(2)$, and $P(3)$, are generated on P-V curve at A, B and C, respectively. Their movements are illustrated in Figure 6-10(b). From

the initial sampling of these three points, B appears to be the best position. Thus, $P(1)$ and $P(3)$ move towards point B in the second iteration. Based on the step size determination suggested in in [37], $P(1)$ moves to point D while $P(3)$ moves to point E. However, during that step, $P(1)$ has already missed GMPP4 and jumped to a further voltage. After the second iteration, E becomes the best position. Since E is located at the rightmost among the three particles, $P(1)$ gives a big jump from point D to the other side of point E and reach at point F. Meanwhile, $P(2)$ moves form point B towards point E. Eventually, all three particles will merge at position E, which is a local peak (LMPP2). This is clearly shown in Figure 6-10(b).

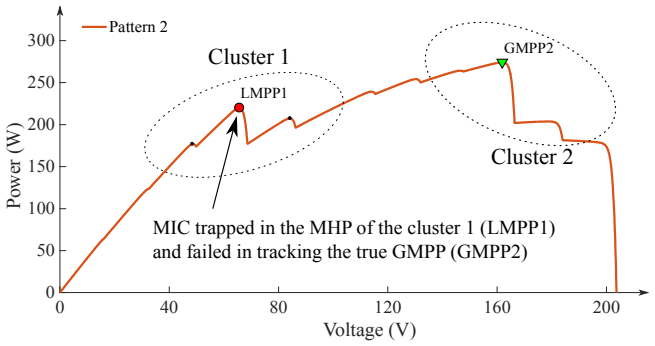

Figure 6-9: Pattern 2 of the shading profile contains two clusters, resulting in MIC tracking failure.

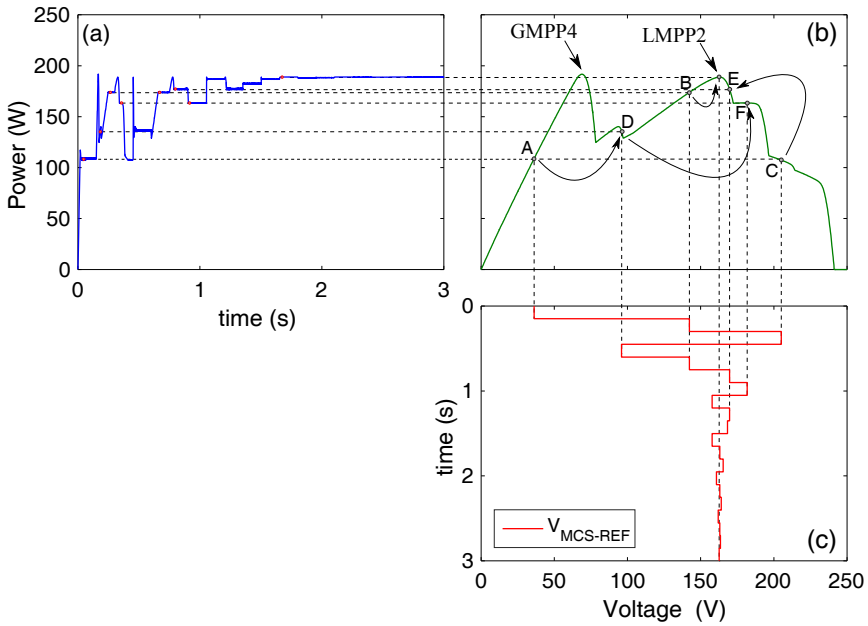

Figure 6-10: Failure of MCS in tracking GMPP4 of Pattern 4. (a) Power fluctuations. (b) Movement of MCS particles on Pattern 4 during the exploring phase. (c) Reference voltage computed by the MCS.

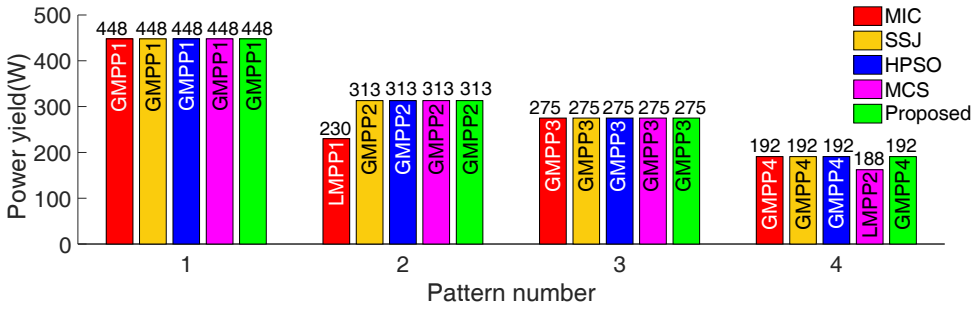

Figure 6-11: The Power output as a result of tracking correctness.

6.5.2.2 Computation Cycle

The computational cycle is defined as the required number of iterations in the reference voltage to reach the GMPP. The reason of including the computational cycles is to give an insight about the number of times the voltage controller is invoked to track the voltage references (computed by the MPPT algorithm) before reaching the GMPP. This is very important because if the voltage controller performance is weak due to noise or imprecise sensors, the computational time (or tracking speed) is affected. Thus, for an efficient tracking, it is desirable to keep the computational cycle to the minimum. For SSJ and MIC, it is proportional to the location of the GMPP (V_{GMPP}). If the V_{GMPP} is closer to V_{oc_str}, the number of computational cycles is higher. This fact can be concluded from Figure 6-12, where V_{GMPP} decreases successively from Pattern 1 to 3. For the HPSO and the proposed MPPT, the computational cycle is not related to V_{GMPP} because the PSO particles are initialized at three separate regions to explore their allocated search space independently.

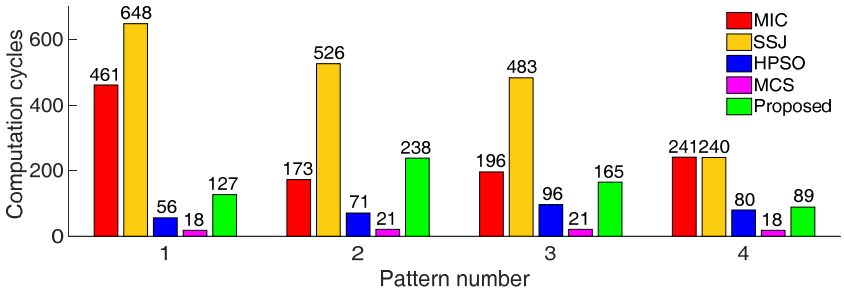

Figure 6-12: The number of computation cycles (iteration) to achieve GMPP.

6.5.2.3 Scanned Interval

From Figure 6-13, the percentage of the interval scanned by SSJ is higher than MIC for all the shading patterns. This is because the MIC only scans the regions around the vicinity of the peaks, i.e. the multiples of $0.8\times V_{oc\_mod}$. For the SSJ, the scanned interval is higher than MIC because it has to start the search from the leftmost side of the *P-V* curve. From there, it needs to perform the search-skip and judge procedures until it locates the V_{GMPP}. For the proposed method, the interval that needs to be scanned is less than the SSJ and MIC. This can be attributed to the improved mechanism for the particles movement and communication. Since the particles utilize the SSJ scheme, the unnecessary intervals are not scanned, thus limiting the movement of the particles. Furthermore, the '*merge&check*' procedure prevents the particles from rescanning the intervals that have been scanned by other particles.

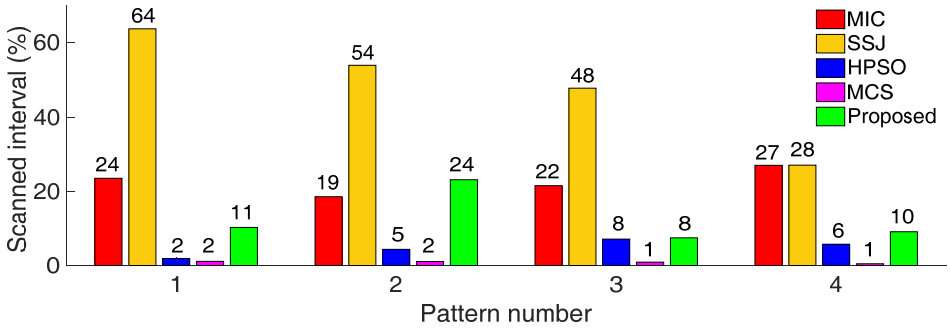

Figure 6-13: Percentage of the interval needed to be scanned.

6.5.2.4 Tracking Time

The tracking time is defined as the time (in millisecond) taken for the algorithm to reach the GMPP. As seen in Figure 6-14, the HPSO is the slowest. Furthermore, the convergence is achieved after large fluctuations in the voltage and power transients. This can be attributed to the random movement of the PSO particles while searching for the GMPP. The SSJ is also slow, particularly when V_{GMPP} is at the higher end of the *P-V* curve. In such case, the SSJ starts the search process from the lower end of the *P-V* curve and performs the search-skip and judge procedures until it locates the V_{GMPP}. On the other hand, the proposed MPPT exhibits rapid convergence to the GMPP due to the improved mechanism for the particles movement and communication (as mentioned above). The proposed method is faster than

SSJ by more than 52, 3, 33 and 8 % for Patterns 1, 2, 3 and 4, respectively. Although the MIC converges very rapidly when the GMPP is located on the lower side of the curve (for Patterns 3 and 4), it is slower if the V_{GMPP} is located near V_{oc_str} (as illustrated by Pattern 1). This is because the MIC needs to scrutinize all the peaks that are located on the left side of the GMPP before converging to GMPP1. Despite this fact, it should be noted that for Pattern 2, MIC fails to track the GMPP; thus, the discussion on its tracking time is irrelevant.

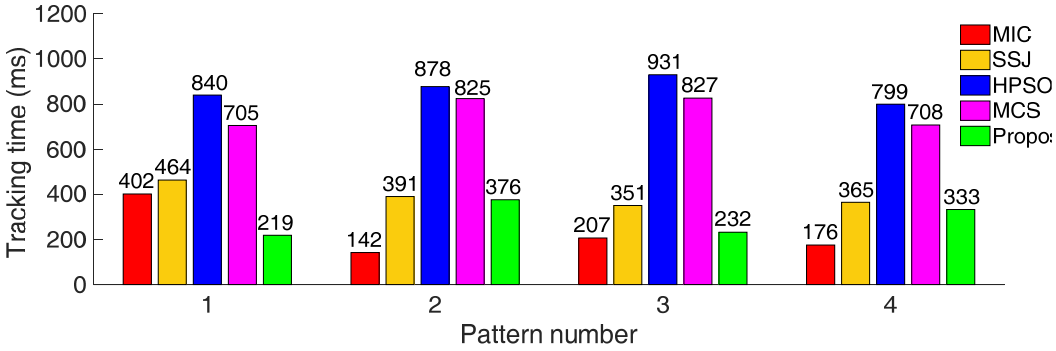

Figure 6-14: Tracking time needed to locate the GMPP.

6.6 Experimental Verification

For verification, a PV string of five modules (emulated using the PVAS) is used. The shading patterns are designed to obtain the *P-V* curves shown in Figure 6-15. Pattern 1 is deliberately chosen to contain two MHP clusters. Its global peak (GMPP1: 90 V, 140 W), is located at the rightmost side of the *P-V* curve. On the other hand, for Pattern 2, the global peak (GMPP2: 35 V, 97 W) is set at the left side of the curve.

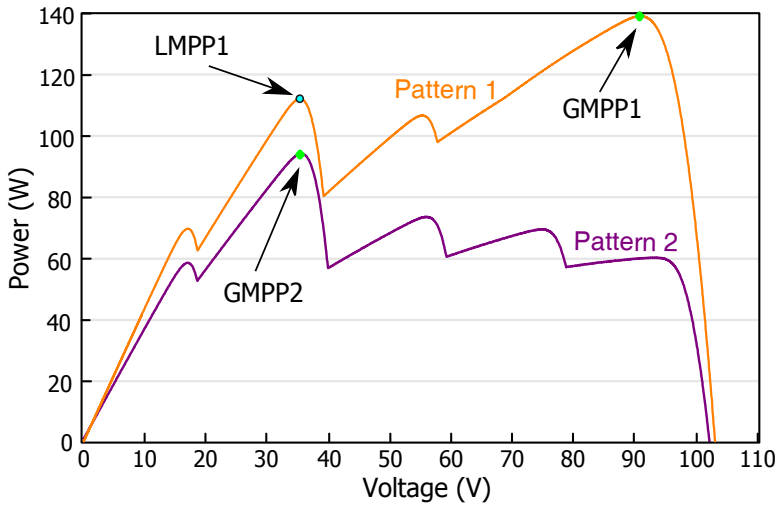

Figure 6-15: *P-V* characteristics of the patterns used in the experiment.

6.7 Results and Discussions

6.7.1 Pattern 1

The tracking performance is illustrated by the oscillograms shown in Figure 6-16. As can be seen from Figure 6-16(a), although the SSJ successfully tracks the global peak (GMPP1), the convergence is slow (3.5 s). This is expected because GMPP1 is located at the rightmost side of the *P-V* curve. Since the SSJ starts the search from the lower end of the curve, it needs to repeat the search-skip-judge process three times before it reaches the vicinity of GMPP1. The MIC also starts the search from the lower end of the curve. After identifying the first cluster that contains MHP, it stops the search because it assumes LMPP1 is the global peak. Thus, it fails to track GMPP1, as indicated in Figure 6-16(b). This observation is consistent with the simulation shown for Pattern 2 of Figure 6-7. On the other hand, the HPSO has successfully tracked GMPP1, as shown in Figure 6-16(c). However, the waveforms show obvious sluggishness (4.8 s). This can be attributed to the haphazard movement of the PSO particles (due to random numbers) before converging to the GMPP1. Finally, the tracking performance of the proposed algorithm is shown in Figure 6-16(d). Its tracking speed is the fastest (2.2 s). This is due to the efficient mechanism that allows skipping the voltage intervals where the GMPP does not exist.

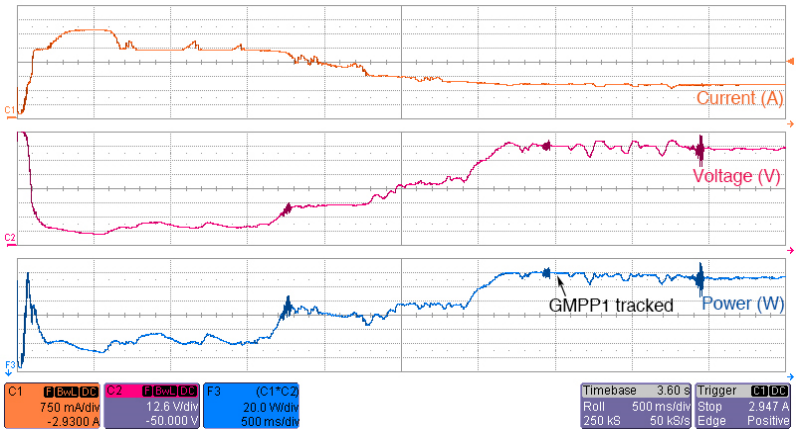

(a)

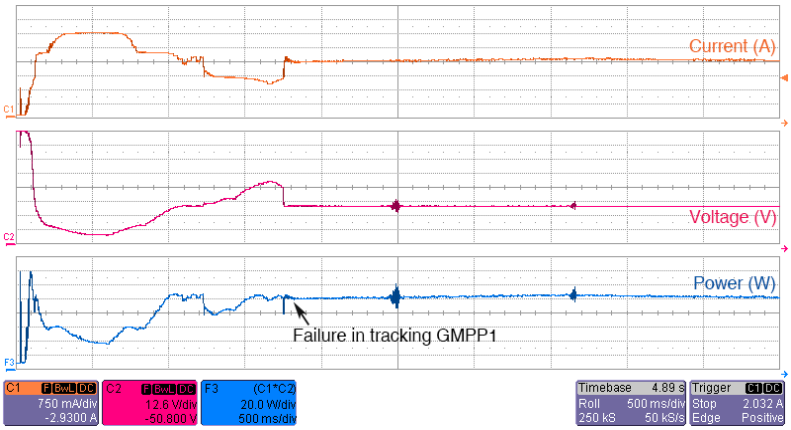

(b)

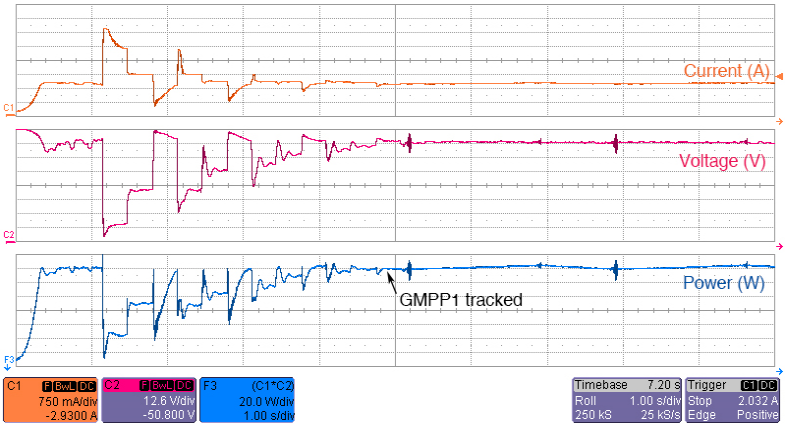

(c)

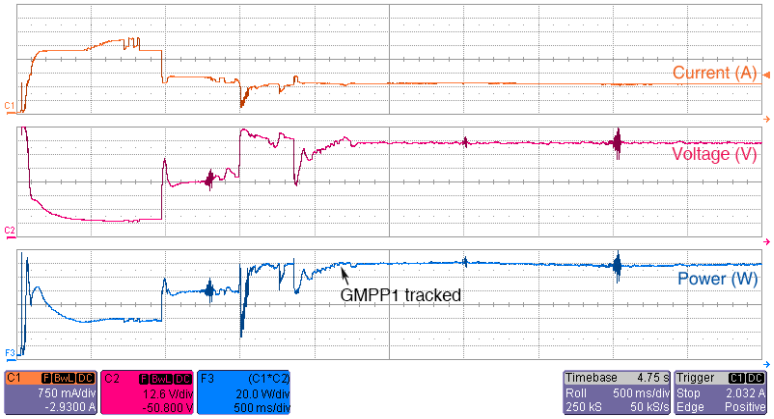

(d)

Figure 6-16: Experimental waveforms of the current, voltage and power while tracking the GMPP of Pattern 1: (a) SSJ (b) MIC (c) HPSO (d) Proposed.

6.7.2 Pattern 2

The global peak for Pattern 2 (GMPP2) is located at the left side of the *P-V* curve. As expected, within a short time, the GMPP2 is tracked successfully by the SSJ (2.5 s) and MIC (2.2 s). These are shown in Figure 6-17(a) and (b), respectively. Similarly, the HPSO is able to track GMPP2 but with a much longer convergence time (8.1 s), as can be seen from Figure 6-17(c). On the other hand, for the proposed method, only the first particle, *P*(1) is involved in the search process. After tracking GMPP2, *P*(1) skips the entire search space using the SSJ scheme; thus the interval scanned by *P*(1) becomes [V_{start}, V_{end}]. Obviously, the initial position of the other two particles, i.e. *P*(2) and *P*(3) are already within this interval. Correspondingly, the information obtained by *P*(1) is communicated to *P*(2) and *P*(3) using the *merge&check()* function. Using this mechanism, particles *P*(2) and *P*(3) are exempted from scanning the interval scanned by *P*(1). As a result, the tracking time is minimized (2.3 s), as shown in Figure 6-17(d). By using these features, the tracking speed is greatly improved compared to the HPSO. From the experimental results, the superiority (in terms of speed and accuracy) of the proposed MPPT scheme is validated. In addition, the practical observation is proven to be consistent with the simulation. In essence, both drawbacks of the original SSJ and the standard PSO are compensated using the proposed control method. This ensures fast convergence towards GMPP and guarantees accurate tracking under complex shading patterns.

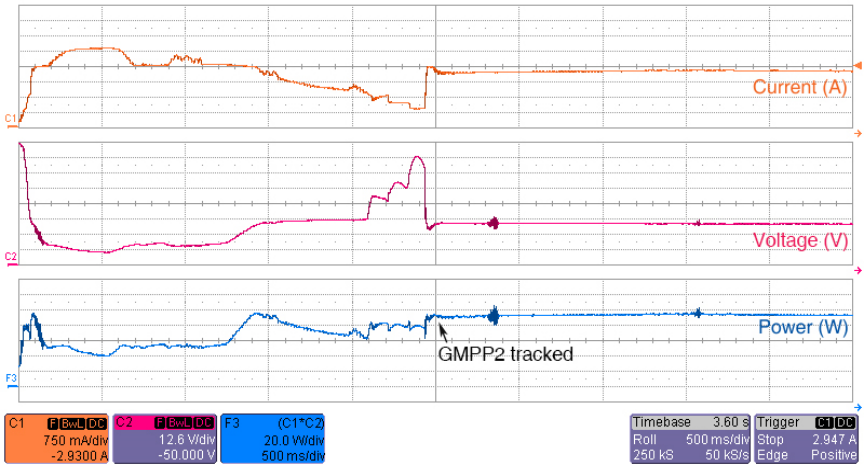

(a)

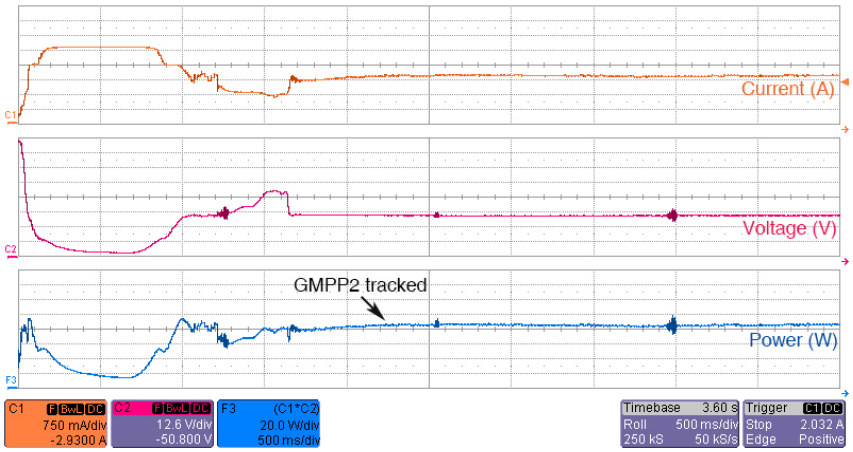

(b)

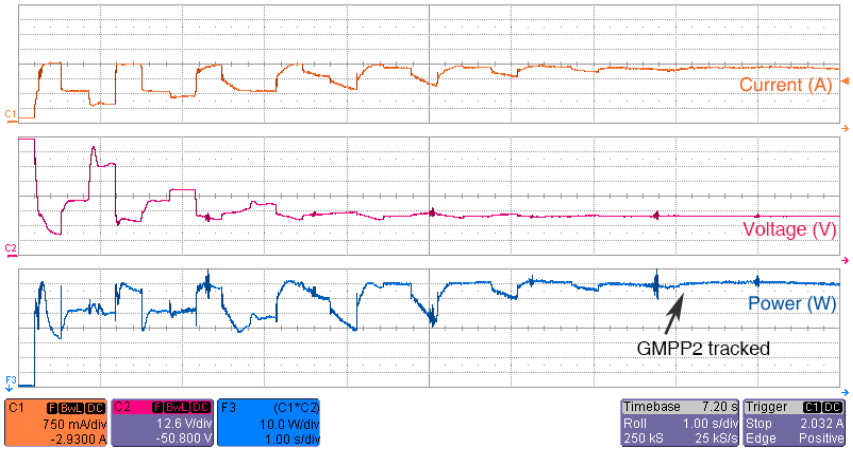

(c)

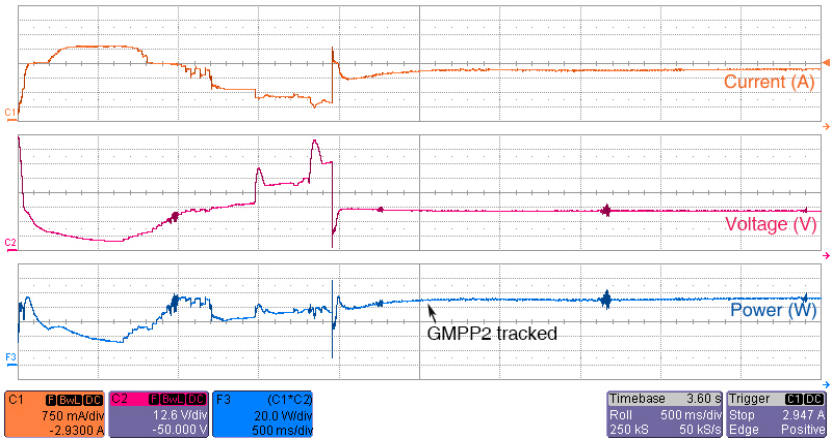

(d)

Figure 6-17: Experimental waveforms of the current, voltage and power while tracking the GMPP of Pattern 2: (a) SSJ (b) MIC (c) HPSO (d) Proposed.

6.8 Comparative Evaluation against the VWS Method

6.8.1 Evaluation of the VWS under Pattern 4

The VWS (described in Section 2.2.3) has high performance and fast tracking speed. However, it is vulnerable to certain shading conditions. As shall be shown below, the VWS fails to handle the shading pattern shown in Figure 6-18 (Pattern 4 of Figure 6-7). Under this pattern, a comparison is made on the tracking performance of the proposed method and VWS.

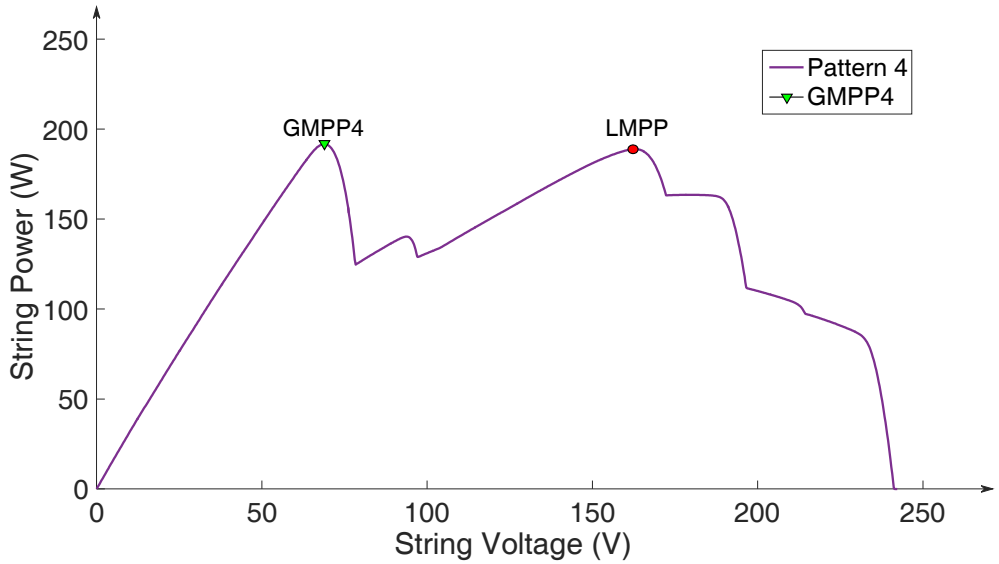

Figure 6-18: Pattern 4 of Figure 6-7 used to evaluate the VWS method.

Figure 6-19 shows the tracking performance of the VWS algorithm. Clearly, it can be seen that the VWS fails to track the GMPP4; instead it trapped at LMPP. On the other hand, the proposed MPPT has successfully tracked GMPP4, as shown in Figure 6-20.

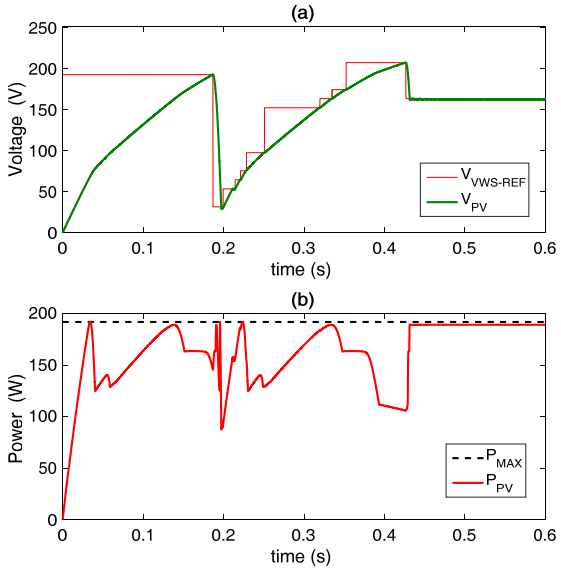

Figure 6-19: Failure of the VWS in tracking the GMPP4. (a) Voltage and (b) power fluctuations.

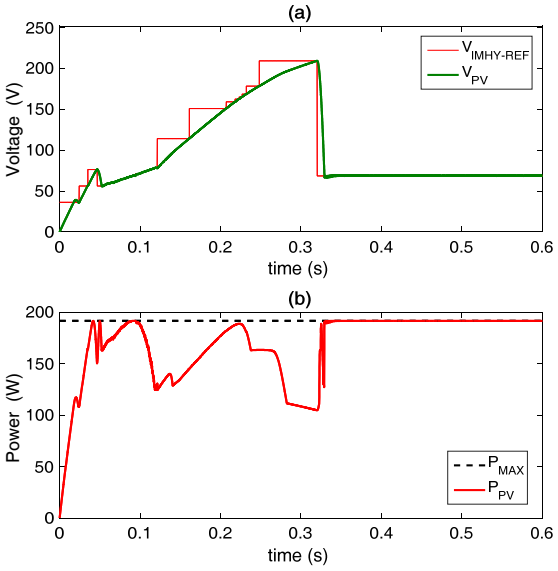

Figure 6-20: The GMPP4 is tracked successfully by the proposed method. (a) Voltage and (b) power fluctuations.

To further explain the reason of failure of the VWS in tracking the GMPP4, Figure 6-21 is considered.

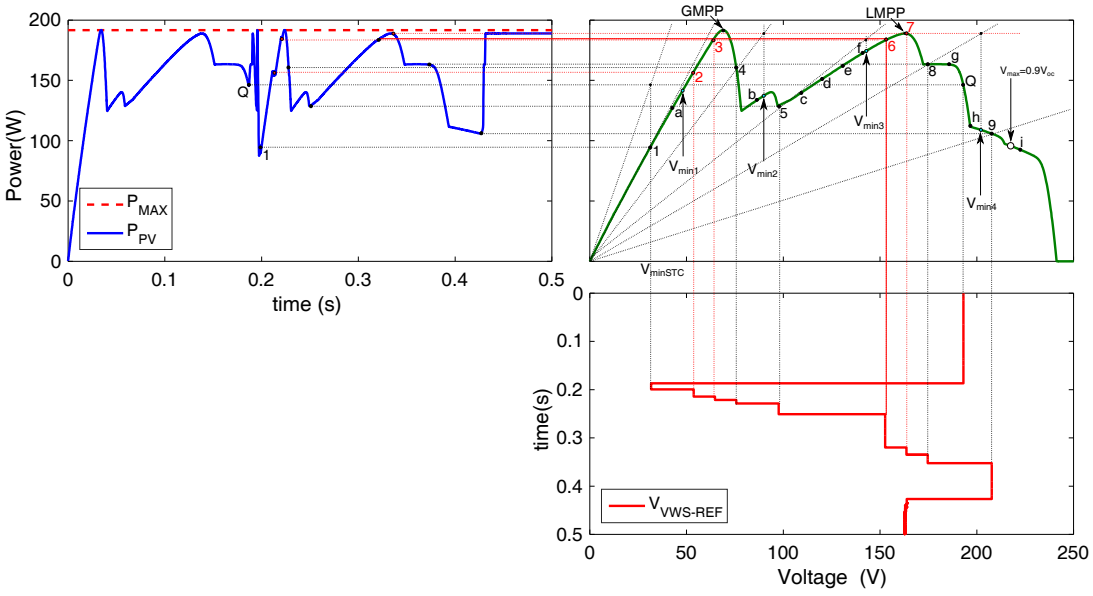

Figure 6-21: Step by step explanation of the VWS failure in tracking the GMPP of Pattern 4.

Assuming an arbitrary starting operating point Q at $0.8V_{oc}$ with power value P_Q (then, $P_{store}=P_Q$). The upper limit of the Voltage Window (VW) remains constant at $V_{max}=0.9V_{oc}$. The lower limit V_{minSTC} is P_{store}/I_{STC} [18]. The VW is restricted to [$V_{minSTC,}$ V_{max}]. The power at point 1 (P_1) is checked. Since $P_1<P_{store}$, a new POT is defined and the lower limit of the VW is updated by V_{min1}. Then, by using V_1, the VWS algorithm calculates the voltages defined as $v=V_1+k\Delta V_{\mathrm{GSTEP}}$ and checks the minimum voltage falling inside the new VW i.e. [V_{min1}, V_{max}]. The voltage of point 2 fulfils this condition, whereas ***a*** is skipped. Since $P_2>P_{store}$, the value of P_2 is stored and retained for further comparisons ($P_{store}=P_2$), and the algorithm checks the next voltage, i.e., $V_3=V_2+\Delta V_{GSTEP}$. Since, for point 3, $P_3>P_{store}$, the value of P_{store} is updated again ($P_{store}=P_3$), and the algorithm checks the next voltage $V_4=V_3+\Delta V_{GSTEP}$. Since, now, $P_4<P_{store}$, a new POT is defined and the new VW now is [V_{min2}, V_{max}]. Then, by using V_4, the VWS algorithm calculates the voltages defined as $v=V_4+k\Delta V_{GSTEP}$, and checks the minimum voltage falling inside [V_{min2}, V_{max}]. The voltage of point 5 fulfils this condition, whereas point b is skipped. Since $P_5<P_{store}$, a new POT is defined and the lower limit of the VW is updated by V_{min3}. Then, by using V_5, the VWS algorithm calculates the voltages defined as $v=V_5+k\Delta V_{GSTEP}$, and checks the minimum voltage falling inside [V_{min3}, V_{max}]. The voltage of point 6 fulfilled this condition, whereas points ***c***, ***d***, ***e*** and ***f*** are skipped. Since $P_6>P_{store}$, the value of P_6 is stored and retained for further comparisons ($P_{\mathrm{store}}=P_6$), and the algorithm checks the next voltage, i.e., $V_7=V_6+\Delta V_{GSTEP}$. Since, for point 7, $P_7>P_{store}$, the value of P_{store} is updated again ($P_{store}=P_7$), and the algorithm checks the next voltage $V_8=V_7+\Delta V_{GSTEP}$. Since, now, $P_8<P_{store}$, a new POT is defined and the new VW now is [V_{min4}, V_{max}]. Then, by using V_8, the VWS algorithm calculates the voltages defined as $v=V_8+k\Delta V_{GSTEP}$, and checks the minimum voltage falling inside [V_{min4}, V_{max}]. The voltage of point 9 fulfilled this condition, whereas points ***g*** and ***h*** are skipped. Since, now, $P_9<P_{store}$, a new POT is defined and since the voltage of point ***i*** located outside the VW, the global searching process ends and sends to the P&O the last retained value of $P_{store}=P_7$ and the corresponding voltage V_7 as the new voltage reference. Hence the VWS algorithm fails in tracking the GMPP.

It can be concluded that, although the VWS MPPT is very fast, but for certain shading patterns, the GMPP can be missed due the large value of the global voltage step ΔV_{GSTEP} used to scan the *P-V* curve.

6.8.2 Experimental Evaluation of the VWS against the Proposed Method

The VWS is experimentally evaluated against the proposed method. Figure 6-22 shows the pattern considered for the test. It is a complex shading pattern contains two MHPs where the higher one is located at the first cluster. The same pattern is implemented on the PVAS for the experimental test. It is shown in Figure 6-23. The GMPP is located at (53.75 V, 124.4 W), while another peak, called LMPP is at (92.3V, 117.5 W).

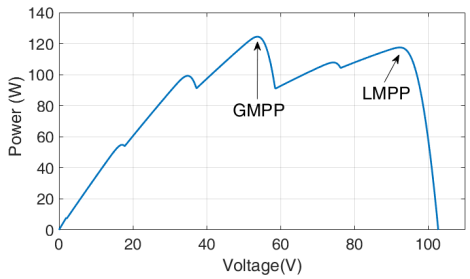

Figure 6-22: Pattern contains two clusters where the GMPP is located in the first one.

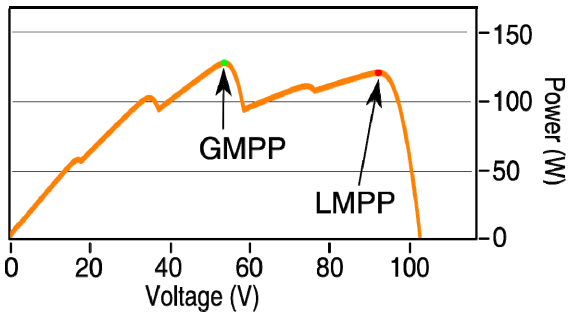

Figure 6-23: Pattern of Figure 6-22 loaded to the PVAS.

Figure 6-24 illustrates the tracking behaviour of VWS when subjected to the shading pattern shown above. By looking at the voltage profile, it is clear that the VWS is not able to track the GMPP. It is instead trapped at LMPP.

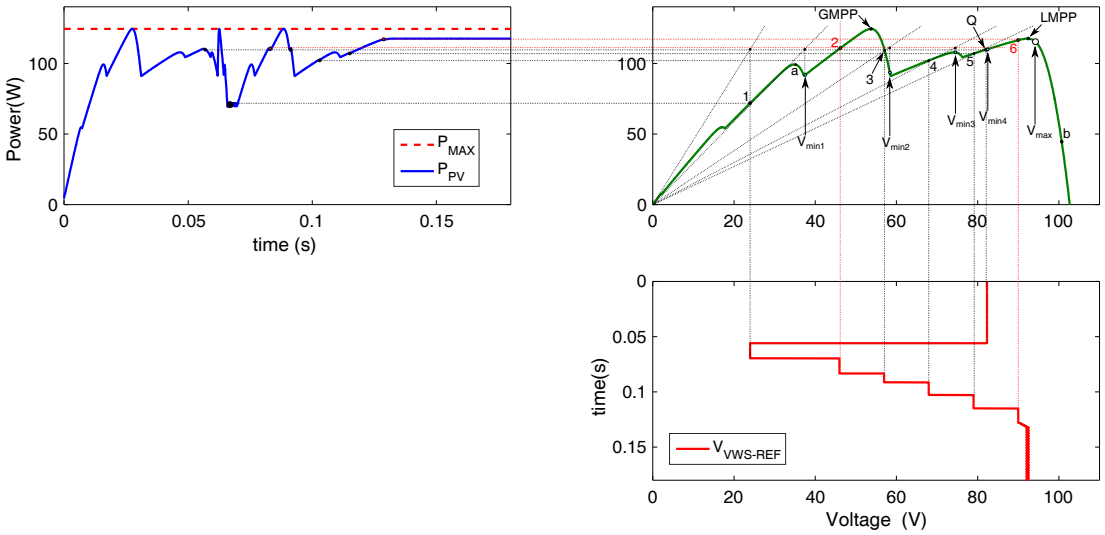

Figure 6-24: A step by step explanation of the VWS failure in tracking the GMPP for Pattern of Figure 6-22.

A brief explanation that collaborates the waveforms in Figure 6-24 is given:

In the beginning, an arbitrary starting point at $0.8V_{oc}$ is chosen. Then, point 1 is checked and the first VW is defined as: [V_{min1}, V_{max}] thus skips point ***a***. Then, point 2 is checked and P_{store} is updated by P_2 since $P_2>P_Q$. Then, points 3, 4 and 5 are checked successively and the VW is updated by V_{min2}, V_{min3} and V_{min4}, respectively. When point 6 is checked, its power is higher than point 2. Thus, P_{store} is updated as: $P_{store}=P_6$ and point ***b*** is ignored since it is outside of the VW. The P&O is turned on starting from the last retained value of P_{store}, i.e. P_6. Thus, the VW fails to identify the region of the GMPP, i.e., [V_2, V_3] and identifies another region which leads to track a LMPP instead.

The VWS algorithm is simulated under this shading pattern. The results is shown in Figure 6-25. As can be seen, the algorithm settles at LMPP after 130 ms and remains there indefinitely. This condition was implemented in the experimental hardware. As can be seen, the experimental results of Figure 6-26 and Figure 6-28 are in very close agreement with the simulation results of Figure 6-25 and Figure 6-27, respectively. The VWS failed in tracking the GMPP and trapped in LMPP while the proposed method successfully tracked the GMPP.

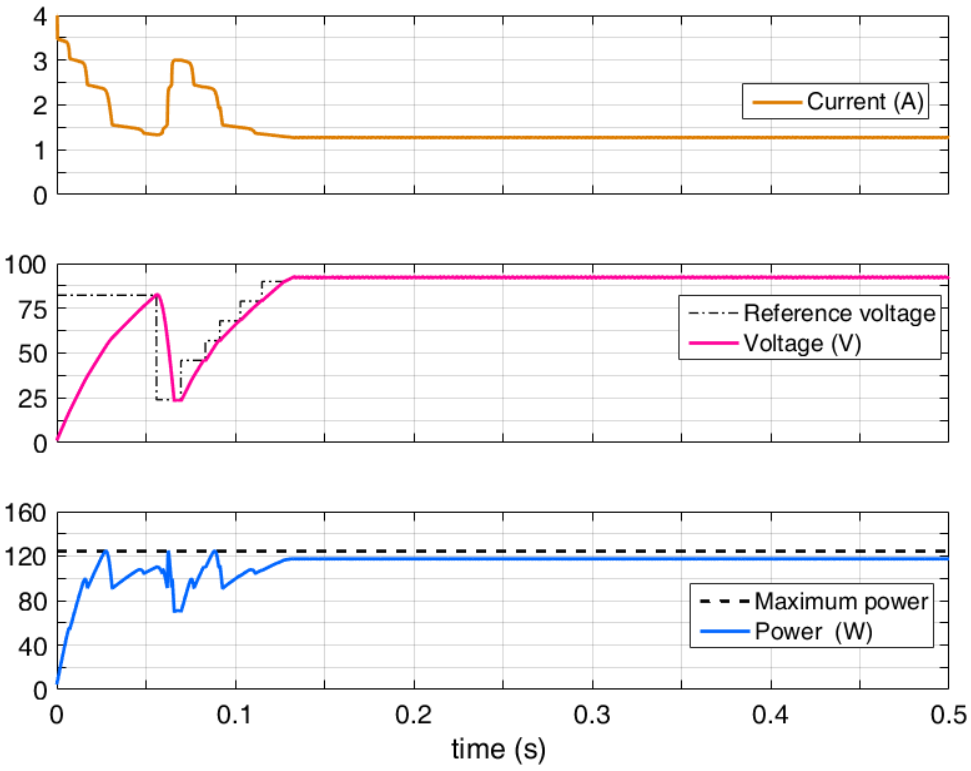

Figure 6-25: Failure of the VWS in tracking the GMPP of the pattern shown in Figure 6-22 (Simulation results).

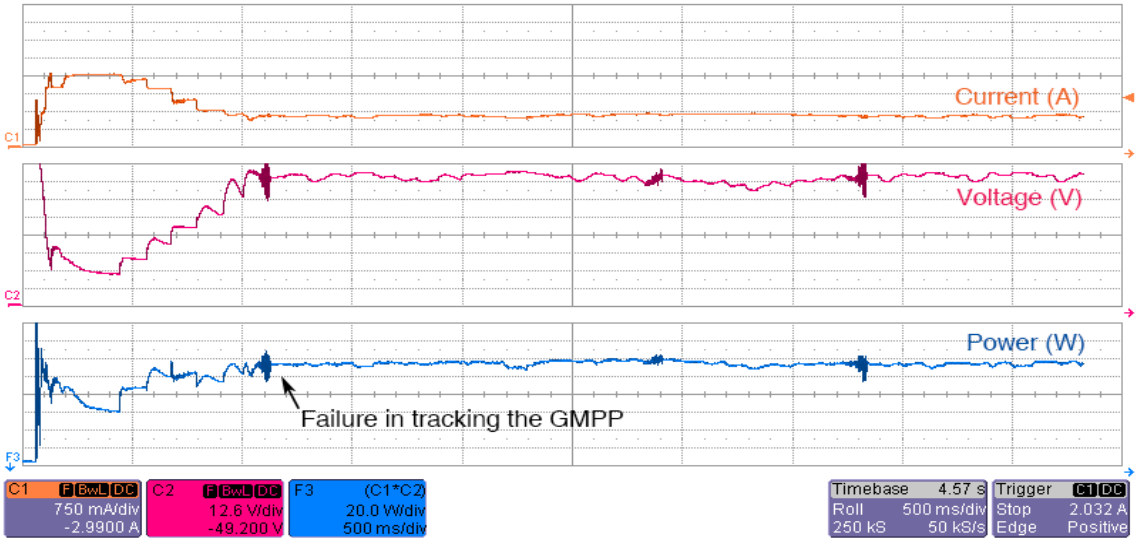

Figure 6-26: The VWS fails in tracking the GMPP of the pattern shown in Figure 6-23 (Experimental results).

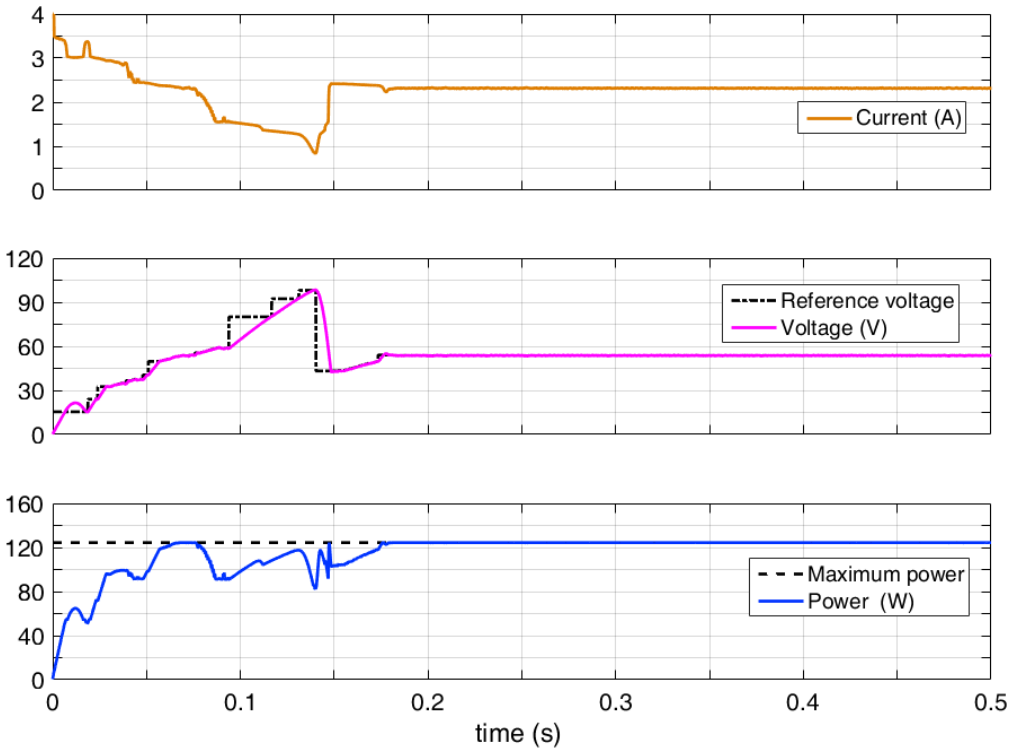

Figure 6-27: The successful tracking of the GMPP using the proposed method (Simulation results).

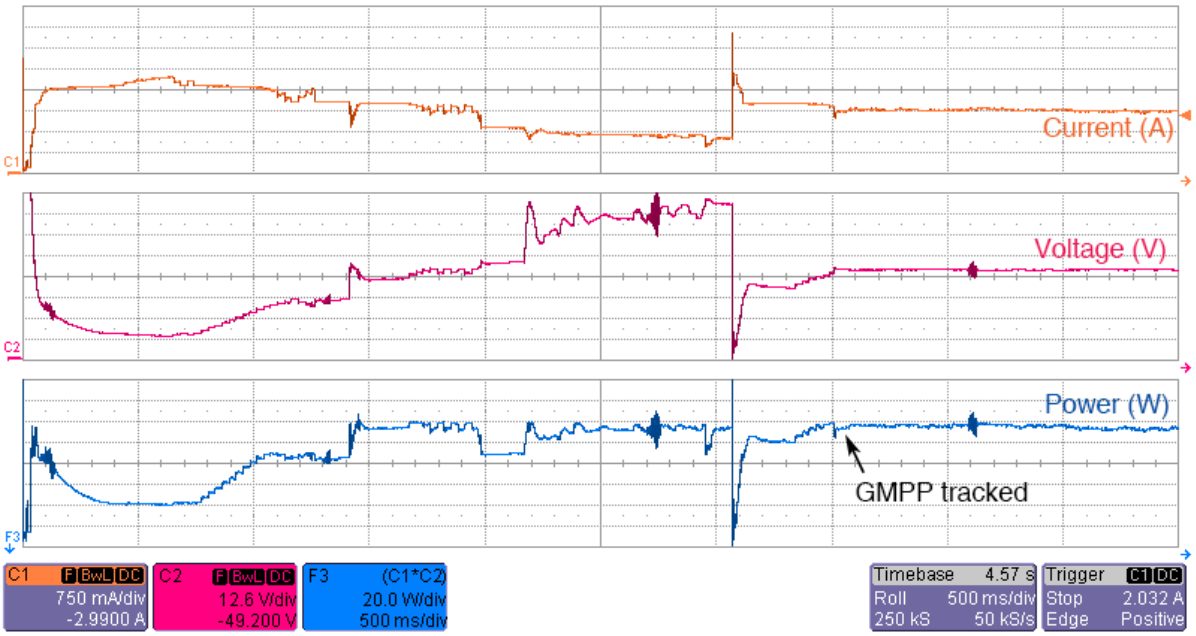

Figure 6-28: The successful tracking of the GMPP using the proposed method (Experimental results).

CHAPTER 7

CONCLUSION AND FUTURE WORK

7.1 Summary of Work

The thesis begins with a critical review on the various MPPT controllers proposed in the literature to deal with partial shading. They are categorized under three groups. First, the improved (modified) conventional MPPT. By incorporating additional intelligence into the MPPT codes, these methods greatly improve the tracking efficiency and overcome the partial shading problem. However, as shown in the results of this work, they failed in handling complex partial shading conditions.

The second group, MPPT based on soft-computing approach such as particle swarm optimization (PSO) and genetic algorithms (GA). These techniques capitalize on their efficient search and optimization capabilities to locate the GMPP. Despite their advantages— particularly in handling partial shading, they exhibit several drawbacks; the most significant is the sluggishness of the tracking speed.

The third group is the hybrid MPPT which is a combination of conventional and metaheuristic approaches. For the metaheuristic PSO, the entire search space is scrutinized so it is very unlikely that the GMPP will be missed. However, this approach exhibits sluggishness in tracking the GMPP despite its effectiveness. This can be attributed to two main reasons. First, the random numbers that are embedded in the PSO velocity equation results in haphazard movement of particles. Second, a PSO particle may explore the space which has been previously scanned by other particles. This unnecessary operation is attributed to the lack of communication between particles.

Later in the thesis, performance assessment of both control methods for MPPT, i.e., the duty cycle (direct) and voltage (indirect) based control methods, is presented. Analysis of the *P-V* characteristics and the (PV+Converter) characteristics (*P-D*) is carried out. The standard P&O technique is implemented using both control methods. For the same test conditions, both control methods are analyzed and their behaviors are studied in terms of steady state oscillation, rapid irradiance change and under load disturbances. The results suggest that the direct method is strongly dependent to the dc-dc converter topology, exhibits higher steady state oscillation and sensitive under rapid irradiance and load changes. On the other hand,

compared to the indirect method. This is conformed the efficiency increase of 1.6% in the steady-state, by up to 30% in the case of rapid irradiance change and by up to 29% in presence of load disturbances.

The main part of this research is to apply a hybrid scheme for the purpose of improving the tracking capability under complex partial shading conditions. This scheme combines the improved P&O and an enhanced PSO. The improved P&O incorporates the search-skip-judge (SSJ) mechanism to minimize the region within *P-V* curve to search by the PSO. The PSO is enhanced by introducing a communication procedure between the particles such that the regions that have been previously explored (by other particle) will not be searched again by (another particle). The proposed scheme offers several advantages: (1) the unnecessary movement of particles is minimized, (2) the convergence time is reduced and (3) the GMPP tracking is guaranteed even under complex partial shading conditions.

The performance of the proposed method is evaluated against four well-established MPPT controllers, namely the original version of SSJ, the modified incremental conductance (MIC), the modified cuckoo search (MCS) and the hybrid PSO (HPSO) using an experimental prototype based on PV array simulator and a buck-boost converter driven by the TMS320F240 DSP on the dSPACE DS1104 platform.

In conclusion, the thesis has demonstrated the viability of the proposed method for tracking the MPP of the PV system regardless of any environmental conditions. The work carried out has proven that the proposed scheme can be suitably used for PV system under challenging and complex partial shading conditions. The main contributions of this thesis can be summarized as follows:

(i) A review discussing the recently proposed MPPT techniques in the literature. The MPPT algorithms have been grouped into three categories: 1- Improved conventional, 2- Soft computing and 3- Hybrid methods.

(ii) A comprehensive comparative analysis for both direct and indirect control methods used for MPPT implementation. It has been found from

the obtained results that the direct method is strongly dependent on the dc-dc converter topology, exhibits higher steady state oscillation and sensitive under rapid irradiance and load changes. From the results, it is suggested to use the indirect method to increase the overall tracking performance in PV systems.

(iii) A comprehensive comparative study for the use of four artificial intelligence-based techniques in the MPPT control under uniform insolation.

(iv) A hybrid MPPT has been proposed to improve the tracking performance of PV systems under complex shading conditions. The scheme is a hybrid between an improved perturb and observe (P&O) and an enhanced particle swarm optimization (PSO). The P&O is improved by incorporating the search-skip-judge (SSJ) mechanism. A communication between the particles has been introduced such that the regions that have been previously explored will not be searched again. Thus, the unnecessary movement is minimized leading to a higher tracking speed.

(v) A critical examination of the proposed method has been carried out against four well-established MPPT controllers in the literature, namely: the modified incremental conductance, the hybrid PSO, the modified cuckoo search and the SSJ (in its original form). The effectiveness of the MPPT methods have been analyzed based on the ability to track GMPP correctly, the number of computation cycles required, the percentage of scanned interval and the tracking time.

(vi) The performance of the proposed method has been verified experimentally using a test bench composed of a PV array simulator, a buck-boost converter, driven by the TMS320F240 DSP on the dSPACE DS1104 platform, and a DC electronic load.

7.2 Future Work

In this thesis, a hybrid MPPT controller has been proposed based on an enhanced PSO incorporating the modified P&O and SSJ scheme. Although the proposed method shows significant improvements in speed and accuracy, the algorithm is quite complex and its implementation requires advanced programming level. Therefore, there remain potentially new findings in the MPPT controller design that can reduce the controller complexity while ensuring the same level of tracking performance and handling major issues in the MPPT area. This simple and compact MPPT controller should be able to:

1) Reduce the effect of steady state oscillation,
2) Integrate an accurate detector differentiating between the partial shading, uniform insolation and the rapid irradiance change,
3) Mitigate the deviation under rapid irradiance increase,
4) Handle the partial shading condition effectively.

REFERENCES

[1] MEM, " Renewable Energy and Energy Efficiency Program," *Ministry of Energy and Mines* March 2011.

[2] M. Kermadi and E. Berkouk, "Techno-economic feasibility study for the use of photovoltaic energy on the south-east algerian farms," *Revue des Energies Renouvelables,* vol. 18, no. 4, pp. 587-594, 2015.

[3] M. Drif, P. J. Pérez, J. Aguilera, and J. D. Aguilar, "A new estimation method of irradiance on a partially shaded PV generator in grid-connected photovoltaic systems," *Renewable Energy,* vol. 33, no. 9, pp. 2048-2056, 2008/09/01/ 2008.

[4] M. A. Green, Y. Hishikawa, E. D. Dunlop, D. H. Levi, J. Hohl-Ebinger, and A. W. Y. Ho-Baillie, "Solar cell efficiency tables (version 51)," *Progress in Photovoltaics: Research and Applications,* vol. 26, no. 1, pp. 3-12, 2018.

[5] F. Dimroth *et al.*, "Four-Junction Wafer-Bonded Concentrator Solar Cells," *IEEE Journal of Photovoltaics,* vol. 6, no. 1, pp. 343-349, 2016.

[6] ISE, "PHOTOVOLTAICS REPORT," *Fraunhofer Institute for Solar Energy Systems, ISE,* Report 26 February 2018.

[7] K. Ishaque and Z. Salam, "A Deterministic Particle Swarm Optimization Maximum Power Point Tracker for Photovoltaic System Under Partial Shading Condition," *IEEE Transactions on Industrial Electronics,* vol. 60, no. 8, pp. 3195-3206, 2013.

[8] S. Mohanty, B. Subudhi, and P. K. Ray, "A New MPPT Design Using Grey Wolf Optimization Technique for Photovoltaic System Under Partial Shading Conditions," *IEEE Transactions on Sustainable Energy,* vol. 7, no. 1, pp. 181-188, 2016.

[9] J. Ahmed and Z. Salam, "A Maximum Power Point Tracking (MPPT) for PV system using Cuckoo Search with partial shading capability," *Applied Energy,* vol. 119, no. 0, pp. 118-130, 4/15/ 2014.

[10] K. Sundareswaran, S. Peddapati, and S. Palani, "MPPT of PV Systems Under Partial Shaded Conditions Through a Colony of Flashing Fireflies," *IEEE Transactions on Energy Conversion* vol. 29, no. 2, pp. 463 - 472, 2014.

[11] N. Kumar, I. Hussain, B. Singh, and B. Panigrahi, "Rapid MPPT for Uniformly and Partial Shaded PV System by using JayaDE Algorithm in Highly Fluctuating Atmospheric Conditions," *IEEE Transactions on Industrial Informatics,* vol. 13, no. 5, pp. 2406 - 2416, 2017.

[12] J. P. Ram and N. Rajasekar, "A Novel Flower Pollination Based Global Maximum Power Point Method for Solar Maximum Power Point Tracking," *IEEE Transactions on Power Electronics,* vol. 32, no. 11, pp. 8486-8499, 2017.

[13] K. Sundareswaran, P. Sankar, P. S. R. Nayak, S. P. Simon, and S. Palani, "Enhanced Energy Output From a PV System Under Partial Shaded Conditions Through Artificial Bee Colony," *IEEE Transactions on Sustainable Energy,* vol. 6, no. 1, pp. 198-209, 2015.

[14] A. M. S. Furtado, F. Bradaschia, M. C. Cavalcanti, and L. R. Limongi, "A Reduced Voltage Range Global Maximum Power Point Tracking Algorithm for Photovoltaic Systems Under Partial Shading Conditions," *IEEE Transactions on Industrial Electronics,* vol. 65, no. 4, pp. 3252-3262, 2018.

[15] Y. Wang, Y. Li, and X. Ruan, "High-Accuracy and Fast-Speed MPPT Methods for PV String Under Partially Shaded Conditions," *IEEE Transactions on Industrial Electronics,* vol. 63, no. 1, pp. 235-245, 2016.

[16] K. S. Tey and S. Mekhilef, "Modified Incremental Conductance Algorithm for Photovoltaic System Under Partial Shading Conditions and Load Variation," *IEEE Transactions on Industrial Electronics,* vol. 61, no. 10, pp. 5384-5392, 2014.

[17] H. Patel and V. Agarwal, "Maximum Power Point Tracking Scheme for PV Systems Operating Under Partially Shaded Conditions," *IEEE Transactions on Industrial Electronics,* vol. 55, no. 4, pp. 1689-1698, 2008.

[18] M. Boztepe, F. Guinjoan, G. Velasco-Quesada, S. Silvestre, A. Chouder, and E. Karatepe, "Global MPPT Scheme for Photovoltaic String Inverters Based on Restricted Voltage Window Search Algorithm," *IEEE Transactions on Industrial Electronics,* vol. 61, no. 7, pp. 3302-3312, 2014.

[19] J. Ahmed and Z. Salam, "An Enhanced Adaptive P&O MPPT for Fast and Efficient Tracking Under Varying Environmental Conditions," *IEEE Transactions on Sustainable Energy,* vol. PP, no. 99, pp. 1-1, 2018.

[20] A. Ramyar, H. Iman-Eini, and S. Farhangi, "Global Maximum Power Point Tracking Method for Photovoltaic Arrays Under Partial Shading Conditions," *IEEE Transactions on Industrial Electronics,* vol. 64, no. 4, pp. 2855-2864, 2017.

[21] S. Elmetennani, T. M. Laleg-Kirati, M. Djemai, and M. Tadjine, "New MPPT algorithm for PV applications based on hybrid dynamical approach," *Journal of Process Control,* vol. 48, pp. 14-24, 2016/12/01/ 2016.

[22] K. Sundareswaran, V. Vigneshkumar, P. Sankar, S. P. Simon, P. S. R. Nayak, and S. Palani, "Development of an Improved P&O Algorithm Assisted Through a Colony of Foraging Ants for MPPT in PV System," *IEEE Transactions on Industrial Informatics,* vol. 12, no. 1, pp. 187-200, 2016.

[23] R. B. A. Koad, A. F. Zobaa, and A. El-Shahat, "A Novel MPPT Algorithm Based on Particle Swarm Optimization for Photovoltaic Systems," *IEEE Transactions on Sustainable Energy,* vol. 8, no. 2, pp. 468-476, 2017.

[24] C. Manickam, G. P. Raman, G. R. Raman, S. I. Ganesan, and N. Chilakapati, "Fireworks Enriched P&O Algorithm for GMPPT and Detection of Partial Shading in PV Systems," *IEEE Transactions on Power Electronics,* vol. 32, no. 6, pp. 4432-4443, 2017.

[25] M. Seyedmahmoudian *et al.*, "Simulation and Hardware Implementation of New Maximum Power Point Tracking Technique for Partially Shaded PV System Using Hybrid DEPSO Method," *IEEE Transactions on Sustainable Energy,* vol. 6, no. 3, pp. 850-862, 2015.

[26] C. Manickam, G. R. Raman, G. P. Raman, S. I. Ganesan, and C. Nagamani, "A Hybrid Algorithm for Tracking of GMPP Based on P&O and PSO With Reduced Power Oscillation in String Inverters," *IEEE Transactions on Industrial Electronics,* vol. 63, no. 10, pp. 6097-6106, 2016.

[27] S. Mohanty, B. Subudhi, and P. K. Ray, "A Grey Wolf-Assisted Perturb & Observe MPPT Algorithm for a PV System," *IEEE Transactions on Energy Conversion,* vol. 32, no. 1, pp. 340-347, 2017.

[28] K. L. Lian, J. H. Jhang, and I. S. Tian, "A Maximum Power Point Tracking Method Based on Perturb-and-Observe Combined With Particle Swarm Optimization," *IEEE Journal of Photovoltaics,* vol. 4, no. 2, pp. 626-633, 2014.

[29] J. Ahmed and Z. Salam, "A Modified P&O Maximum Power Point Tracking Method With Reduced Steady-State Oscillation and Improved Tracking Efficiency," *IEEE Transactions on Sustainable Energy,* vol. 7, no. 4, pp. 1506-1515, 2016.

[30] Y. Shaiek, M. Ben Smida, A. Sakly, and M. F. Mimouni, "Comparison between conventional methods and GA approach for maximum power point tracking of shaded solar PV generators," *Solar Energy,* vol. 90, pp. 107-122, 2013/04/01/ 2013.

[31] Mostefa, "An MPPT controller based on genetic algorithms for photovoltaic systems.," presented at the Proceedings of the Algerian large electrical network conference (CAGRE'15), Algiers, 2015.

[32] H. R. Mohajeri, M. P. Moghaddam, M. Shahparasti, and M. Mohamadian, "Development a new algorithm for maximum power point tracking of partially shaded photovoltaic arrays," in *20th Iranian Conference on Electrical Engineering (ICEE2012)*, 2012, pp. 489-494.

[33] M. Miyatake, M. Veerachary, F. Toriumi, N. Fujii, and H. Ko, "Maximum Power Point Tracking of Multiple Photovoltaic Arrays: A PSO Approach," *IEEE Transactions on Aerospace and Electronic Systems,* vol. 47, no. 1, pp. 367-380, 2011.

[34] K. Ishaque, Z. Salam, M. Amjad, and S. Mekhilef, "An Improved Particle Swarm Optimization (PSO)–Based MPPT for PV With Reduced Steady-State Oscillation," *IEEE Transactions on Power Electronics,* vol. 27, no. 8, pp. 3627-3638, 2012.

[35] M. Kermadi and E. M. Berkouk, "A Hybrid PSO-PI based Maximum Power Point Tracking algorithm using adaptive sampling time strategy," in *2015 4th International Conference on Electrical Engineering (ICEE)*, 2015, pp. 1-6.

[36] M. Kermadi and E. M. Berkouk, "A maximum power point tracker based on particle swarm optimization for PV-battery energy system under partial shading conditions," in *2015 3rd International Conference on Control, Engineering & Information Technology (CEIT)*, 2015, pp. 1-6.

[37] B. R. Peng, K. C. Ho, and Y. H. Liu, "A Novel and Fast MPPT Method Suitable for Both Fast Changing and Partially Shaded Conditions," *IEEE Transactions on Industrial Electronics,* vol. 65, no. 4, pp. 3240-3251, 2018.

[38] C. Huang, L. Wang, R. S. C. Yeung, Z. Zhang, H. S. H. Chung, and A. Bensoussan, "A Prediction Model-Guided Jaya Algorithm for the PV System Maximum Power Point Tracking," *IEEE Transactions on Sustainable Energy,* vol. 9, no. 1, pp. 45-55, 2018.

[39] J. Ahmed and Z. Salam, "A critical evaluation on maximum power point tracking methods for partial shading in PV systems," *Renewable and Sustainable Energy Reviews,* vol. 47, pp. 933-953, 2015/07/01/ 2015.

[40] K. S. Tey, S. Mekhilef, M. Seyedmahmoudian, B. Horan, A. M. T. Oo, and A. Stojcevski, "Improved Differential Evolution-based MPPT Algorithm using SEPIC for PV Systems under Partial Shading Conditions and Load Variation," *IEEE Transactions on Industrial Informatics,* 2018.

[41] P. C. P. Chao, W.-D. Chen, and C.-K. Chang, "Maximum power tracking of a generic photovoltaic system via a fuzzy controller and a two-stage DC–DC converter," *Microsystem Technologies,* vol. 18, no. 9, pp. 1267-1281, 2012/09/01 2012.

[42] A. E. Khateb, N. A. Rahim, J. Selvaraj, and M. N. Uddin, "Fuzzy-Logic-Controller-Based SEPIC Converter for Maximum Power Point Tracking," *IEEE Transactions on Industry Applications,* vol. 50, no. 4, pp. 2349-2358, 2014.

[43] C. Larbes, S. M. Aït Cheikh, T. Obeidi, and A. Zerguerras, "Genetic algorithms optimized fuzzy logic control for the maximum power point tracking in photovoltaic system," *Renewable Energy,* vol. 34, no. 10, pp. 2093-2100, 2009/10/01/ 2009.

[44] F. Chekired, A. Mellit, S. A. Kalogirou, and C. Larbes, "Intelligent maximum power point trackers for photovoltaic applications using FPGA chip: A comparative study," *Solar Energy,* vol. 101, pp. 83-99, 2014/03/01/ 2014.

[45] R. Boukenoui, H. Salhi, R. Bradai, and A. Mellit, "A new intelligent MPPT method for stand-alone photovoltaic systems operating under fast transient variations of shading patterns," *Solar Energy,* vol. 124, pp. 124-142, 2016/02/01/ 2016.

[46] N. Khaehintung, K. Pramotung, and P. Sirisuk, "RISC microcontroller built-in fuzzy logic controller for maximum power point tracking in solar-powered for battery charger," in *2004 IEEE Region 10 Conference TENCON 2004.*, 2004, vol. D, pp. 637-640 Vol. 4.

[47] A. Messai, A. Mellit, A. Massi Pavan, A. Guessoum, and H. Mekki, "FPGA-based implementation of a fuzzy controller (MPPT) for photovoltaic module," *Energy Conversion and Management,* vol. 52, no. 7, pp. 2695-2704, 2011/07/01/ 2011.

[48] P.-C. Cheng, B.-R. Peng, Y.-H. Liu, Y.-S. Cheng, and J.-W. Huang, "Optimization of a Fuzzy-Logic-Control-Based MPPT Algorithm Using the Particle Swarm Optimization Technique," *Energies,* vol. 8, no. 6, 2015.

[49] S. A. Kalogirou, "Artificial neural networks in renewable energy systems applications: a review," *Renewable and Sustainable Energy Reviews,* vol. 5, no. 4, pp. 373-401, 2001/12/01/ 2001.

[50] W. M. Lin, C. M. Hong, and C. H. Chen, "Neural-Network-Based MPPT Control of a Stand-Alone Hybrid Power Generation System," *IEEE Transactions on Power Electronics,* vol. 26, no. 12, pp. 3571-3581, 2011.

[51] Y.-H. Liu, C.-L. Liu, J.-W. Huang, and J.-H. Chen, "Neural-network-based maximum power point tracking methods for photovoltaic systems operating under fast changing environments," *Solar Energy,* vol. 89, pp. 42-53, 2013/03/01/ 2013.

[52] M. Hatti, A. Meharrar, and M. Tioursi, "Power management strategy in the alternative energy photovoltaic/PEM Fuel Cell hybrid system," *Renewable and Sustainable Energy Reviews,* vol. 15, no. 9, pp. 5104-5110, 2011/12/01/ 2011.

[53] A. A. Kulaksız and R. Akkaya, "A genetic algorithm optimized ANN-based MPPT algorithm for a stand-alone PV system with induction motor drive," *Solar Energy,* vol. 86, no. 9, pp. 2366-2375, 2012/09/01/ 2012.

[54] A. Chaouachi, R. M. Kamel, and K. Nagasaka, "A novel multi-model neuro-fuzzy-based MPPT for three-phase grid-connected photovoltaic system," *Solar Energy,* vol. 84, no. 12, pp. 2219-2229, 2010/12/01/ 2010.

[55] F. Mancilla-David, F. Riganti-Fulginei, A. Laudani, and A. Salvini, "A Neural Network-Based Low-Cost Solar Irradiance Sensor," *IEEE Transactions on Instrumentation and Measurement,* vol. 63, no. 3, pp. 583-591, 2014.

[56] L. L. Jiang, D. R. Nayanasiri, D. L. Maskell, and D. M. Vilathgamuwa, "A hybrid maximum power point tracking for partially shaded photovoltaic systems in the tropics," *Renewable Energy,* vol. 76, pp. 53-65, 2015/04/01/ 2015.

[57] S. Daraban, D. Petreus, and C. Morel, "A novel MPPT (maximum power point tracking) algorithm based on a modified genetic algorithm specialized on tracking the global maximum power point in photovoltaic systems affected by partial shading," *Energy,* vol. 74, pp. 374-388, 2014/09/01/ 2014.

[58] S. M. Mirhassani, S. Z. M. Golroodbari, S. M. M. Golroodbari, and S. Mekhilef, "An improved particle swarm optimization based maximum power point tracking strategy with variable sampling time," *International Journal of Electrical Power & Energy Systems,* vol. 64, pp. 761-770, 2015/01/01/ 2015.

[59] Y. H. Liu, S. C. Huang, J. W. Huang, and W. C. Liang, "A Particle Swarm Optimization-Based Maximum Power Point Tracking Algorithm for PV Systems Operating Under Partially Shaded Conditions," *IEEE Transactions on Energy Conversion,* vol. 27, no. 4, pp. 1027-1035, 2012.

[60] K. Sundareswaran, V. Vignesh kumar, and S. Palani, "Application of a combined particle swarm optimization and perturb and observe method for MPPT in PV systems under partial shading conditions," *Renewable Energy,* vol. 75, pp. 308-317, 2015/03/01/ 2015.

[61] S. Messalti, A. G. Harrag, and A. E. Loukriz, "A new neural networks MPPT controller for PV systems," in *IREC2015 The Sixth International Renewable Energy Congress*, 2015, pp. 1-6.

[62] T. Radjai, P. Gaubert Jean, L. Rahmani, and S. Mekhilef, "Experimental verification of P&O MPPT algorithm with direct control based on Fuzzy

logic control using CUK converter," *International Transactions on Electrical Energy Systems,* vol. 25, no. 12, pp. 3492-3508, 2015/12/01 2015.

[63] T. Radjai, L. Rahmani, S. Mekhilef, and J. P. Gaubert, "Implementation of a modified incremental conductance MPPT algorithm with direct control based on a fuzzy duty cycle change estimator using dSPACE," *Solar Energy,* vol. 110, pp. 325-337, 2014/12/01/ 2014.

[64] J. Ahmed and Z. Salam, "An Improved Method to Predict the Position of Maximum Power Point During Partial Shading for PV Arrays," *IEEE Transactions on Industrial Informatics,* vol. 11, no. 6, pp. 1378-1387, 2015.

[65] V. J. Chin, Z. Salam, and K. Ishaque, "Cell modelling and model parameters estimation techniques for photovoltaic simulator application: A review," *Applied Energy,* vol. 154, pp. 500-519, 2015/09/15/ 2015.

[66] K. Ishaque, Z. Salam, and H. Taheri, "Simple, fast and accurate two-diode model for photovoltaic modules," *Solar Energy Materials and Solar Cells,* vol. 95, no. 2, pp. 586-594, 2011/02/01/ 2011.

[67] V. J. Chin, Z. Salam, and K. Ishaque, "An Accurate and Fast Computational Algorithm for the Two-diode Model of PV Module Based on a Hybrid Method," *IEEE Transactions on Industrial Electronics,* vol. 64, no. 8, pp. 6212-6222, 2017.

[68] M. G. Villalva, J. R. Gazoli, and E. R. Filho, "Comprehensive Approach to Modeling and Simulation of Photovoltaic Arrays," *IEEE Transactions on Power Electronics,* vol. 24, no. 5, pp. 1198-1208, 2009.

[69] K. Ishaque, Z. Salam, H. Taheri, and A. Shamsudin, "A critical evaluation of EA computational methods for Photovoltaic cell parameter extraction based on two diode model," *Solar Energy,* vol. 85, no. 9, pp. 1768-1779, 2011/09/01/ 2011.

[70] V. J. Chin, Z. Salam, and K. Ishaque, "An accurate modelling of the two-diode model of PV module using a hybrid solution based on differential evolution," *Energy Conversion and Management,* vol. 124, pp. 42-50, 2016/09/15/ 2016.

[71] M. Kermadi, Z. Salam, and E. M. Berkouk, "An adaptive sliding mode control technique applied in grid-connected PV system with reduced

chattering effect," in *2017 IEEE Conference on Energy Conversion (CENCON)*, 2017, pp. 180-185.

[72] "User's Manual : Programmable Photovoltaic Array Simulator PVAS1," *Arsenal Research,* AIT Austrian Institute of Technology. 2007.

[73] "dSPACE User's Guide for Release 7.4," *dSPACE GmbH,* http://www.dspace.com, Paderborn, Germany. 2012. Paderborn, Germany

[74] I. U. Eisemann, "Modeling Guidelines for Function Development and Production Code Generation," *Embedded World Conference 2006,* February 14th - 16th, 2006. Nuremberg, Germany.

[75] M. A. A. Board, "Control Algorithm Modeling Guidelines Using MATLAB®, Simulink®, and Stateflow®," *V2. 0, The Mathworks, Inc,* 2007.

[76] T. K. Soon and S. Mekhilef, "A Fast-Converging MPPT Technique for Photovoltaic System Under Fast-Varying Solar Irradiation and Load Resistance," *IEEE Transactions on Industrial Informatics,* vol. 11, no. 1, pp. 176-186, 2015.

[77] M. Killi and S. Samanta, "Modified Perturb and Observe MPPT Algorithm for Drift Avoidance in Photovoltaic Systems," *IEEE Transactions on Industrial Electronics,* vol. 62, no. 9, pp. 5549-5559, 2015.

[78] B. I. Rani, G. S. Ilango, and C. Nagamani, "Control Strategy for Power Flow Management in a PV System Supplying DC Loads," *IEEE Transactions on Industrial Electronics,* vol. 60, no. 8, pp. 3185-3194, 2013.

[79] G. Escobar, S. Pettersson, C. N. M. Ho, and R. Rico-Camacho, "Multisampling Maximum Power Point Tracker (MS-MPPT) to Compensate Irradiance and Temperature Changes," *IEEE Transactions on Sustainable Energy,* vol. 8, no. 3, pp. 1096-1105, 2017.

[80] N. Kumar, I. Hussain, B. Singh, and B. K. Panigrahi, "Framework of Maximum Power Extraction from Solar PV Panel using Self Predictive Perturb and Observe Algorithm," *IEEE Transactions on Sustainable Energy,* vol. PP, no. 99, pp. 1-1, 2017.

[81] M. A. Ghasemi, A. Ramyar, and H. Iman-Eini, "MPPT Method for PV Systems Under Partially Shaded Conditions by Approximating I–V Curve," *IEEE Transactions on Industrial Electronics,* vol. 65, no. 5, pp. 3966-3975, 2018.

[82] F. Paz and M. Ordonez, "Zero Oscillation and Irradiance Slope Tracking for Photovoltaic MPPT," *IEEE Transactions on Industrial Electronics,* vol. 61, no. 11, pp. 6138-6147, 2014.

[83] S. K. Kollimalla and M. K. Mishra, "A Novel Adaptive P&O MPPT Algorithm Considering Sudden Changes in the Irradiance," *IEEE Transactions on Energy Conversion,* vol. 29, no. 3, pp. 602-610, 2014.

[84] M. A. Elgendy, B. Zahawi, and D. J. Atkinson, "Assessment of Perturb and Observe MPPT Algorithm Implementation Techniques for PV Pumping Applications," *IEEE Transactions on Sustainable Energy,* vol. 3, no. 1, pp. 21-33, 2012.

[85] M. A. Elgendy, B. Zahawi, and D. J. Atkinson, "Assessment of the Incremental Conductance Maximum Power Point Tracking Algorithm," *IEEE Transactions on Sustainable Energy,* vol. 4, no. 1, pp. 108-117, 2013.

[86] "Solarex MSX60 and MSX64 Solar Arrays Datasheet," http://www.solarelectricsupply.com/solarex-msx-60-w-junction-box-548. 1997.

[87] S. Kolesnik and A. Kuperman, "On the Equivalence of Major Variable-Step-Size MPPT Algorithms," *IEEE Journal of Photovoltaics,* vol. 6, no. 2, pp. 590-594, 2016.

[88] N. H. R. Bründlinger, H. Häberlin, B. Burger, A. Bergmann, and F. Baumgartner "prEN 50530–The New European Standard for Performance Characterisation of PV Inverters," presented at the Proc. 24th European Photovoltaic Solar Energy Conf, 2009.

[89] I. G. Zurbriggen and M. Ordonez, "PV Energy Harvesting under Extremely Fast Changing Irradiance: State-plane Direct MPPT," *IEEE Transactions on Industrial Electronics,* pp. 1-1, 2018.

[90] M. Kermadi and E. M. Berkouk, "Artificial intelligence-based maximum power point tracking controllers for Photovoltaic systems: Comparative study," *Renewable and Sustainable Energy Reviews,* vol. 69, pp. 369-386, 2017/03/01/ 2017.

[91] B. Subudhi and R. Pradhan, "A Comparative Study on Maximum Power Point Tracking Techniques for Photovoltaic Power Systems," *IEEE Transactions on Sustainable Energy,* vol. 4, no. 1, pp. 89-98, 2013.

[92] D. Verma, S. Nema, A. M. Shandilya, and S. K. Dash, "Maximum power point tracking (MPPT) techniques: Recapitulation in solar photovoltaic systems," *Renewable and Sustainable Energy Reviews,* vol. 54, pp. 1018-1034, 2016/02/01/ 2016.

[93] P. Manganiello, M. Balato, and M. Vitelli, "A Survey on Mismatching and Aging of PV Modules: The Closed Loop," *IEEE Transactions on Industrial Electronics,* vol. 62, no. 11, pp. 7276-7286, 2015.

[94] B. Nehme, N. K. M'Sirdi, T. Akiki, and A. Naamane, "Contribution to the Modeling of Ageing Effects in PV Cells and Modules," *Energy Procedia,* vol. 62, pp. 565-575, 2014/01/01/ 2014.

[95] T. Esram and P. L. Chapman, "Comparison of Photovoltaic Array Maximum Power Point Tracking Techniques," *IEEE Transactions on Energy Conversion,* vol. 22, no. 2, pp. 439-449, 2007.

[96] Z. Salam, J. Ahmed, and B. S. Merugu, "The application of soft computing methods for MPPT of PV system: A technological and status review," *Applied Energy,* vol. 107, pp. 135-148, 2013/07/01/ 2013.

[97] A. Mellit and S. A. Kalogirou, "MPPT-based artificial intelligence techniques for photovoltaic systems and its implementation into field programmable gate array chips: Review of current status and future perspectives," *Energy,* vol. 70, pp. 1-21, 2014/06/01/ 2014.

[98] M. Kermadi, Z. Salam, J. Ahmed, and E. M. Berkouk, "An Effective Hybrid Maximum Power Point Tracker of Photovoltaic Arrays for Complex Partial Shading Conditions," *IEEE Transactions on Industrial Electronics,* pp. 1-1, 2018.

[99] J. Ahmed and Z. Salam, "An Accurate Method for MPPT to Detect the Partial Shading Occurrence in a PV System," *IEEE Transactions on Industrial Informatics,* vol. 13, no. 5, pp. 2151-2161, 2017.

[100] M. Stateflow® User's Guide, "The MathWorks," ed: Inc, 2011.

[101] M. Kermadi, Z. Salam, and E. M. Berkouk, "A Rule-based Power Management Controller using Stateflow for Grid-Connected PV-Battery Energy System supplying Household load," in *2018 9th IEEE International Symposium on Power Electronics for Distributed Generation Systems (PEDG)*, 2018, pp. 1-6.

APPENDIX A

LIST OF PUBLICATIONS AND CONFERENCES

International Journal Publications:

1. **M. Kermadi,** Z. Salam, J. Ahmed and E. M. Berkouk, "An Effective Hybrid Maximum Power Point Tracker of PV Arrays for Complex Partial Shading Conditions" in *IEEE Transactions on Industrial Electronics*. Doi: 10.1109/TIE.2018.2877202, October 2018.
2. **M. Kermadi,** Z. Salam and E. M. Berkouk, “Comparative Assessment of Maximum Power Point Trackers Performance using Direct and Indirect Control Methods" in *IEEE Transactions on Industrial Electronics*, **under review.**
3. **M. Kermadi** and E. M. Berkouk, "Artificial intelligence-based maximum power point tracking controllers for Photovoltaic systems: Comparative study," *Renewable and Sustainable Energy Reviews,* vol. 69, pp. 369-386, 2017/03/01/ 2017.

National Journal Publications :

4. **M. Kermadi** and E. M. Berkouk, Techno-economic feasibility study for the use of photovoltaic energy on the south-east algerian farms, Revue des Energies Renouvelables Vol. 18 No 4 (2015) 587-594.

International Conference Publications :

5. **M. Kermadi**, E. M. Berkouk and Z. Salam, "An Adaptive Sliding Mode Control Technique Applied in Grid-Connected PV System with Reduced Chattering Effect", in *The 3rd IEEE Conference on Energy Conversion (CENCON 2017)* October 30-31th, 2017, Kuala Lumpur, Malaysia. ***Best Paper Award*** (*3rd Prize*).

6. **M. Kermadi**, Z. Salam and E. M. Berkouk, "A Rule-based Power Management Controller using Stateflow for Grid-Connected PV-Battery Energy System supplying Household load," *2018 9th IEEE International Symposium on Power Electronics for Distributed Generation Systems (PEDG)*, Charlotte, NC, USA, 2018, pp. 1-6. doi: 10.1109/PEDG.2018.8447566

7. **M. Kermadi** and E. M. Berkouk, "A Hybrid PSO-PI based Maximum Power Point Tracking algorithm using adaptive sampling time strategy," in 2015 *4th International Conference on Electrical Engineering (ICEE)*, Boumerdes 2015.

8. **M. Kermadi** and E. M. Berkouk, "A maximum power point tracker based on particle swarm optimization for PV-battery energy system under partial shading conditions," in *2015 3rd International Conference on Control, Engineering & Information Technology (CEIT)*, Tlemcen 2015, pp. 1-6.

9. **M. Kermadi,** *et al.*, "Design of discrete PI-based current controller for reversible buck boost converter. Digital implementation using Arduino Due board," in *2016 8th International Conference on Modelling, Identification and Control (ICMIC)*, Algiers 2016, pp. 863-866.

National Conference Publications :

10. **M. Kermadi** and E. M. Berkouk, "Real time implementation of space vector pulse width modulation using arduino UNO board", *in 9 eme Conference sur le Genie Electrique (CGE09)* April 2015 — EMP, Bordj El Bahri, Algeria

11. **M. Kermadi** et al, "Overview of arduino development platform and its applications in control systems", in *2nd International Conference on Power Electronics and their Applications (ICPEA 2015)*— Djelfa, Algeria.

12. **M.Kermadi** and E. M. Berkouk, "An MPPT controller based on Genetic Algorithms for Photovoltaic systems", in *Algerian Large Electrical Network Conference (CAGRE'15)* March 2015— Algiers, Algeria.

13. **M. Kermadi** and E. M. Berkouk, "Controle par Mode Glissant de l'injection de la Puissance dans une Source d'energie Renouvelable Connectee au Reseau", *in 2eme conference Internationale des energies renouvelables CIER-2014,* December 2014— Monastir, Tunisia.

14. **M. Kermadi** and E. M. Berkouk, "Direct SVPWM control for Matrix converter. Implementation using dSpace ds1104 board", in Third International Conference on Power Electronics and Electrical Drives ICPEED'14 December 2014— Oran, Algeria

Co-Authored publications :

15. Z. E. A. Kherroubi, F. Akel, **M. Kermadi** and E.M. Berkouk, "Real time implementation of space vector pulse width modulation using Arduino DUE board," in *IECON 2016 - 42nd Annual Conference of the IEEE Industrial Electronics Society*, 2016, pp. 3576-3581.

16. Z. E. A. Kherroubi, **M. Kermadi**, E. M. Berkouk and Z. Salam," Real Time Implementation of Space Vector Pulse Width Modulation for Three Level Neutral Point Clamped (NPC) inverter using Arduino DUE board", in *the 3rd IEEE Conference on Energy Conversion (CENCON 2017)* October 30-31th, 2017, Kuala Lumpur, Malaysia.

17. A. Alalei, **M. Kermadi**, A. Nesba and A. Hazzab, "Adaptive Sliding Mode Control of DFIG fed by Matrix Converter during Grid Faults", in *the 3rd IEEE Conference on Energy Conversion (CENCON 2017)* October 30-31th, 2017, Kuala Lumpur, Malaysia.

18. Charles Kho, J. Ahmed, Yi Lung Then, **M. Kermadi** "Mitigating the Effect of Partial Shading by Triple-Tied Configuration of PV Modules" *in 10th IEEE PES Asia-Pacific Power and Energy Engineering Conference 2018 (APPEEC).* Sabah, Malaysia.